

XYZ-like Spectra from Laplace Sum Rule at N2LO in the Chiral Limit

R. Albuquerque

Faculty of Technology, Rio de Janeiro State University (FAT, UERJ), Brazil

Email address: raphael.albuquerque@uerj.br

S. Narison

*Laboratoire Univers et Particules de Montpellier (LUPM), CNRS-IN2P3,
Case 070, Place Eugène Bataillon, 34095 - Montpellier, France.*

Email address: snarison@yahoo.fr

F. Fanomezana*, A. Rabemananjara, D. Rabetiarivony* and G. Randriamanatrika*

Institute of High-Energy Physics of Madagascar (iHEPMAD)

University of Antakatso, Antananarivo 101, Madagascar

We present new compact integrated expressions of QCD spectral functions of heavy-light molecules and four-quark XYZ -like states at lowest order (LO) of perturbative (PT) QCD and up to $d = 8$ condensates of the Operator Product Expansion (OPE). Then, we improve previous LO results from QCD spectral sum rules (QSSR), on the XYZ -like masses and decay constants (which suffer from the ill-defined heavy quark mass) by including up to next-to-next leading order (N2LO) PT QCD corrections, which we have estimated by assuming the factorization of the four-quark spectral functions. PT N3LO corrections are estimated using a geometric growth of the PT series and are included in the systematic errors. Our optimal results based on stability criteria with respect to the variations of the τ -Laplace sum rule (LSR) variable, QCD continuum threshold t_c and subtraction constant μ are summarized in Tables 11 to 14 and compared with experimental candidates and some LO QSSR results in Section 11. We conclude that the masses of the XZ observed states are compatible with (almost) pure $J^{PC} = 1^{+\pm}, 0^{++}$ molecule or/and four-quark states. The predicted masses of the $1^{-\pm}, 0^{-\pm}$ molecule / four-quark states are about 1.5 GeV above the $Y_{c,b}$ mesons experimental candidates and hadronic thresholds which may suggest that these predicted states are broad or/and weakly bounded. The observed $Y_{c,b}(1^{--})$ mesons may result from large mixing of the exotics with ordinary $J/\psi, \Upsilon$ states. We also find that the $\bar{D}D, \bar{B}B$ -like molecule and four-quark states couple weakly to the associated interpolating currents than ordinary D, B mesons ($f_{DD} \approx 10^{-3} f_D$) while, our numerical results indicate an approximate $1/\bar{m}_b^{3/2}$ (resp. $1/\bar{m}_b$) behaviour for the $1^+, 0^+$ (resp. $1^-, 0^-$) states compared to the usual $1/\bar{m}_b^{1/2}$ one of f_B , which can stimulate further theoretical studies of these decay constants.

Keywords: QCD spectral sum rules, Perturbative and Non-Perturbative calculations, Exotic mesons masses and decay constants.

Pac numbers: 11.55.Hx, 12.38.Lg, 13.20-v

* PhD Students.

1. Introduction and Experimental Facts

- A large amount of exotic hadrons which differ from the “standard” $\bar{c}c$ charmonium and $\bar{b}b$ bottomonium radial excitation states have been discovered in D and B -factories through e.g. $J/\psi\pi^+\pi^-$ and $\Upsilon\pi^+\pi^-$ processes. These states are the^a:

- $X_c(3872)$ 1^{++} state found by BELLE,¹ BABAR,^{2,3} CDF,⁴ D0⁵ from $B^- \rightarrow \pi^- [X \rightarrow J/\psi\pi^+\pi^-]$ and $B^- \rightarrow K^- [X \rightarrow J/\psi\pi^+\pi^-]$ decays and LHCb⁶ from $B^+ \rightarrow K^+ [X \rightarrow \psi(2S)\gamma]$ and $B^+ \rightarrow K^+ [X \rightarrow \psi\gamma]$ with a full width less than 1.2 MeV (90% CL).⁷
- $Y_c(4260, 4360, 4660)$ 1^{--} states by BELLE,¹³ BABAR,¹⁴ CLEO¹⁵ and BESIII¹⁶^b discovered through the initial-state-radiation (ISR) process: $e^+e^- \rightarrow \gamma_{ISR}\pi^+\pi^-J/\psi$ and the one: $e^+e^- \rightarrow \pi^+\pi^-J/\psi$ in the charmonium region, with a respective total width of (88.0 ± 23.5) , (48.0 ± 15.3) and $(92.0^{+41.2}_{-31.9})$ MeV.
- $Z_c(3900)$ 1^{++} by BELLE^{18,19} and BESIII¹⁶ from $e^+e^- \rightarrow \pi^\pm [Z_c \rightarrow \pi^\pm J/\psi]$. However, the $Z_c(3900)$ is now quoted in PDG⁷ as a 0^{++} state.
- $Z_c(4025)$ found by BESIII,²⁰⁻²² through $e^+e^- \rightarrow D^*\bar{D}^*\pi$, $\pi\pi h_c$. The charged [resp. neutral] one having a width of (24.8 ± 9.5) [resp. (23.0 ± 6.1)] MeV.
- $Z_c(4050)$ found by BELLE²³ through $\pi^\pm J/\psi(2S)$.
- $Z_c(4430)$ from $B \rightarrow K [Z_c \rightarrow \psi'\pi^\pm]$ decays by BELLE²⁴ and confirmed recently by LHCb²⁵ with a width of (35 ± 7) MeV.⁷

and the observed bottomonium states. The:

- $Y_b(9898, 10260)$ seen by BELLE²⁶ through $e^+e^- \rightarrow \Upsilon(5S) \rightarrow h_b(nP)\pi^+\pi^-$ ($n = 1, 2, 3$).
- $Y_b(10860)$ near the $\Upsilon(5S)$ peak seen by BELLE²⁷ where the partial widths to $\Upsilon(nS)\pi^+\pi^-$ ($n = 1, 2, 3$) of (1.79 ± 0.24) MeV and to $\Upsilon(1S)K^+K^-$ of (0.067 ± 0.021) MeV are much larger than the one of a standard $\bar{b}b$ state.
- $Z_b(10610, 10650)$ by BELLE²⁸ through $\Upsilon(5S) \rightarrow \Upsilon(nS)\pi^+\pi^-$ ($n = 1, 2, 3$) and $h_b(mP)\pi^+\pi^-$ ($m = 1, 2$) decay analyses where they have a respective total width of (18.4 ± 2.4) and (11.5 ± 2.2) MeV.

- The observations of these unconventional states^c, which have some properties beyond the standard quark model (BSQM), have motivated different theoretical interpretations such as molecule and four-quark states^d or simply cusps/rescattering effects where no resonance is needed for explaining the data.⁴⁹⁻⁵¹

^aWe postpone in a future publication⁸ the analysis of the states decaying to $J/\psi\phi$ such as the: $X_c(4147, 4273)$ 1^{++} states found recently by LHCb⁹ which confirm previous CDF^{10,11} results, the $X_c(4350)$ by BELLE,¹² the $X_c(4506, 4704)$ 0^{++} states by LHCb⁹ and the $Y_c(4140)$ 1^{--} by CDF.¹⁰

^bFor a recent review on BESIII results, see e.g.¹⁷

^cA recent analysis of the BELLE collaboration from $\Upsilon(1S)$ inclusive decays does not confirm the existence of some of these states.²⁹

^dFor reviews, see e.g.^{30-34, 36-46}

- The existence of molecule states has been speculated long ago for charmonium systems.^{52,53} They can be weakly bound states of the Van Der Waals-type of two mesons from a long range potential due to one meson exchange.^{54–56}
- The four-quark states have been introduced earlier by⁵⁷ for interpreting the complex spectra of light scalar mesons and used recently by^{58,59} for explaining the $X(3872)$ meson firstly found by BELLE.¹ Recent analysis based on $1/N_c$ expansion have shown that the four-quark states should be narrow^{60–62} which do not then favour the four-quark interpretation of the light scalar meson $f_0(500)$. In fact, the latter can eventually have a large gluon component in its wave function.^{63–68}
- In previous papers,^{69–73} we have studied like various authors,^{69–86} to lowest order (LO) of perturbation theory (PT) and including non-perturbative condensates of dimension $d \leq 6–8$, the masses of the $J^P = 1^\pm$, and 0^\pm molecules and four-quark states using Exponential/Borel/inverse Laplace (hereafter denoted as LSR^e) or by combining it with Finite Energy (FESR)^{91,92} QCD spectral sum rules (QSSR)^{93,94}^f and the double ratio of sum rules (DRSR)¹⁰²^g. These LO results for the masses and couplings agree in many cases with the observed XZ charmonium and bottomium states and have encouraged some authors to estimate within QSSR (but still to LO) the hadronic widths^{114–118} and mixing^{114,119} (for reviews, see e.g.^{32–34}).
- Unfortunately, these previous results obviously suffer from the ill-defined heavy quark mass definition used at LO. The favoured numerical input values: $m_c \approx (1.23 – 1.26)$ GeV and $m_b \approx 4.17$ GeV used in the current literature correspond numerically to the one of the running masses though there is no reason to discard the values: $m_c \approx 1.5$ GeV and $m_b \approx 4.7$ GeV of the on-shell quark masses which are more natural because the spectral functions have been evaluated using the on-shell heavy quark propagator.
- Some of the previous LO results have been improved in conference communications^{120,121} where we have included next-to-leading (NLO) and next-to-next leading (N2LO) order α_s^2 PT QCD corrections in the analysis. Pursuing the analysis, we have recently improved, in,¹²² the existing LO analysis^{123–127} interpreting, as a molecule or four-quark state, the recent experimental candidate $X(5568)$ seen by D0¹²⁸ through the sequential decay to $B_s^0\pi^\pm$: $B_s^0 \rightarrow J/\psi\phi$, $J/\psi \rightarrow \mu^+\mu^-$, $\phi \rightarrow K^+K^-$, where a $J^P = 0^+$ is favoured, but this observation was not confirmed by LHCb.¹²⁹ A conclusion which is consistent with our findings.
- In this paper, we pursue and complete the previous program by reconsidering the existing estimate of the masses of the XYZ-like states obtained at LO from QSSR, namely the spin one and spin zero $\bar{D}D$, $\bar{B}B$ -like molecules (see Table 1) and four-quark $[Qq\bar{Q}\bar{q}]$ (see Table 4) states. In so doing, we include the NLO and N2LO

^eThe inverse Laplace transform properties of the Exponential sum rule have been noticed in⁸⁷ sum rules when NLO PT corrections are included. A comprehensive interpretation of the LSR using the harmonic oscillator can be found in.^{88,89}

^fFor reviews where complete references can be found, see e.g.^{95–101}

^gFor some other successful applications, see.^{103–113}

4 *R. Albuquerque et al.*

PT contributions to the QCD two-point correlator by assuming the factorization of the four-quark correlator into a convolution of two quark correlators built from bilinear quark currents. We add to it the contribution of the order α_s^3 N3LO contribution estimated from a geometric growth of the PT series.¹³⁰ To these new higher order (HO) PT contributions, we add the contributions of condensates having a dimension ($d \leq 6$) already available in the literature but rederived in this paper. Due to the uncertainties on the size (violation of the factorization assumption^{131–135} and mixing of operators¹³⁶) and contributions (only one class of contributions are only computed in the literature) of higher dimension ($d \geq 8$), we do not include them into the analysis but only consider their effects as a source of errors in the truncation of the Operator Product Expansion (OPE).

- Our results are summarized in Tables 11 to 14 and in the section : Summary and Conclusions.
- A confrontation with different experimental candidate is given in Section 11.

2. QCD expressions of the Spectral Functions

- Compared to previous LO QCD expressions of the spectral functions given in the literature, we provide integrated compact expressions which are more easier to handle for the numerical analysis. These expressions are tabulated in the Appendix.
- The PT expression of the spectral function obtained using on-shell renormalization has been transformed into the \overline{MS} -scheme by using the relation between the \overline{MS} running mass $\overline{m}_Q(\mu)$ and the on-shell mass M_Q , to order α_s^2 :^{137–146}

$$\begin{aligned} M_Q = \overline{m}_Q(\mu) & \left[1 + \frac{4}{3}a_s + (16.2163 - 1.0414n_l)a_s^2 \right. \\ & + \text{Log}\left(\frac{\mu}{M_Q}\right)^2 (a_s + (8.8472 - 0.3611n_l)a_s^2) \\ & \left. + \text{Log}^2\left(\frac{\mu}{M_Q}\right)^2 (1.7917 - 0.0833n_l)a_s^2 \dots \right], \end{aligned} \quad (1)$$

for n_l light flavours and where μ is the arbitrary subtraction point and $a_s \equiv \alpha_s/\pi$.

- Higher order PT corrections are obtained using the factorization assumption of the four-quark correlators into a convolution of bilinear current correlators as we shall discuss later on.

3. QSSR analysis of the Heavy-Light Molecules

3.1. Molecule currents and the QCD two-point function

- For describing these molecule states, we shall consider the usual lowest dimension local interpolating currents used in existing literature where each bilinear current has the quantum number of the corresponding open $D(0^-)$, $D_0^*(0^+)$ and $D^*(1^-)$, $D_1(1^+)$ states and the corresponding states in the b -quark channel^h. The

^hFor convenience, we shall not consider colored and more general combinations of interpolating

previous assignment is consistent with the definition of a molecule to be a weakly bound state of two mesons within a Van der Waals force other than a gluon exchange, which can justify the approximate use (up to order $1/N_c$) of the factorization of the four-quark currents as a convolution of two bilinear quark-antiquark currents when estimating the HO PT corrections. These states and the corresponding interpolating currents are given in Table 1.

Table 1. Interpolating currents with a definite C -parity describing the molecule-like states. $Q \equiv c$ (resp. b) for the $\bar{D}D$ (resp. $\bar{B}B$)-like molecules. $q \equiv u, d$.

States	J^{PC}	Molecule Currents $\equiv \mathcal{O}_{mol}(x)$
	0⁺⁺	
$\bar{D}D, \bar{B}B$		$(\bar{q}\gamma_5 Q)(\bar{Q}\gamma_5 q)$
$\bar{D}^*D^*, \bar{B}^*B^*$		$(\bar{q}\gamma_\mu Q)(\bar{Q}\gamma^\mu q)$
$\bar{D}_0^*D_0^*, \bar{B}_0^*B_0^*$		$(\bar{q}Q)(\bar{Q}q)$
	1⁺⁺	
\bar{D}^*D, \bar{B}^*B		$\frac{i}{\sqrt{2}} \left[(\bar{Q}\gamma_\mu q)(\bar{q}\gamma_5 Q) - (\bar{q}\gamma_\mu Q)(\bar{Q}\gamma_5 q) \right]$
$\bar{D}_0^*D_1, \bar{B}_0^*B_1$		$\frac{1}{\sqrt{2}} \left[(\bar{q}Q)(\bar{Q}\gamma_\mu\gamma_5 q) + (\bar{Q}q)(\bar{q}\gamma_\mu\gamma_5 Q) \right]$
	0^{-±}	
$\bar{D}_0^*D, \bar{B}_0^*B$		$\frac{1}{\sqrt{2}} \left[(\bar{q}Q)(\bar{Q}\gamma_5 q) \pm (\bar{Q}q)(\bar{q}\gamma_5 Q) \right]$
$\bar{D}^*D_1, \bar{B}^*B_1$		$\frac{1}{\sqrt{2}} \left[(\bar{Q}\gamma_\mu q)(\bar{q}\gamma^\mu\gamma_5 Q) \mp (\bar{Q}\gamma_\mu\gamma_5 q)(\bar{q}\gamma^\mu Q) \right]$
	1^{-±}	
$\bar{D}_0^*D^*, \bar{B}_0^*B^*$		$\frac{1}{\sqrt{2}} \left[(\bar{q}Q)(\bar{Q}\gamma_\mu q) \mp (\bar{Q}q)(\bar{q}\gamma_\mu Q) \right]$
$\bar{D}D_1, \bar{B}B_1$		$\frac{i}{\sqrt{2}} \left[(\bar{Q}\gamma_\mu\gamma_5 q)(\bar{q}\gamma_5 Q) \pm (\bar{q}\gamma_\mu\gamma_5 Q)(\bar{Q}\gamma_5 q) \right]$

- The two-point correlators associated to the (axial)-vector interpolating operators are:

$$\begin{aligned} \Pi_{mol}^{\mu\nu}(q) &\equiv i \int d^4x e^{iq.x} \langle 0 | T[\mathcal{O}_{mol}^\mu(x) \mathcal{O}_{mol}^{\nu\dagger}(0)] | 0 \rangle \\ &= -\Pi_{mol}^{(1)}(q^2)(g^{\mu\nu} - \frac{q^\mu q^\nu}{q^2}) + \Pi_{mol}^{(0)}(q^2) \frac{q^\mu q^\nu}{q^2}, \end{aligned} \quad (2)$$

The two invariants, $\Pi_{mol}^{(1)}$ and $\Pi_{mol}^{(0)}$, appearing in Eq. (2) are independent and have respectively the quantum numbers of the spin 1 and 0 mesons.

operators discussed e.g in^{84,117} as well as higher dimension ones involving derivatives.

- $\Pi_{mol}^{(0)}$ is related via Ward identities^{95,96} to the (pseudo)scalar two-point functions $\psi_{mol}^{(s,p)}(q^2)$ built directly from the (pseudo)scalar currents given in Table 1:

$$\psi_{mol}^{(s,p)}(q^2) = i \int d^4x e^{iq.x} \langle 0 | T[\mathcal{O}_{mol}^{(s,p)}(x) \mathcal{O}_{mol}^{(s,p)}(0)] | 0 \rangle , \quad (3)$$

with which, we shall work in the following.

- Thanks to their analyticity, the invariant functions $\Pi_{mol}^{(1,0)}(q^2)$ in Eq. (2) and the two-point correlator $\psi_{mol}^{(s,p)}(q^2)$ in Eq. 3 obey the dispersion relation:

$$\Pi_{mol}^{(1,0)}(q^2); \psi_{mol}^{(s,p)}(q^2) = \frac{1}{\pi} \int_{4m_c^2}^{\infty} dt \frac{\text{Im } \Pi_{mol}^{(1,0)}(t); \text{Im } \psi_{mol}^{(s,p)}(t)}{t - q^2 - i\epsilon} + \dots , \quad (4)$$

where $\text{Im } \Pi_{mol}^{(1,0)}(t); \text{Im } \psi_{mol}^{(s,p)}(t)$ are the spectral functions and \dots indicate subtraction points which are polynomial in q^2 .

3.2. LO PT and NP corrections to the molecule two-point function

The different LO expressions including non-perturbative (NP) corrections up to dimension $d=6-8$ used in the analysis are tabulated in Appendix A.

- Compared to the ones in the literature, the expressions of the spectral functions are in integrated and compact forms which are more easier to handle for the numerical phenomenological analysis. However, one should note that most of the expressions given in the literature do not agree each others. Due to the few informations given by the authors on their derivation, it is difficult to trace back the origin of such discrepancies. Hopefully, within the accuracy of the approach, such discrepancies affect only slightly the final results if the errors are taken properly.

- In the chiral limit $m_q = 0$ and $\langle \bar{u}u \rangle = \langle \bar{d}d \rangle$, we have checked that the orthogonal combinations of $\bar{D}^* D, \bar{B}^* B(1^{++}), \bar{D}_0^* D_1, \bar{B}_0^* B_1(0^{--})$ and $\bar{D}^* D_1, \bar{B}^* B_1(0^{--})$ molecules give the same results up to the $d = 6$ contributions. This is due to the presence of one γ_5 matrix in the current which neutralizes the different traces appearing in each pair. This is not the case of the $\bar{D}_0^* D^*, \bar{B}_0^* B^*$ (without γ_5) and $\bar{D} D_1, \bar{B} B_1$ (with two γ_5).

3.3. $1/q^2$ tachyonic gluon mass and large order PT corrections

The $1/q^2$ corrections due to a tachyonic gluon mass corrections discussed in^{147,148} (for reviews see:^{149,150}) will not be included here. Instead, we shall consider the fact that they are dual to the sum of the large order PT series¹³⁰ such that, with the inclusion of the N3LO term estimated from the geometric growth of the QCD PT series¹³⁰ as a source of the PT errors, we expect to give a good approximation of these uncalculated higher order terms. The estimate of these errors is given in Tables 7 to 10.

3.4. NLO and N2LO PT corrections using factorization

Assuming a factorization of the four-quark interpolating current as a natural consequence of the molecule definition of the state, we can write the corresponding spectral function as a convolution of the spectral functions associated to quark bilinear currentⁱ as illustrated by the Feynman diagrams in Fig. 1. In this way, we obtain^{151,j} for the $\bar{D}D^*$ and $\bar{D}_0^*D^*$ spin 1 states:

$$\frac{1}{\pi} \text{Im}\Pi_{mol}^{(1)}(t) = \theta(t - 4M_Q^2) \left(\frac{1}{4\pi}\right)^2 t^2 \int_{M_Q^2}^{(\sqrt{t}-M_Q)^2} dt_1 \int_{M_Q^2}^{(\sqrt{t}-\sqrt{t_1})^2} dt_2 \\ \times \lambda^{3/2} \frac{1}{\pi} \text{Im}\Pi^{(1)}(t_1) \frac{1}{\pi} \text{Im}\psi^{(s,p)}(t_2). \quad (5)$$

For the $\bar{D}D$ spin 0 state, one has:

$$\frac{1}{\pi} \text{Im}\psi_{mol}^{(s)}(t) = \theta(t - 4M_Q^2) \left(\frac{1}{4\pi}\right)^2 t^2 \int_{m_Q^2}^{(\sqrt{t}-M_Q)^2} dt_1 \int_{m_Q^2}^{(\sqrt{t}-\sqrt{t_1})^2} dt_2 \\ \times \lambda^{1/2} \left(\frac{t_1}{t} + \frac{t_2}{t} - 1\right)^2 \\ \times \frac{1}{\pi} \text{Im}\psi^{(p)}(t_1) \frac{1}{\pi} \text{Im}\psi^{(p)}(t_2), \quad (6)$$

and for the \bar{D}^*D^* spin 0 state:

$$\frac{1}{\pi} \text{Im}\psi_{mol}(t) = \theta(t - 4M_Q^2) \left(\frac{1}{4\pi}\right)^2 t^2 \int_{m_Q^2}^{(\sqrt{t}-M_Q)^2} dt_1 \int_{m_Q^2}^{(\sqrt{t}-\sqrt{t_1})^2} dt_2 \\ \times \lambda^{1/2} \left[\left(\frac{t_1}{t} + \frac{t_2}{t} - 1\right)^2 + \frac{8t_1 t_2}{t^2}\right] \\ \times \frac{1}{\pi} \text{Im}\Pi^{(1)}(t_1) \frac{1}{\pi} \text{Im}\Pi^{(1)}(t_2), \quad (7)$$

where:

$$\lambda = \left(1 - \frac{(\sqrt{t_1} - \sqrt{t_2})^2}{t}\right) \left(1 - \frac{(\sqrt{t_1} + \sqrt{t_2})^2}{t}\right), \quad (8)$$

is the phase space factor and M_Q is the on-shell heavy quark mass. $\text{Im}\Pi^{(1)}(t)$ is the spectral function associated to the bilinear $\bar{c}\gamma_\mu(\gamma_\mu\gamma_5)q$ vector or axial-vector current, while $\text{Im}\psi^{(5)}(t)$ is associated to the $\bar{c}(\gamma_5)q$ scalar or pseudoscalar current^k. This representation simplifies the evaluation of the PT α_s^n -corrections as we can use the PT expression of the spectral functions for heavy-light bilinear currents known to order α_s (NLO) from¹⁵⁵ and to order α_s^2 (N2LO) from^{156,157} which are available

ⁱIt is called properly sesquilinear instead of bilinear current as it is formed by a quark field and its anti-particle. We thank Professor Raoelina Andriambololona for this remark.

^jFor some applications to the $\bar{B}B$ mixing, see e.g.^{152–154}

^kIn the limit where the light quark mass $m_q = 0$, the PT expressions of the vector (resp. scalar) and axial-vector (resp. pseudoscalar) spectral functions are the same.

as a Mathematica Program Rvs. From this above representation, the anomalous dimension of the correlator comes from the (pseudo)scalar current and the corresponding renormalization group invariant interpolating current reads to NLO¹:

$$\bar{\mathcal{O}}_{mol}^{(s,p)}(\mu) = a_s(\mu)^{4/\beta_1} \mathcal{O}_{mol}^{(s,p)}, \quad \bar{\mathcal{O}}_{mol}^{(1)}(\mu) = a_s(\mu)^{2/\beta_1} \mathcal{O}_{mol}^{(1)}. \quad (9)$$

Within the above procedure, we have checked that we reproduce the factorized PT LO contributions obtained using for example the PT expressions of $\bar{D}_0^* D_0^*$ and $\bar{D}_0^* D^*$ given in Appendix A.

3.5. The inverse Laplace transform sum rule (LSR)

The exponential sum rules firstly derived by SVZ^{93,94} have been called Borel sum rules due to the factorial suppression factor of the condensate contributions in the OPE. Their quantum mechanics version have been studied by Bell-Bertlmann in^{88–90} through the harmonic oscillator where τ has the property of an imaginary time, while the derivation of their radiative corrections has been firstly shown by Narison-de Rafael⁸⁷ to have the properties of the inverse Laplace sum rule (LSR). The LSR and its ratio read:

$$\mathcal{L}_{mol}(\tau, t_c, \mu) = \int_{4M_Q^2}^{t_c} dt e^{-t\tau} \frac{1}{\pi} \text{Im}\Pi_{mol}^{(1,0)}(t, \mu), \quad (10)$$

$$\mathcal{R}_{mol}(\tau, t_c, \mu) = \frac{\int_{4M_Q^2}^{t_c} dt t e^{-t\tau} \frac{1}{\pi} \text{Im}\Pi_{mol}^{(1,0)}(t, \mu)}{\int_{4M_Q^2}^{t_c} dt e^{-t\tau} \frac{1}{\pi} \text{Im}\Pi_{mol}^{(1,0)}(t, \mu)} \simeq M_R^2, \quad (11)$$

where μ is the subtraction point which appears in the approximate QCD series when radiative corrections are included and τ is the sum rule variable replacing q^2 . Similar sum rules are obtained for the (pseudo)scalar two-point function $\psi^{(s,p)}(q^2)$. The variables τ, μ and t_c are, in principle, free parameters. We shall use stability criteria (if any), with respect to these free 3 parameters, for extracting the optimal results.

3.6. Parametrization of the Spectral Function within MDA

- We shall use the Minimal Duality Ansatz (MDA) given in Eq. 12 for parametrizing the spectral function (generic notation):

$$\frac{1}{\pi} \text{Im}\Pi_{mol}(t) \simeq f_{mol}^2 M_{mol}^8 \delta(t - M_{mol}^2) + \text{“QCD continuum”} \theta(t - t_c), \quad (12)$$

where f_{mol} is the decay constant defined as:

$$\langle 0 | \mathcal{O}_{mol}^{(s,p)} | mol \rangle = f_{mol}^{(s,p)} M_{mol}^4, \quad \langle 0 | \mathcal{O}_{mol}^\mu | mol \rangle = f_{mol}^{(1)} M_{mol}^5 \epsilon_\mu, \quad (13)$$

¹The spin 0 current built from two (axial)-vector currents has no anomalous dimension.

respectively for spin 0 and 1 molecule states with ϵ_μ the vector polarization. The higher states contributions are smeared by the “QCD continuum” coming from the discontinuity of the QCD diagrams and starting from a constant threshold t_c .

- Within MDA, the ratio of sum rules $\mathcal{R}(\tau, \mu)$ is useful, as it is equal to the resonance mass squared M_{mol}^2 at the τ -stability region.
- Noting that in the previous definition in Table 1, the bilinear (pseudo)scalar current acquires an anomalous dimension due to its normalization, thus the decay constants run to order α_s^2 as^m:

$$f_{mol}^{(s,p)}(\mu) = \hat{f}_{mol}^{(s,p)} (-\beta_1 a_s)^{4/\beta_1} / r_m^2, \quad f_{mol}^{(1)}(\mu) = \hat{f}_{mol}^{(1)} (-\beta_1 a_s)^{2/\beta_1} / r_m, \quad (14)$$

where we have introduced the renormalization group invariant coupling \hat{f}_{mol} ; $-\beta_1 = (1/2)(11 - 2n_f/3)$ is the first coefficient of the QCD β -function for n_f flavours and $a_s \equiv (\alpha_s/\pi)$. The QCD corrections numerically read;

$$r_m(n_f = 4) = 1 + 1.014a_s + 1.389a_s^2, \quad r_m(n_f = 5) = 1 + 1.176a_s + 1.501a_s^2. \quad (15)$$

3.7. Tests of MDA and Stability Criteria

- In the standard Minimal Duality Ansatz (MDA) given in Eq. 12 for parametrizing the spectral function, the “QCD continuum” threshold t_c is constant and is independent on the subtraction point μ ⁿ. One should notice that this standard MDA with constant t_c describes quite well the properties of the lowest ground state as explicitly demonstrated in^{159,160} and in various examples,^{95,96} while it has been also successfully tested in the large N_c limit of QCD in.^{161,162}
- Ref.^{159,160} has explicitly tested this simple model by confronting the predictions of the integrated spectral function within this simple parametrization with the full data measurements. One can notice in Figs. 1 and 2 of Ref.^{159,160} the remarkable agreement of the model predictions and of the measured data of the J/ψ charmonium and Υ bottomonium systems for a large range of the inverse sum rule variable τ . Though it is difficult to estimate with a good precision the systematic error related to this simple model, this feature indicates the ability of the model for reproducing accurately the data. We expect that the same feature is reproduced for the case of the XYZ discussed here where complete data are still lacking.

- In order to extract an optimal information for the lowest resonance parameters from this rather crude description of the spectral function and from the approximate QCD expression, one often applies the stability criteria at which an optimal result can be extracted. This stability is signaled by the existence of a stability plateau, an extremum or an inflection point (so-called “sum rule window”) versus the changes of the external sum rule variables τ and t_c where the simultaneous requirement on the dominance over the continuum contribution and on the convergence of the OPE

^mThe coupling of the (pseudo)scalar molecule built from two (axial)-vector currents has no anomalous dimension and does not run.

ⁿSome model with a μ -dependence of t_c has been discussed e.g in.¹⁵⁸

is automatically satisfied. This optimization criterion demonstrated in series of papers by Bell-Bertlmann,^{88–90} in the case of the τ -variable, by taking the examples of harmonic oscillator and charmonium sum rules and extended to the case of the t_c -parameter in^{95,96} gives a more precise meaning of the so-called “sum rule window” originally discussed by SVZ^{93,94} and used in the sum rules literature. Similar applications of the optimization method to the pseudoscalar D and B open meson states have been successful when compared with results from some other determinations as discussed in Ref.^{159,160} and reviewed in^{95,96,163–165} and in some other recent reviews.^{166,167}

- In this paper, we shall add to the previous well-known τ - and t_c -stability criteria, the one associated to the requirement of stability versus the arbitrary subtraction constant μ often put by hand in the current literature and which is often the source of large errors from the PT series in the sum rule analysis. The μ -stability procedure has been applied recently in^{159,160,164,165,168–170} o which gives a much better meaning on the choice of μ -value at which the observable is extracted, while the errors in the determinations of the results have been reduced due to a better control of the μ region of variation which is not the case in the existing literature.

Table 2. QCD input parameters: the original errors for $\langle \alpha_s G^2 \rangle$, $\langle g^3 G^3 \rangle$ and $\rho \langle \bar{q}q \rangle^2$ have been multiplied by about a factor 3 for a conservative estimate of the errors (see also the text).

Parameters	Values	Ref.
$\alpha_s(M_\tau)$	0.325(8)	131, 176, 177
$\overline{m}_c(m_c)$	1261(12) MeV	average ^{7, 178–183}
$\overline{m}_b(m_b)$	4177(11) MeV	average ^{7, 178–181}
$\hat{\mu}_q$	(253 ± 6) MeV	95, 107, 109, 169, 184, 185
M_0^2	(0.8 ± 0.2) GeV ²	108, 133–135, 186–188
$\langle \alpha_s G^2 \rangle$	$(7 \pm 3) \times 10^{-2}$ GeV ⁴	88–90, 131, 132, 179–181, 189–194
$\langle g^3 G^3 \rangle$	(8.2 ± 2.0) GeV ² $\times \langle \alpha_s G^2 \rangle$	179–181
$\rho \alpha_s \langle \bar{q}q \rangle^2$	$(5.8 \pm 1.8) \times 10^{-4}$ GeV ⁶	131–135

3.8. QCD Input Parameters

- The QCD parameters which shall appear in the following analysis will be the charm and bottom quark masses $m_{c,b}$ (we shall neglect the light quark masses $q \equiv u, d$), the light quark condensate $\langle \bar{q}q \rangle$, the gluon condensates $\langle \alpha_s G^2 \rangle \equiv \langle \alpha_s G_{\mu\mu}^a G_{a\mu\mu}^a \rangle$ and $\langle g^3 G^3 \rangle \equiv \langle g^3 f_{abc} G_{\mu\mu}^a G_{\mu\rho}^b G_{\rho\mu}^c \rangle$, the mixed condensate $\langle \bar{q}Gq \rangle \equiv \langle \bar{q}g\sigma^{\mu\mu}(\lambda_a/2)G_{\mu\mu}^a q \rangle = M_0^2 \langle \bar{q}q \rangle$ and the four-quark condensate $\rho \alpha_s \langle \bar{q}q \rangle^2$, where $\rho \simeq 3 - 4$ indicates the deviation from the four-quark vacuum saturation. Their values are given in Table 2.

^oSome other alternative approaches for optimizing the PT series can be found in.^{171–175}

- We shall work with the running light quark condensates and masses, which read to leading order in α_s :

$$\langle \bar{q}q \rangle(\tau) = -\hat{\mu}_q^3 (-\beta_1 a_s)^{2/\beta_1}, \quad \langle \bar{q}Gq \rangle(\tau) = -M_0^2 \hat{\mu}_q^3 (-\beta_1 a_s)^{1/3\beta_1}, \quad (16)$$

where $\beta_1 = -(1/2)(11 - 2n_f/3)$ is the first coefficient of the β function for n_f flavours; $a_s \equiv \alpha_s(\tau)/\pi$; $\hat{\mu}_q$ is the spontaneous RGI light quark condensate.¹⁹⁷ We shall use:

$$\alpha_s(M_\tau) = 0.325(8) \implies \alpha_s(M_Z) = 0.1192(10) \quad (17)$$

from τ -decays^{131, 176, 177}^p which agree with the 2016 world average:¹⁹⁶

$$\alpha_s(M_Z) = 0.1181(11). \quad (18)$$

The value of the running $\langle \bar{q}q \rangle$ condensate is deduced from the well-known GMOR relation:

$$(m_u + m_d)\langle \bar{u}u + \bar{d}d \rangle = -m_\pi^2 f_\pi^2, \quad (19)$$

where $f_\pi = 130.4(2)$ MeV¹⁶⁶ and the value of $(\bar{m}_u + \bar{m}_d)(2) = (7.9 \pm 0.6)$ MeV obtained in^{107, 109} agrees with the PDG in⁷ and lattice averages in.¹⁶⁷ Then, we deduce the RGI light quark spontaneous mass $\hat{\mu}_q$ given in Table 2.

- For the heavy quarks, we shall use the running mass and the corresponding value of α_s evaluated at the scale μ . These sets of correlated parameters are given in Table 3 for different values of μ and for a given number of flavours n_f .
- For the $\langle \alpha_s G^2 \rangle$ condensate, we have enlarged the original error by a factor about 3 in order to have a conservative result in order to recover the original SVZ estimate and the alternative extraction in^{182, 183} from charmonium sum rules. However, a direct comparison of this range of values obtained within short QCD series (few terms) with the one from lattice calculations¹⁹⁸ obtained within a long QCD series remains to be clarified.¹⁹⁹
- Some other estimates of the gluon and four-quark condensates using τ -decay and $e^+e^- \rightarrow I = 1$ hadrons data can be found in.^{91, 92, 200, 201} Due to the large uncertainties induced by the different resummations of the QCD series and by the less-controlled effects of some eventual duality violation, we do not consider explicitly these values in the following analysis. However, we shall see later on that the effects of the gluon and four-quark condensates on the values of the decay constants and masses are almost negligible though they play an important rôle in the stability analysis.

4. Accuracy of the Factorization Assumption

4.1. PT Lowest order tests

To lowest order of PT QCD, the four-quark correlator can be subdivided into its factorized (Fig. 1a) and its non-factorized (Fig. 1b) parts. In the following, we shall

^pA recent update is done in¹⁹⁵ where the same central value is obtained and more complete references are given.

Table 3. $\alpha_s(\mu)$ and correlated values of $\overline{m}_Q(\mu)$ used in the analysis for different values of the subtraction scale μ . The error in $\overline{m}_Q(\mu)$ has been induced by the one of $\alpha_s(\mu)$ to which one has added the error on their determination given in Table 2.

Input for $\bar{D}D, \dots, [cq\bar{c}\bar{q}]$, : $n_f = 4$		
$\mu[\text{GeV}]$	$\alpha_s(\mu)$	$\overline{m}_c(\mu)[\text{GeV}]$
Input: $\overline{m}_c(m_c)$	0.4084(144)	1.26
1.5	0.3649(110)	1.176(5)
2	0.3120(77)	1.069(9)
2.5	0.2812(61)	1.005(10)
3.0	0.2606(51)	0.961(10)
3.5	0.2455(45)	0.929(11)
4.0	0.2339(41)	0.903(11)
4.5	0.2246(37)	0.882(11)
5.0	0.2169(35)	0.865(11)
5.5	0.2104(33)	0.851(12)
6.0	0.2049(30)	0.838(12)
Input for $\bar{B}B, \dots, [bq\bar{b}\bar{q}]$: $n_f = 5$		
$\mu[\text{GeV}]$	$\alpha_s(\mu)$	$\overline{m}_b(\mu)[\text{GeV}]$
3	0.2590(26)	4.474(4)
3.5	0.2460(20)	4.328(2)
Input: $\overline{m}_b(m_b)$	0.2320(20)	4.177
4.5	0.2267(20)	4.119(1)
5.0	0.2197(18)	4.040(1)
5.5	0.2137(17)	3.973(2)
6.0	0.2085(16)	3.914(2)
6.5	0.2040(15)	3.862(2)
7.0	0.2000(15)	3.816(3)

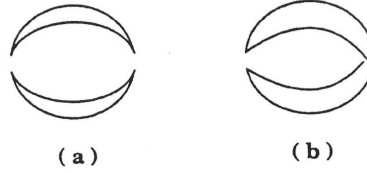


Fig. 1. (a) Factorized contribution to the four-quark correlator at lowest order of PT; (b) Non-factorized contribution at lowest order of PT (the figure comes from ¹⁵¹).

further test the factorization assumption if one does it at lowest order (LO) of PT by taking the example of the $\bar{M}_0^* M^*(1^-)$ molecule states where $M \equiv D$ (resp. B) meson in the charm (resp. bottom) quark channels. The factorized expression corresponds to the value $\epsilon = 0$ and the full one to $\epsilon = 1$ in the QCD expressions of the spectral functions given in Appendix A.

- *Decay Constants and Masses of the $\bar{M}_0^* M^*(1^-)$ Molecules*

We study in Fig. 2 the effect of factorization for a given value of $t_c = 42 \text{ GeV}^2$ and $\mu = 4.5 \text{ GeV}$ at lowest order of PT for the $\bar{D}_0^* D^*(1^-)$ molecule. An analogous analysis is done for the $\bar{B}_0^* B^*$ molecule which presents the same qualitative behaviour as the one in Fig. 2.

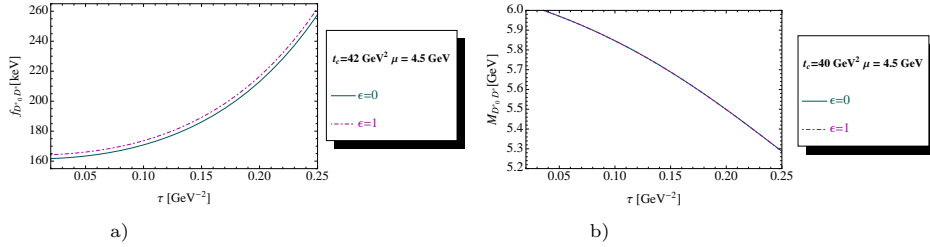


Fig. 2. **a)** Factorized ($\epsilon = 0$) and full ($\epsilon = 1$) lowest order PT contributions to $f_{D_0^* D^*}$ as function of τ for a given value of $t_c = 42 \text{ GeV}^2$, $\mu = 4.5 \text{ GeV}$, $\bar{m}_c(\bar{m}_c) = 1.26 \text{ GeV}$ and using the QCD parameters in Tables 2 and 3; **b)** The same as a) but for the mass $M_{D_0^* D^*}$.

- *Conclusions from the PT lowest order analysis*

We conclude from the previous two examples that assuming a factorization of the PT contributions at LO induces an almost negligible effect on the decay constant ($\simeq 1.5\%$) and mass ($\simeq 7 \times 10^{-4}$) determinations for the $\bar{D}_0^* D^*$ and $\bar{B}_0^* B^*$ vector molecules.

4.2. Factorization tests for PT \oplus NP contributions at LO

One can notice from the QCD expression including NP contributions that the factorization assumption modifies the structure of the OPE due to the vanishing of some contributions at LO.

- *Decay Constants and Masses of the $\bar{M}_0^* M^*(1^{--})$ Molecules*

We study in Fig. 3 the effect of factorization for PT \oplus NP at LO for a given value of $t_c = 42 \text{ GeV}^2$ and $\mu = 4.5 \text{ GeV}$ at lowest order of PT for the $\bar{D}_0^* D^*(1^-)$ molecule. An analogous analysis is done for the $\bar{B}_0^* B^*$ molecule which presents the same qualitative behaviour as the one in Fig. 3.

- *Conclusions for the PT \oplus NP analysis*

One can notice from Fig. 3 that the effect of factorization of the PT \oplus NP at LO is about 2.2% for the decay constant and 0.5% for the mass which is quite tiny. However, to avoid this small effect, we shall work in the following with the full non-factorized PT \oplus NP at LO expressions.

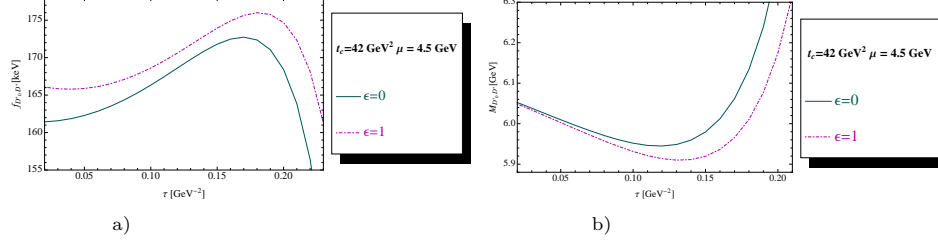


Fig. 3. a) Factorized ($\epsilon = 0$) and full ($\epsilon = 1$) lowest order PT contributions to $f_{D_0^* D^*}$ as function of τ for a given value of $t_c = 42 \text{ GeV}^2$, $\mu = 4.5 \text{ GeV}$, $\bar{m}_c(\bar{m}_c) = 1.26 \text{ GeV}$ and using the QCD parameters in Tables 2 and 3; b) The same as a) but for the mass $M_{D_0^* D^*}$.

4.3. Test at NLO of PT

- Example of the $B^0 \bar{B}^0$ four-quark correlator

For extracting the PT α_s^n corrections to the correlator and due to the technical complexity of the calculations, we shall assume that these radiative corrections are dominated by the ones from the factorized diagrams (Fig. 4a,b) while the ones from non-factorized (Fig. 4c to f) are negligible. This fact has been proven explicitly by ^{153,154} in the case of the $\bar{B}^0 B^0$ systems (very similar correlator as the ones discussed in the following) where the non-factorized α_s corrections do not exceed 10% of the total α_s corrections.

- Conclusions of the PT NLO analysis

We expect from the previous LO examples that the masses of the molecules are known with a good accuracy while, for the coupling, we shall have in mind the systematics induced by the radiative corrections estimated by keeping only the factorized diagrams. The contributions of the factorized diagrams will be extracted from the convolution integrals given in Eq. 5. Here, the suppression of the NLO corrections will be more pronounced for the extraction of the meson masses from the ratio of sum rules compared to the case of the $\bar{B}^0 B^0$ systems.

5. The (0^{++}) Heavy-Light Scalar Molecule States

We shall study the $\bar{D}D$, \bar{D}^*D^* and $\bar{D}_0^*D_0^*$ and their beauty analogue using the same approaches and strategies. The qualitative behaviours of the curves in these different channels are very similar such that we shall only illustrate explicitly the analysis for the $\bar{D}D$ and $\bar{B}B$ molecules and will only quote the results for the others.

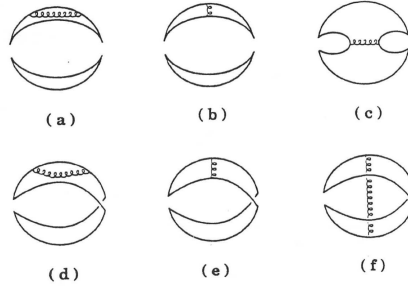


Fig. 4. **(a,b)** Factorized contributions to the four-quark correlator at NLO of PT; **(c to f)** Non-factorized contributions at NLO of PT (the figure comes from¹⁵¹).

5.1. Decay constant and mass of the $\bar{D}D$ molecule

- τ and t_c stabilities

We study the behavior of the coupling^q f_{DD} and mass M_{DD} in terms of LSR variable τ at different values of t_c as shown in Fig.5 at LO, in Fig. 6 at NLO and in Fig. 7 at N2LO. We consider as final and conservative result the one corresponding

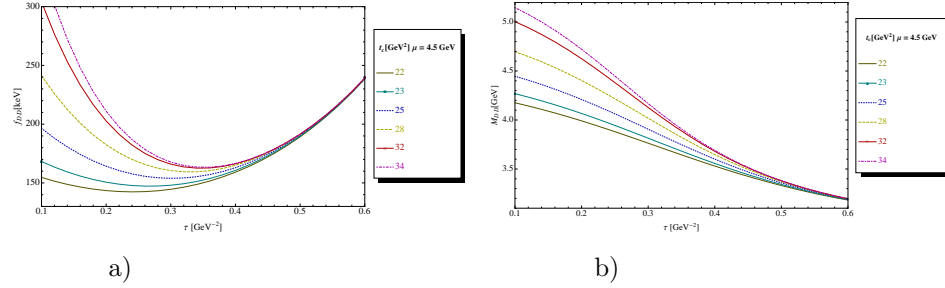


Fig. 5. **a)** f_{DD} at LO as function of τ for different values of t_c , for $\mu = 4.5$ GeV and for the QCD parameters in Tables 2 and 3; **b)** The same as a) but for the mass M_{DD} .

to the beginning of the τ -stability ($\tau \simeq 0.25$ GeV $^{-2}$) for $t_c=22$ GeV 2 until the one where t_c -stability starts to be reached for $t_c \simeq 32$ GeV 2 and for $\tau \simeq 0.35$ GeV $^{-2}$. In these stability regions, the requirement that the pole contribution is larger than the one of the continuum is automatically satisfied (see e.g.³⁴).

- *Running versus the pole quark mass definitions*

We show in Fig. 8 the effect of the definitions (running or pole) of the heavy quark mass used in the analysis at LO which is relatively important. The difference should

^qHere and in the following : decay constant is the same as : coupling.

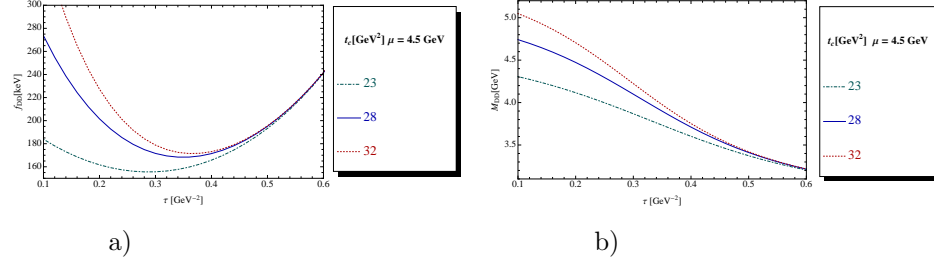


Fig. 6. **a)** f_{DD} at NLO as function of τ for different values of t_c , for $\mu = 4.5$ GeV and for the QCD parameters in Tables 2 and 3; **b)** The same as a) but for the mass M_{DD} .

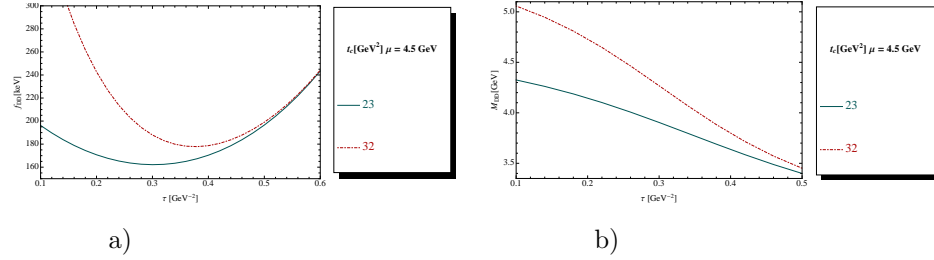


Fig. 7. **a)** f_{DD} at N2LO as function of τ for different values of t_c , for $\mu = 4.5$ GeV and for the QCD parameters in Tables 2 and 3; **b)** The same as a) but for the mass M_{DD} .

be added as errors in the LO analysis. This source of errors is never considered in the current literature.

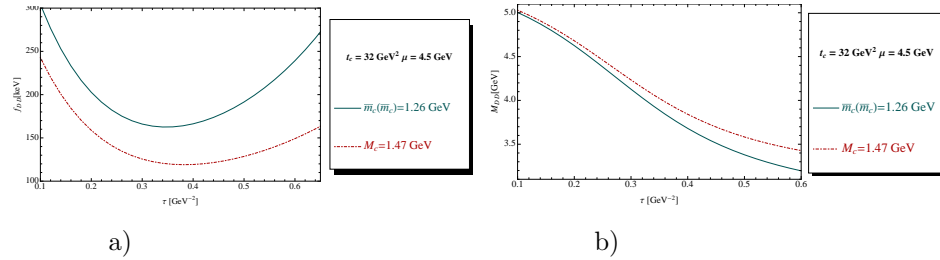


Fig. 8. **a)** f_{DD} at LO as function of τ for $t_c = 32$ GeV 2 , for $\mu = 4.5$ GeV, for values of the running $\bar{m}_c(\bar{m}_c) = 1.26$ GeV and pole mass $M_c = 1.47$ GeV. We use the QCD parameters in Tables 2 and 3; **b)** The same as a) but for the mass M_{DD} .

• Convergence of the PT series

Using $t_c = 32$ GeV 2 , we study in Fig. 9 the convergence of the PT series for a given value of $\mu = 4.5$ GeV. We observe (see Table 11) that from NLO to N2LO the mass decreases by about only 1 per mil indicating the good convergence of the PT series.

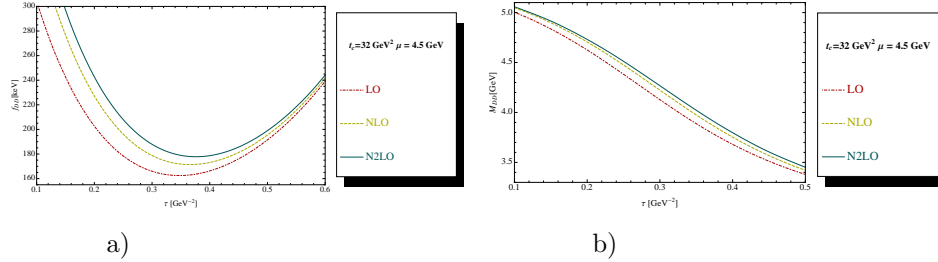


Fig. 9. a) f_{DD} as function of τ for a given value of $t_c = 32 \text{ GeV}^2$, for $\mu = 4.5 \text{ GeV}$, for different truncation of the PT series and for the QCD parameters in Tables 2 and 3; b) The same as a) but for the mass M_{DD} .

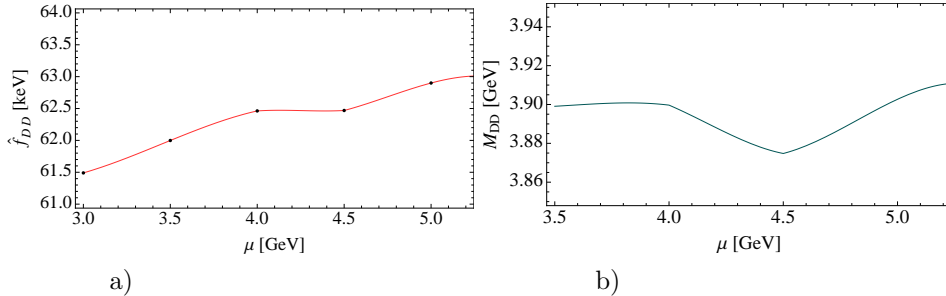


Fig. 10. a) Renormalization group invariant coupling \hat{f}_{DD} at NLO as function of μ , for the corresponding τ -stability region, for $t_c \simeq 18 \text{ GeV}^2$ and for the QCD parameters in Tables 2 and 3; b) The same as a) but for the mass M_{DD} .

• μ -stability

We improve our previous results by using different values of μ (Fig. 10). Using the fact that the final result must be independent of the arbitrary parameter μ (plateau / inflexion point for the coupling and minimum for the mass), we consider as an optimal result the one at $\mu \simeq 4.5 \text{ GeV}$ where we deduce the result given in Table 11.

5.2. Coupling and mass of the $\bar{B}B$ molecule

We extend the analysis to the b -quark sector which we show in Figs. 11 to 16. The optimal results of the analysis, given in Table 12, are obtained for the set:

$$\tau \simeq 0.08 \text{ GeV}^{-2}, \quad t_c \simeq (160 - 190) \text{ GeV}^2 \quad \text{and} \quad \mu \simeq 5.5 \text{ GeV}. \quad (20)$$

6. The $(1^{+\pm})$ Heavy-Light Axial-Vector Molecule States

We shall study here the masses and couplings of the $J^{PC} = 1^{+\pm}$ axial-vector molecule states : \bar{D}^*D , \bar{B}^*B and $\bar{D}_0^*D_1$, $\bar{B}_0^*B_1$. States with opposite C -parity are degenerated in this channel. The analysis will be illustrated by the study of \bar{D}^*D and \bar{B}^*B molecule states.

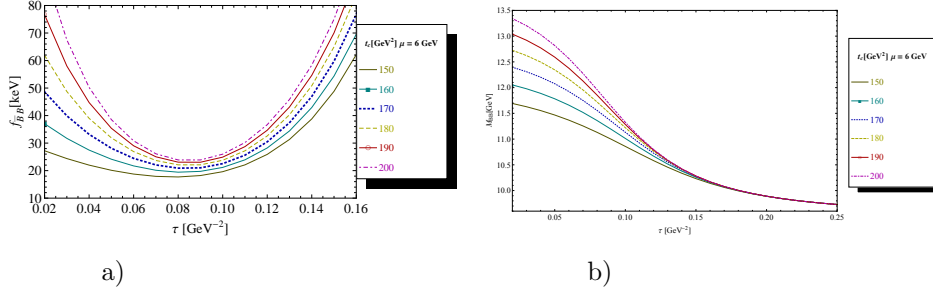


Fig. 11. **a)** f_{BB} at LO as function of τ for different values of t_c , for $\mu = 6$ GeV and for the QCD parameters in Tables 2 and 3; **b)** The same as a) but for the mass M_{BB} .

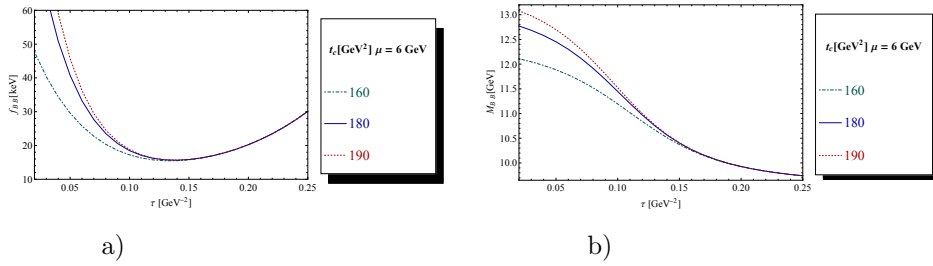


Fig. 12. **a)** f_{BB} at NLO as function of τ for different values of t_c , for $\mu = 6$ GeV and for the QCD parameters in Tables 2 and 3; **b)** The same as a) but for the mass M_{BB} .

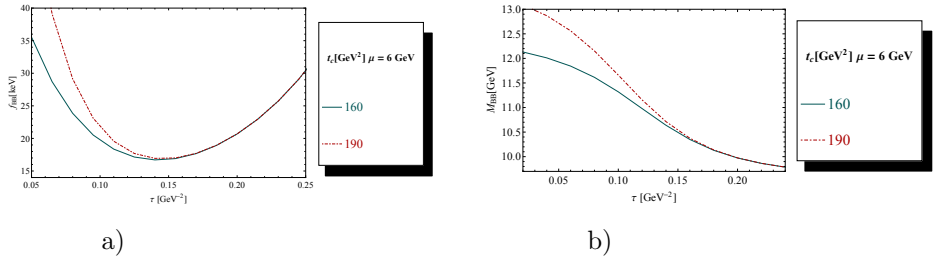


Fig. 13. **a)** f_{BB} at N2LO as function of τ for different values of t_c , for $\mu = 6$ GeV and for the QCD parameters in Tables 2 and 3; **b)** The same as a) but for the mass M_{BB} .

6.1. Coupling and mass of the \bar{D}^*D molecule

• τ and t_c stabilities

We study the behavior of the coupling f_{D^*D} and mass M_{D^*D} in terms of LSR variable τ at different values of t_c as shown in Fig.17 at LO and in Fig.18 at NLO. We consider as a final and conservative result the one corresponding to the beginning of the τ -stability for $t_c=21$ GeV 2 until the one where t_c -stability starts to be reached for $t_c \simeq 32$ GeV 2 . In these stability regions, the requirement that the pole contribution is larger than the one of the continuum (see e.g.³⁴) is automatically

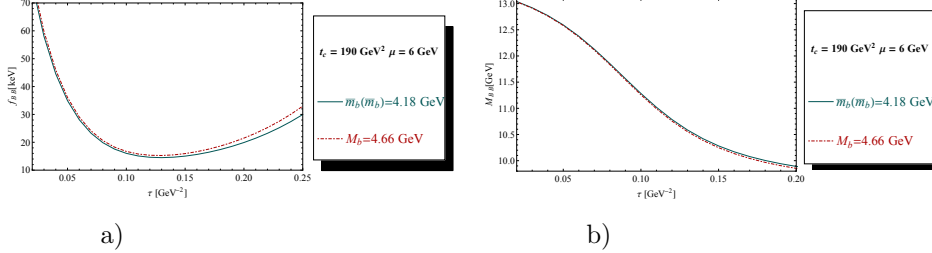


Fig. 14. a) f_{BB} at LO as function of τ for $t_c = 190$ GeV 2 , for $\mu = 6$ GeV, for values of the running $\overline{m}_b(\overline{m}_b) = 4.18$ GeV and pole mass $M_b = 4.66$ GeV. We use the QCD parameters in Tables 2 and 3; b) The same as a) but for the mass M_{BB} .

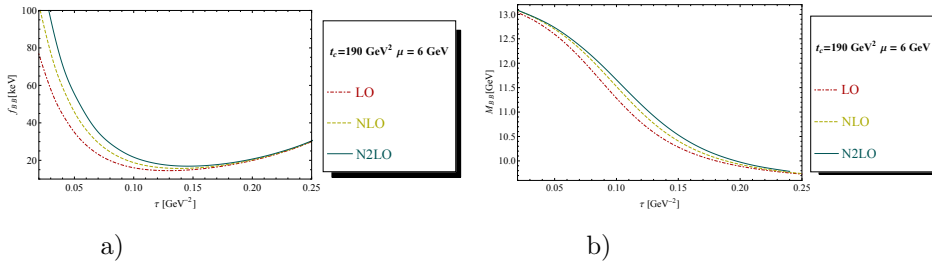


Fig. 15. a) f_{BB} as function of τ for a given value of $t_c = 190$ GeV 2 , for $\mu = 6$ GeV, for different truncation of the PT series and for the QCD parameters in Tables 2 and 3; b) The same as a) but for the mass M_{BB} .

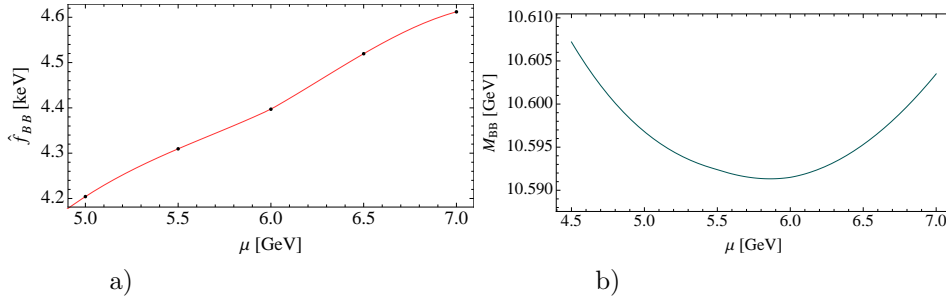


Fig. 16. a) Renormalization group invariant coupling \hat{f}_{BB} at NLO as function of μ , for the corresponding τ -stability region, for $t_c \simeq 190$ GeV 2 and for the QCD parameters in Tables 2 and 3; b) The same as a) but for the mass M_{BB} .

satisfied.

- *Running versus the pole quark mass definitions*

We show in Fig. 20 the effect of the definitions (running or pole) of the heavy quark mass used in the analysis at LO where the effect is large for the coupling.

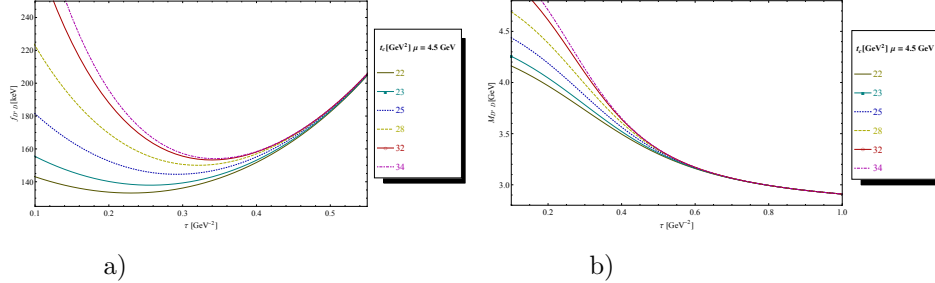


Fig. 17. **a)** f_{D^*D} at LO as function of τ for different values of t_c , for $\mu = 4.5$ GeV and for the QCD parameters in Tables 2 and 3; **b)** The same as a) but for the mass M_{D^*D} .

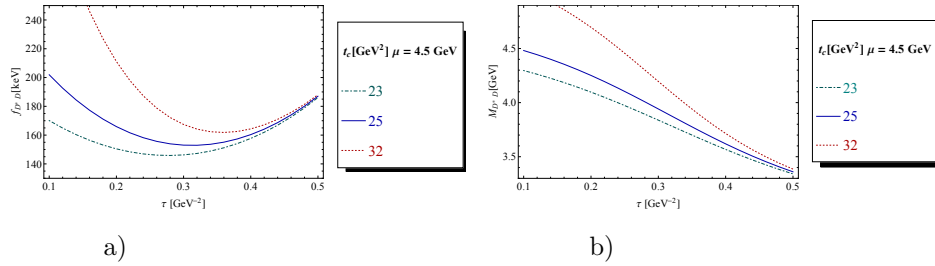


Fig. 18. **a)** f_{D^*D} at NLO as function of τ for different values of t_c , for $\mu = 4.5$ GeV and for the QCD parameters in Tables 2 and 3; **b)** The same as a) but for the mass M_{D^*D} .

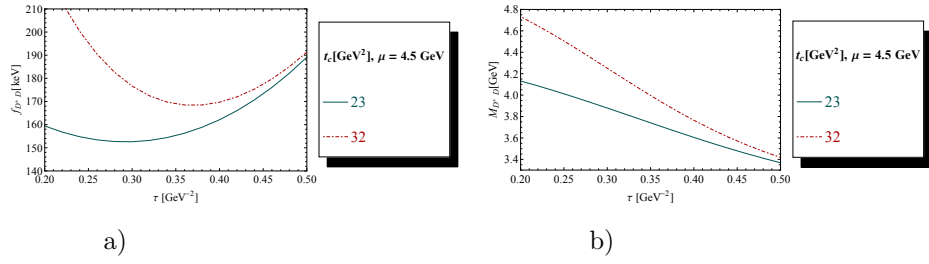


Fig. 19. **a)** f_{D^*D} at N2LO as function of τ for different values of t_c , for $\mu = 4.5$ GeV and for the QCD parameters in Tables 2 and 3; **b)** The same as a) but for the mass M_{D^*D} .

• Convergence of the PT series

Using $t_c \simeq 32$ GeV 2 , we study in Fig. 21 the convergence of the PT series for a given value of $\mu = 4.5$ GeV. We observe in Table 11 that from NLO to N2LO the mass decreases by about 1% only while the coupling increases by about 4% which are smaller than the errors in their determinations.

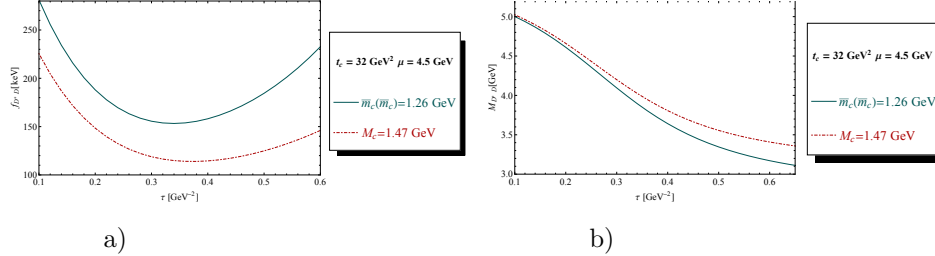


Fig. 20. a) f_{D^*D} at LO as function of τ for $t_c = 32$ GeV 2 , for $\mu = 4.5$ GeV, for values of the running $\bar{m}_c(\bar{m}_c) = 1.26$ GeV and pole mass $M_c = 1.47$ GeV. We use the QCD parameters in Tables 2 and 3; b) The same as a) but for the mass M_{D^*D} .

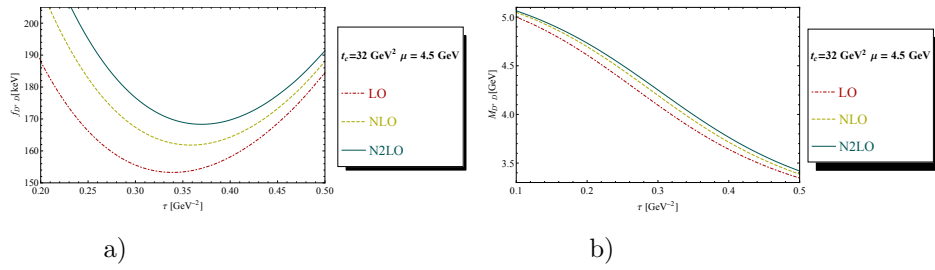


Fig. 21. a) f_{D^*D} as function of τ for a given value of $t_c = 32$ GeV 2 , for $\mu = 4.5$ GeV, for different truncation of the PT series and for the QCD parameters in Tables 2 and 3; b) The same as a) but for the mass M_{D^*D} .

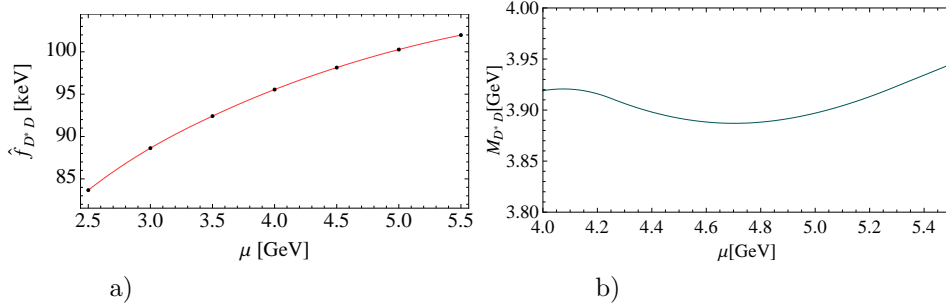


Fig. 22. a) Renormalization group invariant coupling \hat{f}_{D^*D} at NLO as function of μ , for the corresponding τ -stability region, for $t_c \simeq 32$ GeV 2 and for the QCD parameters in Tables 2 and 3; b) The same as a) but for the mass M_{D^*D} .

• μ -stability

We improve our previous results by using different values of μ (Fig. 22). Using the fact that the final result must be independent of the arbitrary parameter μ , we consider as an optimal results the one for $\mu \simeq 4.6$ GeV (inflection point for the coupling and minimum for the mass) which we give in Table 11.

6.2. Coupling and mass of the \bar{B}^*B molecule

We extend the analysis to the b -quark sector which we show in Figs. 23 to 28. The optimal values of the mass and coupling are given in Table 12 for the set:

$$\tau \simeq 0.14 \text{ GeV}^{-2}, \quad t_c \simeq (140 - 170) \text{ GeV}^2 \quad \text{and} \quad \mu \simeq (6 - 6.5) \text{ GeV}. \quad (21)$$

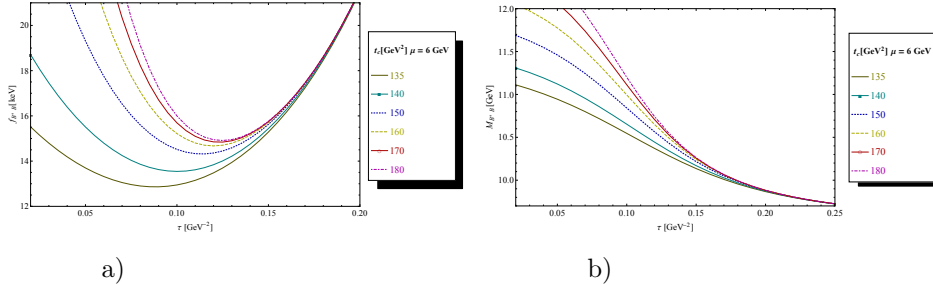


Fig. 23. a) f_{B^*B} at LO as function of τ for different values of t_c , for $\mu = 6$ GeV and for the QCD parameters in Tables 2 and 3; b) The same as a) but for the mass M_{B^*B} .

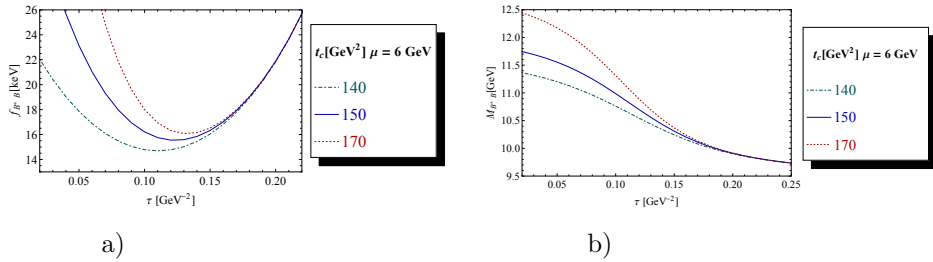


Fig. 24. a) f_{B^*B} at NLO as function of τ for different values of t_c , for $\mu = 6$ GeV and for the QCD parameters in Tables 2 and 3; b) The same as a) but for the mass M_{B^*B} .

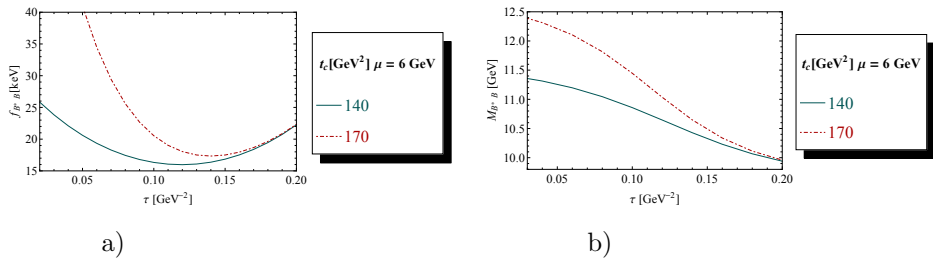


Fig. 25. a) f_{B^*B} at N2LO as function of τ for different values of t_c , for $\mu = 6$ GeV and for the QCD parameters in Tables 2 and 3; b) The same as a) but for the mass M_{B^*B} .

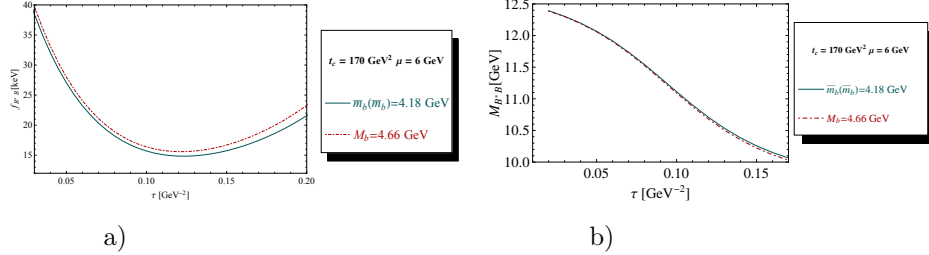


Fig. 26. a) f_{B^*B} at LO as function of τ for $t_c = 170$ GeV 2 , for $\mu = 6$ GeV, for values of the running $\bar{m}_b(\bar{m}_b) = 4.18$ GeV and pole mass $M_b = 4.66$ GeV. We use the QCD parameters in Tables 2 and 3; b) The same as a) but for the mass M_{B^*B} .

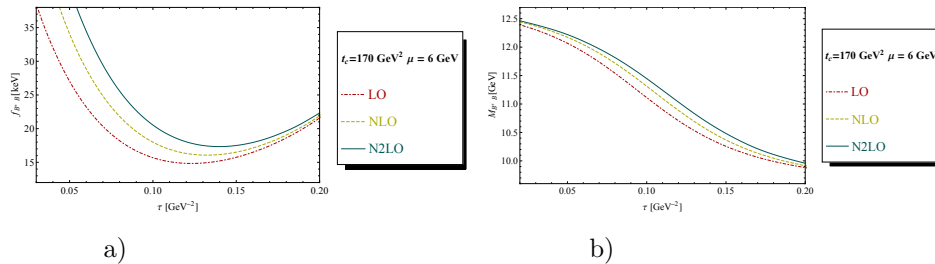


Fig. 27. a) f_{B^*B} as function of τ for a given value of $t_c = 170$ GeV 2 , for $\mu = 6$ GeV, for different truncation of the PT series and for the QCD parameters in Tables 2 and 3; b) The same as a) but for the mass M_{B^*B} .

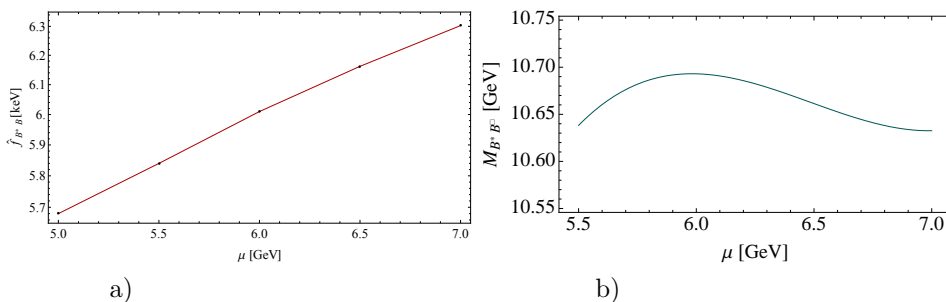


Fig. 28. a) Renormalization group invariant coupling \hat{f}_{B^*B} at NLO as function of μ , for the corresponding τ -stability region, for $t_c \simeq 170$ GeV 2 and for the QCD parameters in Tables 2 and 3; b) The same as a) but for the mass M_{B^*B} .

7. The $(0^{-\pm})$ Heavy-Light Pseudoscalar Molecule States

Here, we shall analyze the masses and couplings of the pseudoscalar $\bar{D}_0^* D$, $\bar{D}^* D_1$ and their beauty analogue, which will be illustrated by the case of $\bar{D}_0^* D$ and $\bar{B}_0^* B$. States with opposite C -parities are degenerated in this channel.

7.1. Coupling and mass of the $\bar{D}_0^* D$ molecule

- τ and t_c stabilities

We study the behavior of the coupling $f_{D_0^* D}$ and mass $M_{D_0^* D}$ in terms of LSR variable τ at different values of t_c as shown in Fig.29 at LO, in Fig. 30 at NLO and in Fig. 31 at N2LO. We consider as a final and conservative result the one

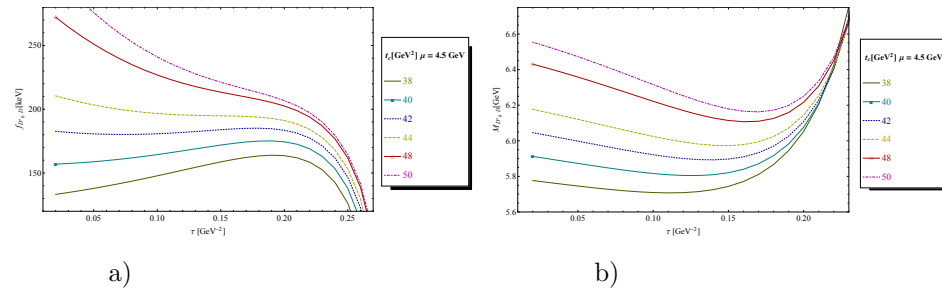


Fig. 29. **a)** $f_{D_0^* D}$ at LO as function of τ for different values of t_c , for $\mu = 4.5$ GeV and for the QCD parameters in Tables 2 and 3; **b)** The same as a) but for the mass $M_{D_0^* D}$.

corresponding to the beginning of the τ -stability for $t_c=42$ GeV^2 until the one where t_c -stability starts to be reached for $t_c \simeq 48$ GeV^2 . In these stability regions, the requirement that the pole contribution is larger than the one of the continuum (see e.g. ³⁴) is automatically satisfied.

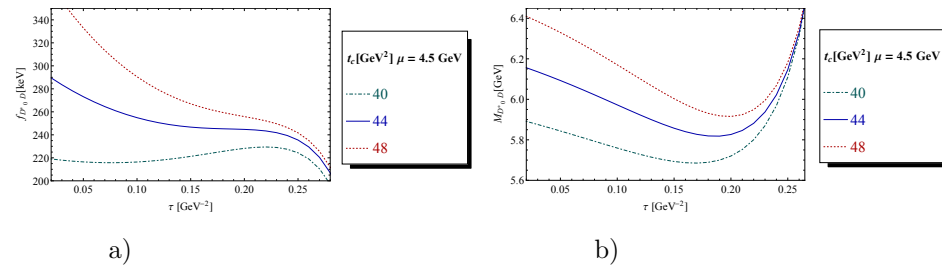


Fig. 30. **a)** $f_{D_0^* D}$ at NLO as function of τ for different values of t_c , for $\mu = 4.5$ GeV and for the QCD parameters in Tables 2 and 3; **b)** The same as a) but for the mass $M_{D_0^* D}$.

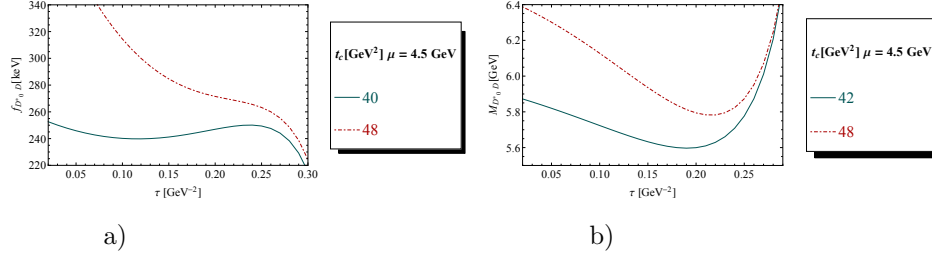


Fig. 31. **a)** $f_{D_0^* D}$ at N2LO as function of τ for different values of t_c , for $\mu = 4.5$ GeV and for the QCD parameters in Tables 2 and 3; **b)** The same as a) but for the mass $M_{D_0^* D}$.

• Running versus the pole quark mass definitions

We show in Fig. 32 the effect of the definitions (running or pole) of the heavy quark mass used in the analysis at LO which is important for the coupling and the mass.

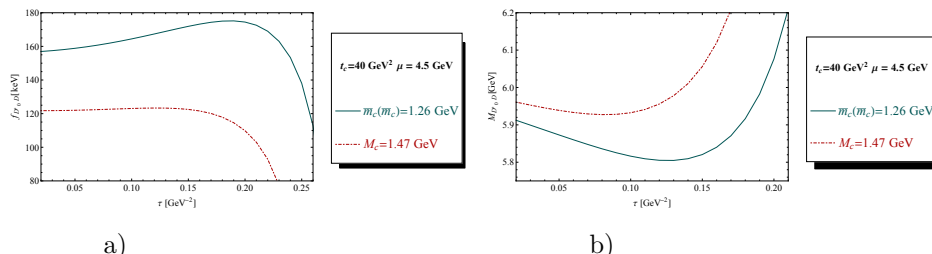


Fig. 32. **a)** $f_{D_0^* D}$ at LO as function of τ for $t_c = 42$ GeV 2 , for $\mu = 4.5$ GeV, for values of the running $\bar{m}_c(\bar{m}_c) = 1.26$ GeV and pole mass $M_c = 1.47$ GeV. We use the QCD parameters in Tables 2 and 3; **b)** The same as a) but for the mass $M_{D_0^* D}$.

• Convergence of the PT series

Using $t_c \simeq 32$ GeV 2 , we study in Fig. 33 the convergence of the PT series for a given value of $\mu = 4.5$ GeV. We observe that from NLO to N2LO the mass decreases by about only 1.5% indicating the good convergence of the PT series.

• μ -stability

We improve our previous results by using different values of μ (Fig. 34). Using the fact that the final result must be independent of the arbitrary parameter μ , we consider as an optimal result the one at the inflection point for $\mu \simeq (4.5 - 5.0)$ GeV at which we deduce the result in Table 11.

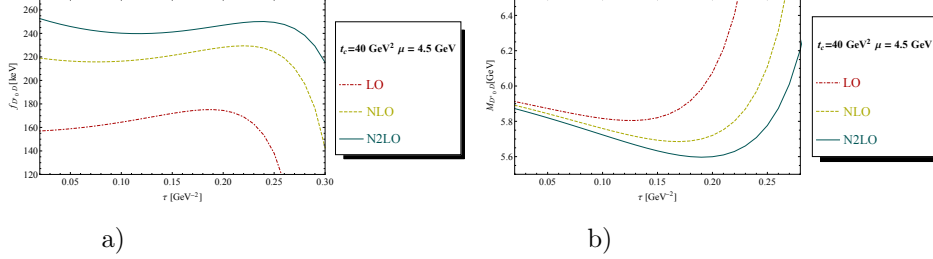


Fig. 33. **a)** $f_{D_0^* D}$ as function of τ for a given value of $t_c = 42 \text{ GeV}^2$, for $\mu = 4.5 \text{ GeV}$, for different truncation of the PT series and for the QCD parameters in Tables 2 and 3; **b)** The same as a) but for the mass $M_{D_0^* D}$.

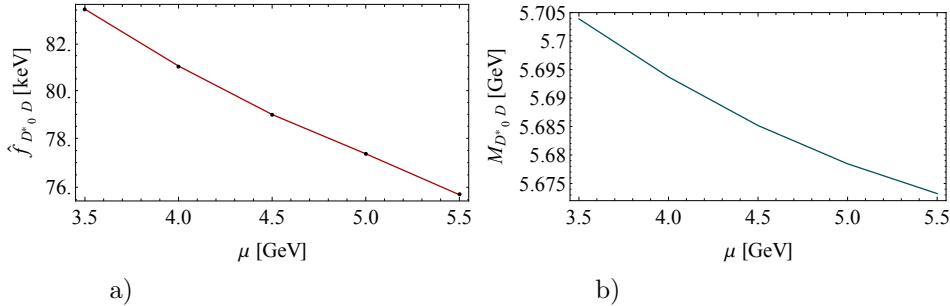


Fig. 34. **a)** Renormalization group invariant coupling $\hat{f}_{D_0^* D}$ at NLO as function of μ , for the corresponding τ -stability region, for $t_c \simeq 42 \text{ GeV}^2$ and for the QCD parameters in Tables 2 and 3; **b)** The same as a) but for the mass $M_{D_0^* D}$.

7.2. Coupling and mass of the $\bar{B}_0^* B$ molecule

We extend the analysis to the b -quark sector which we show in Figs. 35 to 40. The result is shown in Table 12.

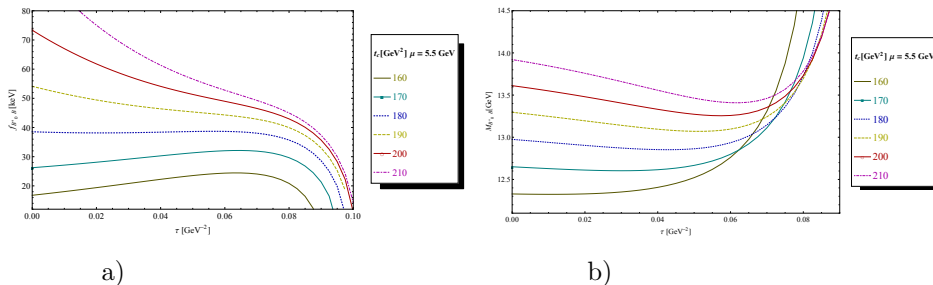


Fig. 35. **a)** $f_{B_0^* B}$ at LO as function of τ for different values of t_c , for $\mu = 6 \text{ GeV}$ and for the QCD parameters in Tables 2 and 3; **b)** The same as a) but for the mass $M_{B_0^* B}$.

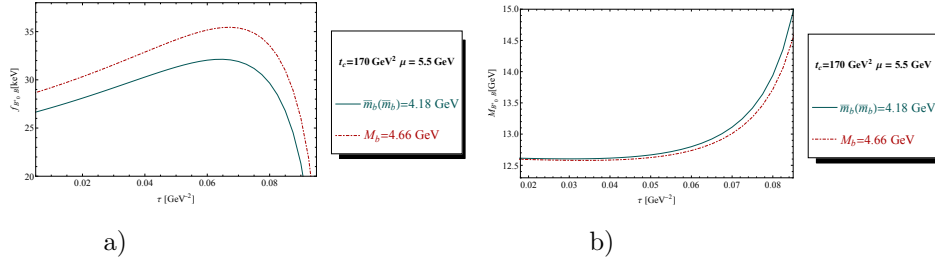


Fig. 36. **a**) $f_{B_0^* B}$ at LO as function of τ for $t_c = 170 \text{ GeV}^2$, for $\mu = 6 \text{ GeV}$, for values of the running $\bar{m}_b(\bar{m}_b) = 4.18 \text{ GeV}$ and pole mass $M_b = 4.66 \text{ GeV}$. We use the QCD parameters in Tables 2 and 3; **b)** The same as a) but for the mass $M_{B_0^* B}$.

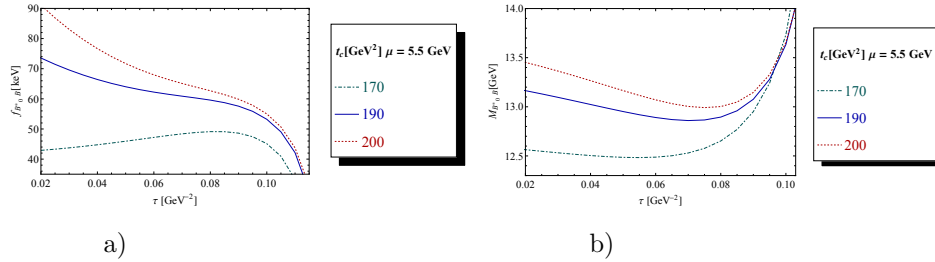


Fig. 37. a) $f_{B_0^* B}^{**}$ at NLO as function of τ for different values of t_c , for $\mu = 6$ GeV and for the QCD parameters in Tables 2 and 3; b) The same as a) but for the mass $M_{B_0^* B}$.

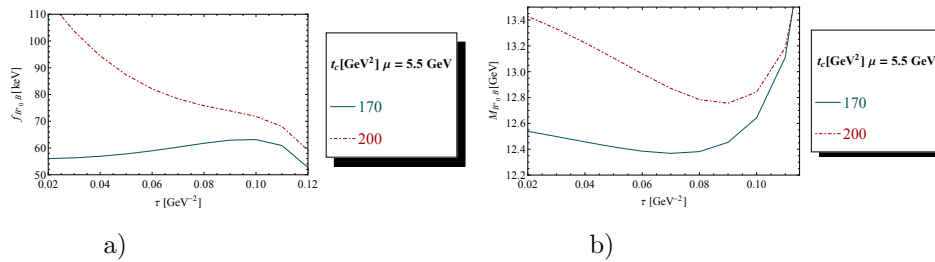


Fig. 38. a) $f_{B_0^* B}^{**}$ at N2LO as function of τ for different values of t_c , for $\mu = 6$ GeV and for the QCD parameters in Tables 2 and 3; b) The same as a) but for the mass $M_{B_0^* B}$.

8. The (1^{--}) Heavy-Light Vector Molecule states

We shall study the $\bar{D}_0^* D^*$, $\bar{D} D_1$ and their beauty analogue which will be illustrated by the analysis of the $\bar{D}_0^* D^*$ and $\bar{B}_0^* B^*$ molecules.

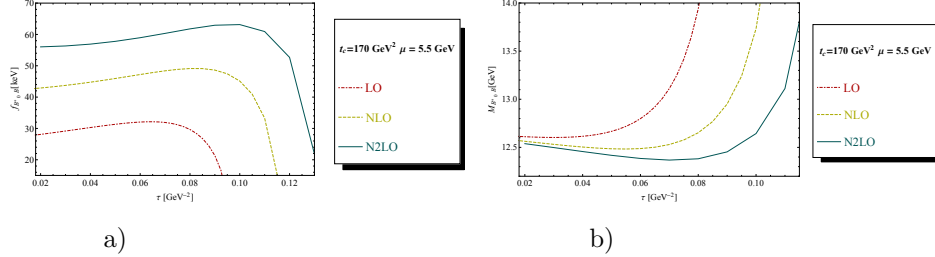


Fig. 39. **a)** $f_{B_0^* B}$ as function of τ for a given value of $t_c = 170 \text{ GeV}^2$, for $\mu = 6 \text{ GeV}$, for different truncation of the PT series and for the QCD parameters in Tables 2 and 3; **b)** The same as a) but for the mass $M_{B_0^* B}$.

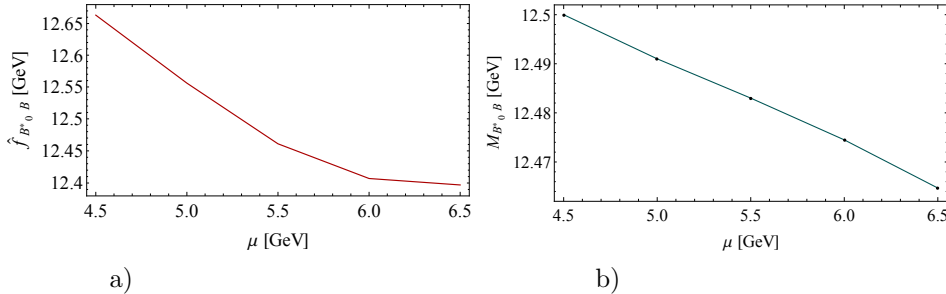


Fig. 40. **a)** Renormalization group invariant coupling $\hat{f}_{B_0^* B_1}$ at NLO as function of μ , for the corresponding τ -stability region, for $t_c \simeq 170 \text{ GeV}^2$ and for the QCD parameters in Tables 2 and 3; **b)** The same as a) but for the mass $M_{B_0^* B_1}$.

8.1. Coupling and mass of the $\bar{D}_0^* D^*$ molecule

- τ and t_c stabilities

We study the behavior of the coupling $f_{D_0^* D^*}$ and mass $M_{D_0^* D^*}$ in terms of LSR variable τ at different values of t_c as shown in Fig. 41 at LO to Fig. 43 at N2LO. We

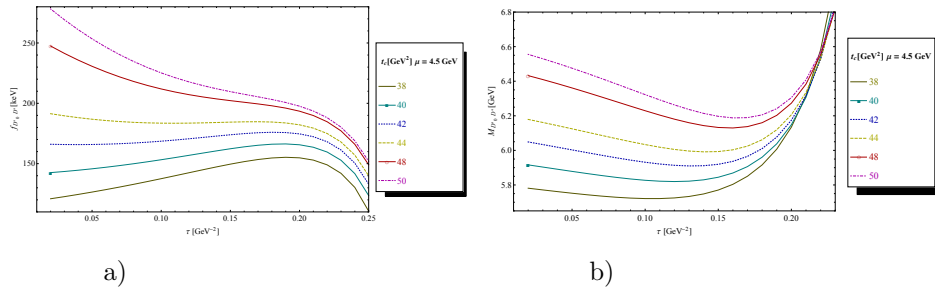


Fig. 41. **a)** $f_{D_0^* D^*}$ at LO as function of τ for different values of t_c , for $\mu = 4.5 \text{ GeV}$ and for the QCD parameters in Tables 2 and 3; **b)** The same as a) but for the mass $M_{D_0^* D^*}$.

consider as a final and conservative result the one corresponding to the beginning of the τ -stability for $t_c=42 \text{ GeV}^2$ until the one where t_c -stability starts to be reached for $t_c \simeq 48 \text{ GeV}^2$. In these stability regions, the requirement that the pole contribution is larger than the one of the continuum (see e.g.³⁴⁾ is automatically satisfied.

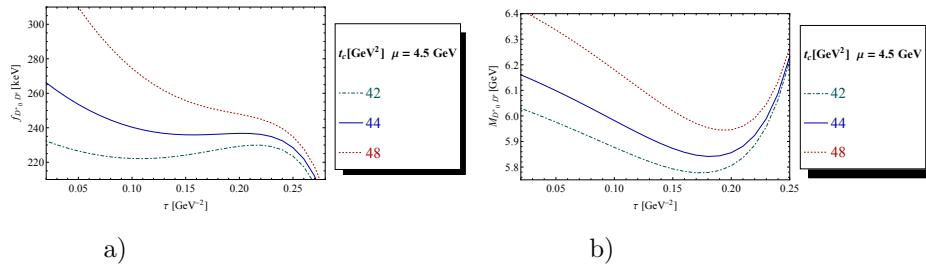


Fig. 42. **a)** $f_{D_0^* D^*}$ at NLO as function of τ for different values of t_c , for $\mu = 4.5 \text{ GeV}$ and for the QCD parameters in Tables 2 and 3; **b)** The same as a) but for the mass $M_{D_0^* D^*}$.

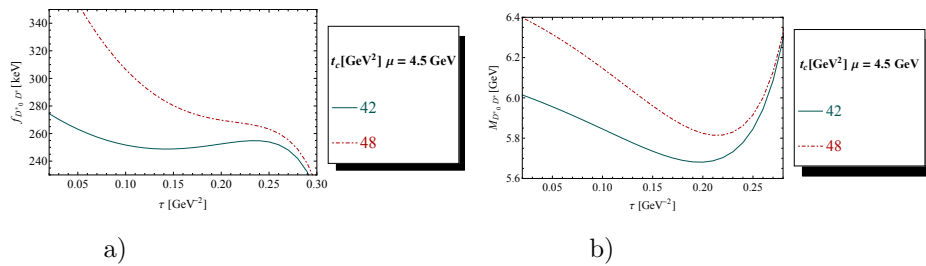


Fig. 43. **a)** $f_{D_0^* D^*}$ at N2LO as function of τ for different values of t_c , for $\mu = 4.5 \text{ GeV}$ and for the QCD parameters in Tables 2 and 3; **b)** The same as a) but for the mass $M_{D_0^* D^*}$.

• Running versus the pole quark mass definitions

We show in Fig. 44 the effect of the definitions (running or pole) of the heavy quark mass used in the analysis at LO which is large.

• Convergence of the PT series

Using $t_c \simeq 42 \text{ GeV}^2$, we study in Fig. 45 the convergence of the PT series for a given value of $\mu = 4.5 \text{ GeV}$. We observe that from NLO to N2LO the mass decreases by about 2% only showing the good convergence of the PT series.

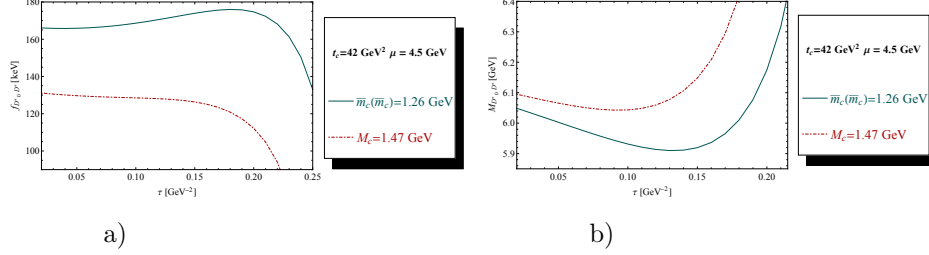


Fig. 44. a) $f_{D_0^* D^*}$ at LO as function of τ for $t_c = 42$ GeV 2 , for $\mu = 4.5$ GeV, for values of the running $\bar{m}_c(\bar{m}_c) = 1.26$ GeV and pole mass $M_c = 1.47$ GeV. We use the QCD parameters in Tables 2 and 3; b) The same as a) but for the mass $M_{D_0^* D^*}$.

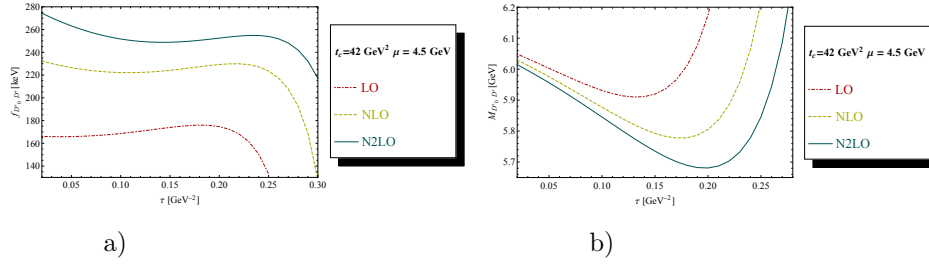


Fig. 45. a) $f_{D_0^* D^*}$ as function of τ for a given value of $t_c = 42$ GeV 2 , for $\mu = 4.5$ GeV, for different truncation of the PT series and for the QCD parameters in Tables 2 and 3; b) The same as a) but for the mass $M_{D_0^* D^*}$.

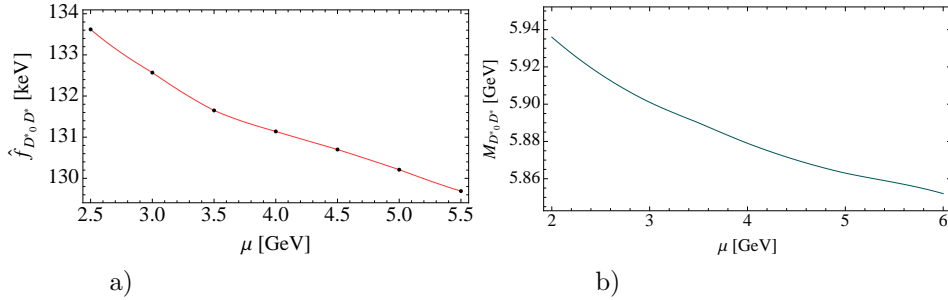


Fig. 46. a) Renormalization group invariant coupling $\hat{f}_{D_0^* D^*}$ at NLO as function of μ , for the corresponding τ -stability region, for $t_c \simeq 42$ GeV 2 and for the QCD parameters in Tables 2 and 3; b) The same as a) but for the mass $M_{D_0^* D^*}$.

• μ -stability

We improve our previous results by using different values of μ (Fig. 46). Using the fact that the final result must be independent of the arbitrary parameter μ , we consider as an optimal result the one at the inflection point for $\mu \simeq (4.0 - 4.5)$ GeV at which we deduce the result in Table 11.

8.2. Coupling and mass of the $\bar{B}_0^* B^*$ molecule

We extend the analysis to the b -quark sector which we show in Figs. 47 to 52.

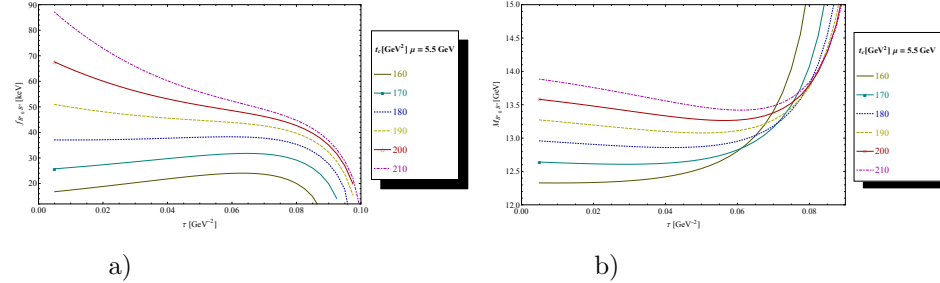


Fig. 47. a) $f_{B_0^* B^*}$ at LO as function of τ for different values of t_c , for $\mu = 5.5$ GeV and for the QCD parameters in Tables 2 and 3; b) The same as a) but for the mass $M_{B_0^* B^*}$.

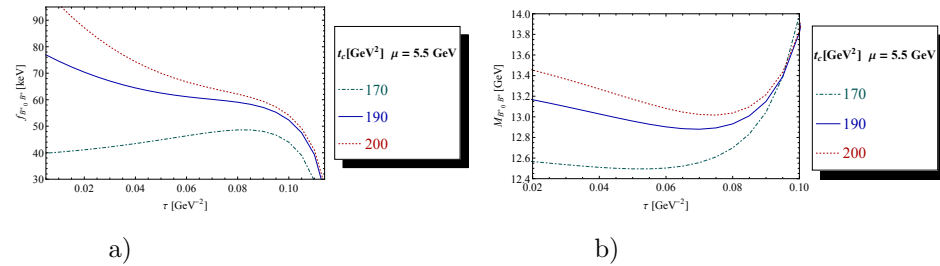


Fig. 48. a) $f_{B_0^* B^*}$ at NLO as function of τ for different values of t_c , for $\mu = 5.5$ GeV and for the QCD parameters in Tables 2 and 3; b) The same as a) but for the mass $M_{B_0^* B^*}$.

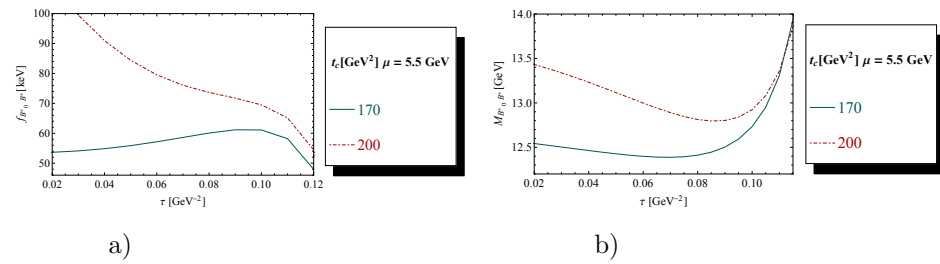


Fig. 49. a) $f_{B_0^* B^*}$ at N2LO as function of τ for different values of t_c , for $\mu = 5.5$ GeV and for the QCD parameters in Tables 2 and 3; b) The same as a) but for the mass $M_{B_0^* B^*}$.

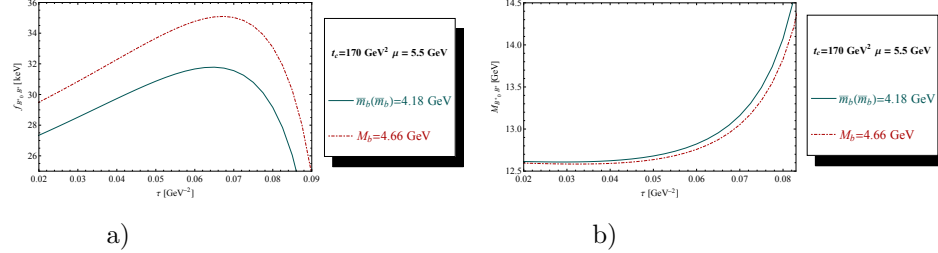


Fig. 50. **a)** $f_{B_0^* B^*}$ at LO as function of τ for $t_c = 170$ GeV 2 , for $\mu = 5.5$ GeV, for values of the running $\bar{m}_b(\bar{m}_b) = 4.18$ GeV and pole mass $M_b = 4.66$ GeV. We use the QCD parameters in Tables 2 and 3; **b)** The same as a) but for the mass $M_{B_0^* B^*}$.

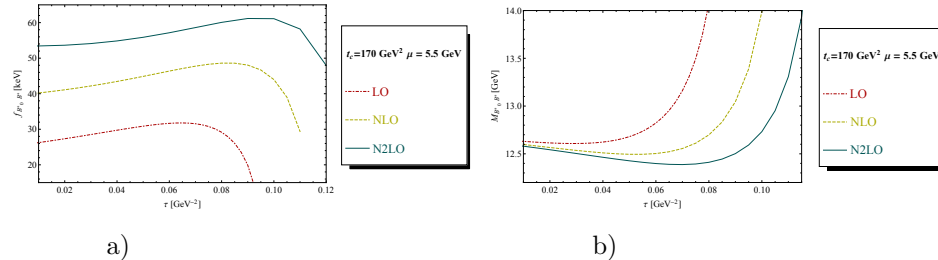


Fig. 51. **a)** $f_{B_0^* B^*}$ as function of τ for a given value of $t_c = 170$ GeV 2 , for $\mu = 6$ GeV, for different truncation of the PT series and for the QCD parameters in Tables 2 and 3; **b)** The same as a) but for the mass $M_{B_0^* B^*}$.

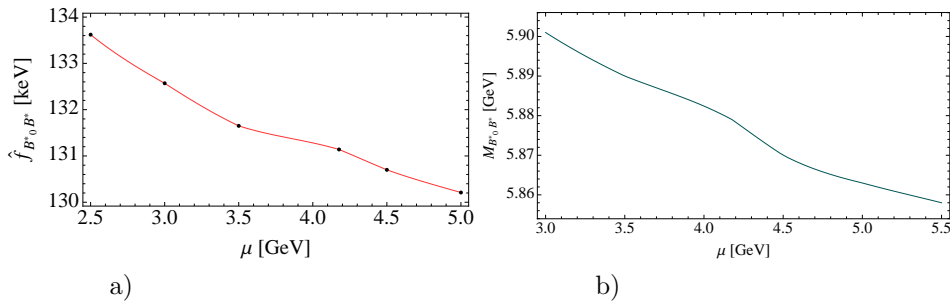


Fig. 52. **a)** Renormalization group invariant coupling $\hat{f}_{B_0^* B^*}$ at NLO as function of μ , for the corresponding τ -stability region, for $t_c \simeq 170$ GeV 2 and for the QCD parameters in Tables 2 and 3; **b)** The same as a) but for the mass $M_{B_0^* B^*}$.

9. The (1^{-+}) Heavy-Light Vector Molecule states

We shall study here the $\bar{D}_0^* D^*$, $\bar{D} D_1$ and their beauty analogue with positive C -parity using the currents in Table 1. The analysis is very similar to the previous case as well as the shape of different curves. The results are quoted in Table 7 to 12.

10. The heavy-light four-quark states

10.1. The QCD interpolating currents

The four-quark states $[Qq\bar{Q}\bar{q}]$ will be described by the interpolating currents given in Table 4:

Table 4. Interpolating currents with a definite P -parity describing the four-quark states. $Q \equiv c$ (resp. b) in the charm and bottom channels. $q \equiv u, d$.

J^P	Four-Quark Currents $\equiv \mathcal{O}_{4q}(x)$
0⁺	$\epsilon_{abc}\epsilon_{dec} \left[(q_a^T C \gamma_5 Q_b)(\bar{q}_d \gamma_5 C \bar{Q}_e^T) + k(q_a^T C Q_b)(\bar{q}_d C \bar{Q}_e^T) \right]$
1⁺	$\epsilon_{abc}\epsilon_{dec} \left[(q_a^T C \gamma_5 Q_b)(\bar{q}_d \gamma_\mu C \bar{Q}_e^T) + k(q_a^T C Q_b)(\bar{q}_d \gamma_\mu \gamma_5 C \bar{Q}_e^T) \right]$
0⁻	$\epsilon_{abc}\epsilon_{dec} \left[(q_a^T C \gamma_5 Q_b)(\bar{q}_d C \bar{Q}_e^T) + k(q_a^T C Q_b)(\bar{q}_d \gamma_5 C \bar{Q}_e^T) \right]$
1⁻	$\epsilon_{abc}\epsilon_{dec} \left[(q_a^T C \gamma_5 Q_b)(\bar{q}_d \gamma_\mu \gamma_5 C \bar{Q}_e^T) + k(q_a^T C Q_b)(\bar{q}_d \gamma_\mu C \bar{Q}_e^T) \right]$

The corresponding spectral functions are defined analogously to Eq. 2 as: $\frac{1}{\pi} \text{Im}\Pi_{4q}^{(1)}(t)$ for spin 1 particles and $\frac{1}{\pi} \text{Im}\psi_{4q}^{(s,p)}(t)$ from Eq. 3 from spin 0 ones. k is the mixing of the two operators. We shall take the optimal choice $k = 0$ as demonstrated in.^{72,73} The expressions of the spectral functions to LO of PT and including the contributions of condensates of dimension $d \leq 8$ are given in Appendix B.

10.2. Coupling and mass of the $S_c(0^+)$ four-quark state

Like in the previous case of the molecule states, we study the coupling and mass of the scalar $S_c(0^+)$ four-quark state which we show in Figs. 53 to 58. We shall in the following different analysis that the one of the four-quark states is very similar to the analysis of the molecules and present analogous features (presence of minimas or/and inflexion points, good convergence of the PT series and the OPE). The results are summarized in Tables 9 and 13.

10.3. Coupling and mass of the $S_b(0^+)$ four-quark state

We extend the analysis to the b -quark sector which we show in Figs. 59 to 64. The results are summarized in Tables 10 and 14.

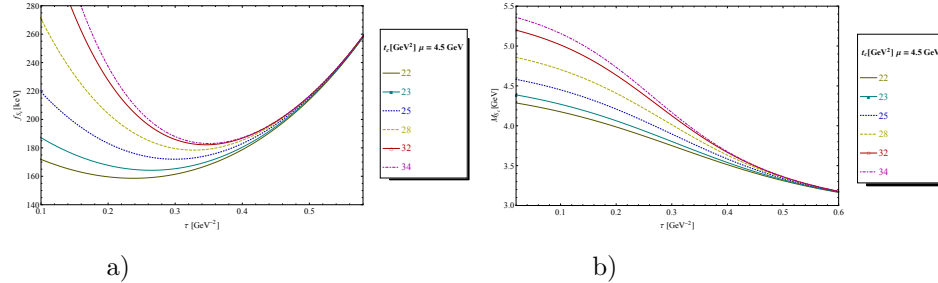


Fig. 53. a) f_{S_c} at LO as function of τ for different values of t_c , for $\mu = 4.5$ GeV and for the QCD parameters in Tables 2 and 3; b) The same as a) but for the mass M_{S_c} .

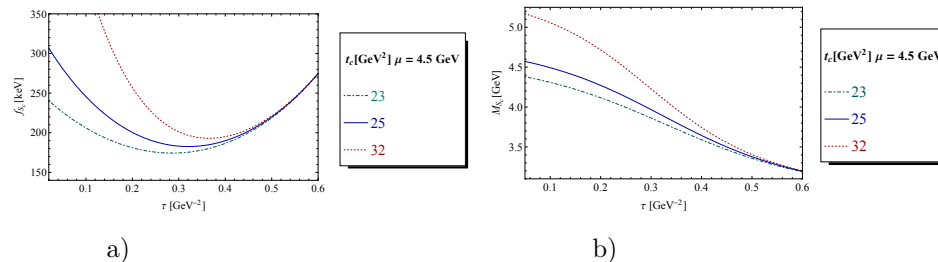


Fig. 54. a) f_{S_c} at NLO as function of τ for different values of t_c , for $\mu = 4.5$ GeV and for the QCD parameters in Tables 2 and 3; b) The same as a) but for the mass M_{S_c} .

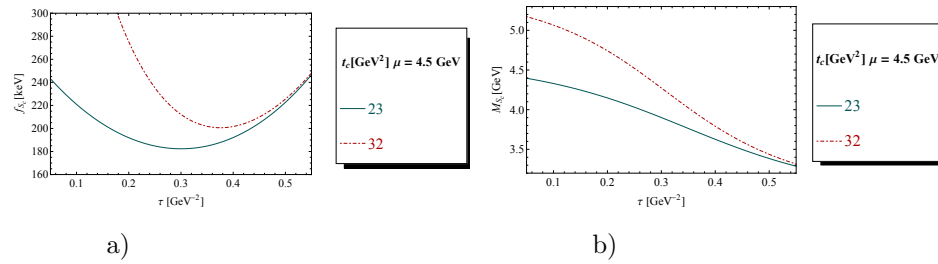


Fig. 55. a) f_{S_c} at N2LO as function of τ for different values of t_c , for $\mu = 4.5$ GeV and for the QCD parameters in Tables 2 and 3; b) The same as a) but for the mass M_{S_c} .

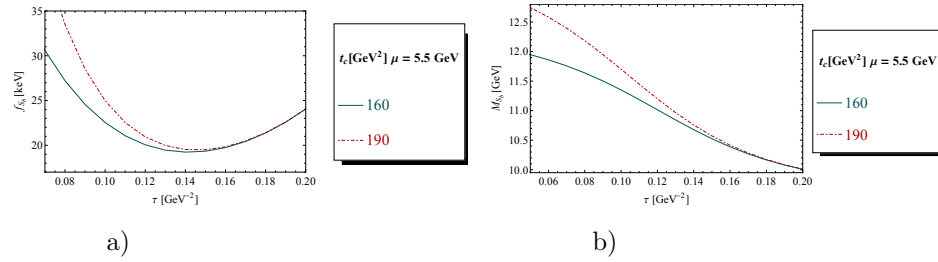


Fig. 61. a) f_{S_b} at N2LO as function of τ for different values of t_c , for $\mu = 5.5$ GeV and for the QCD parameters in Tables 2 and 3; b) The same as a) but for the mass M_{S_b} .

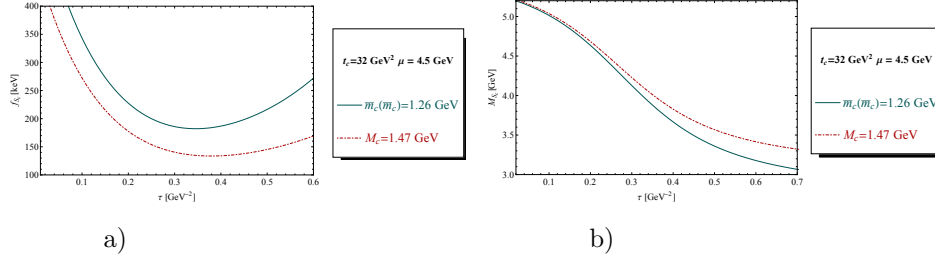


Fig. 56. **a)** f_{S_c} at LO as function of τ for $t_c = 32 \text{ GeV}^2$, for $\mu = 4.5 \text{ GeV}$, for values of the running $\bar{m}_c(\bar{m}_c) = 1.26 \text{ GeV}$ and pole mass $M_c = 1.47 \text{ GeV}$. We use the QCD parameters in Tables 2 and 3; **b)** The same as a) but for the mass M_{S_c} .

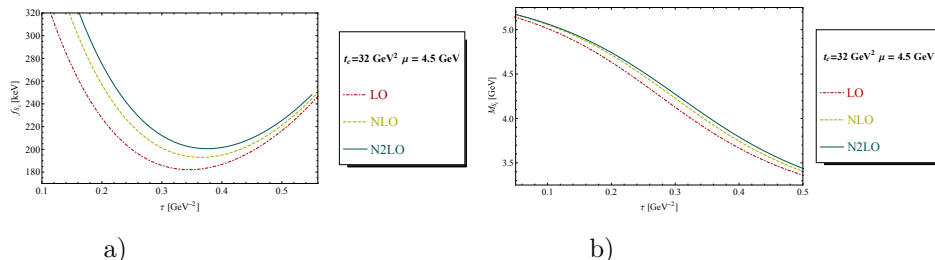


Fig. 57. **a)** f_{S_c} as function of τ for a given value of $t_c = 32 \text{ GeV}^2$, for $\mu = 4.5 \text{ GeV}$, for different truncation of the PT series and for the QCD parameters in Tables 2 and 3; **b)** The same as a) but for the mass M_{S_b} .

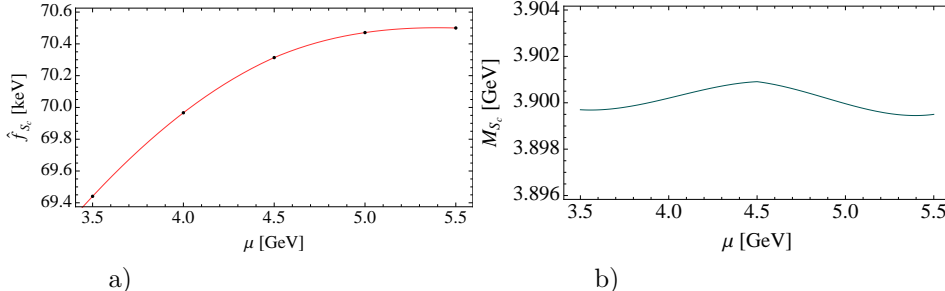


Fig. 58. **a)** Renormalization group invariant coupling \hat{f}_{S_c} at NLO as function of μ , for the corresponding τ -stability region, for $t_c \simeq 32 \text{ GeV}^2$ and for the QCD parameters in Tables 2 and 3; **b)** The same as a) but for the mass M_{S_c} .

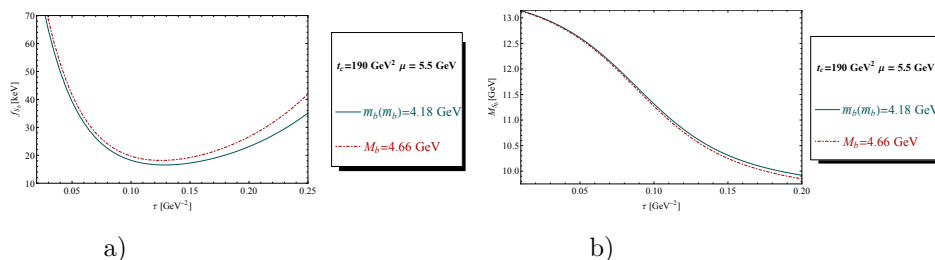


Fig. 62. **a)** f_{S_b} at LO as function of τ for $t_c = 170 \text{ GeV}^2$, for $\mu = 5.5 \text{ GeV}$, for values of the running $\bar{m}_b(\bar{m}_b) = 4.18 \text{ GeV}$ and pole mass $M_b = 4.66 \text{ GeV}$. We use the QCD parameters in Tables 2 and 3; **b)** The same as a) but for the mass M_{S_b} .

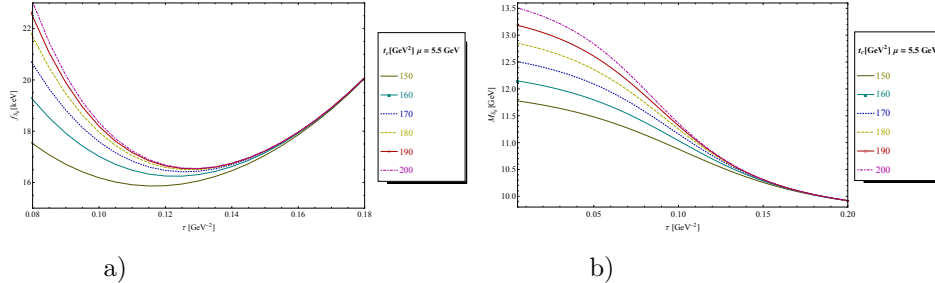


Fig. 59. a) f_{S_b} at LO as function of τ for different values of t_c , for $\mu = 5.5$ GeV and for the QCD parameters in Tables 2 and 3; b) The same as a) but for the mass M_{S_b} .

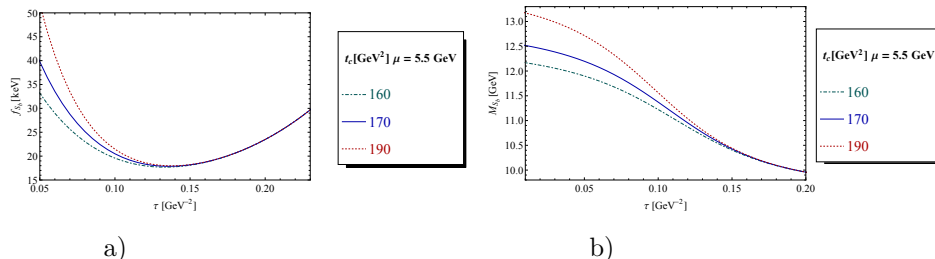


Fig. 60. **a)** f_{S_b} at NLO as function of τ for different values of t_c , for $\mu = 5.5$ GeV and for the QCD parameters in Tables 2 and 3; **b)** The same as a) but for the mass M_{S_b} .

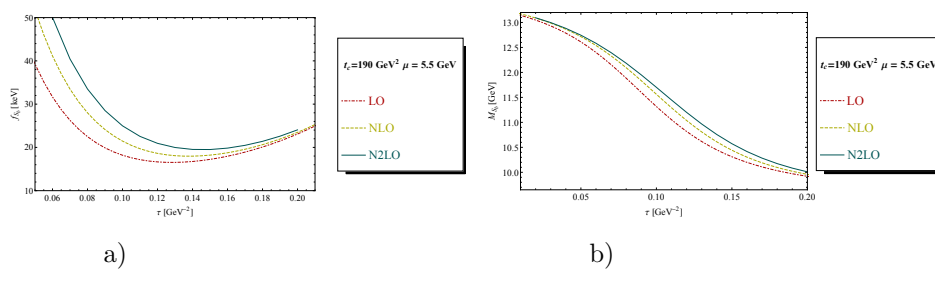


Fig. 63. **a**) f_{S_b} as function of τ for a given value of $t_c = 190 \text{ GeV}^2$, for $\mu = 5.5 \text{ GeV}$, for different truncation of the PT series and for the QCD parameters in Tables 2 and 3; **b**) The same as a) but for the mass M_{S_b} .

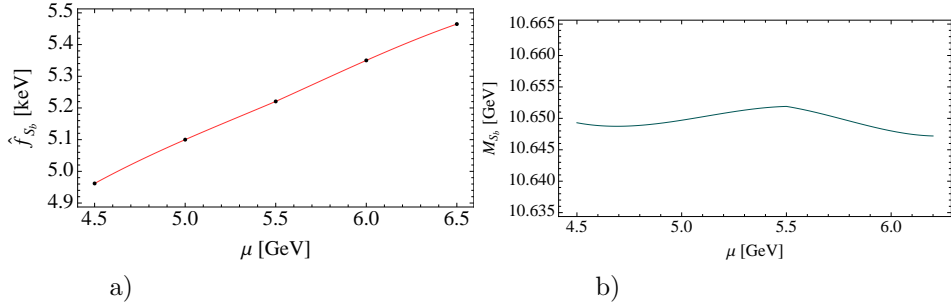


Fig. 64. a) Renormalization group invariant coupling \hat{f}_{S_b} at NLO as function of μ , for the corresponding τ -stability region, for $t_c \simeq 190$ GeV 2 and for the QCD parameters in Tables 2 and 3; b) The same as a) but for the mass M_{S_b} .

10.4. Coupling and mass of the $A_c(1^+)$ four-quark state

Like in the previous cases, we study the coupling and mass of the axial-vector $A_c(1^+)$ four-quark state which we show in Figs. 65 to 70. The results are summarized in Tables 9 and 13.

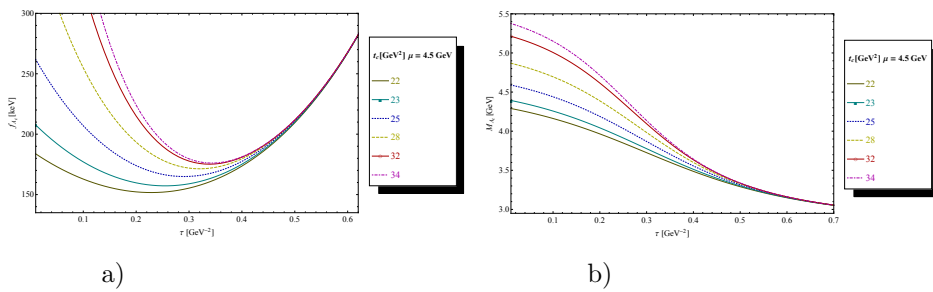


Fig. 65. a) f_{A_c} at LO as function of τ for different values of t_c , for $\mu = 4.5$ GeV and for the QCD parameters in Tables 2 and 3; b) The same as a) but for the mass M_{A_c} .

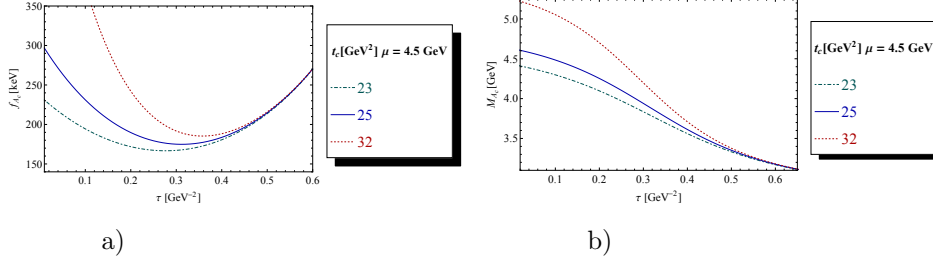


Fig. 66. **a)** f_{A_c} at NLO as function of τ for different values of t_c , for $\mu = 4.5$ GeV and for the QCD parameters in Tables 2 and 3; **b)** The same as a) but for the mass M_{A_c} .

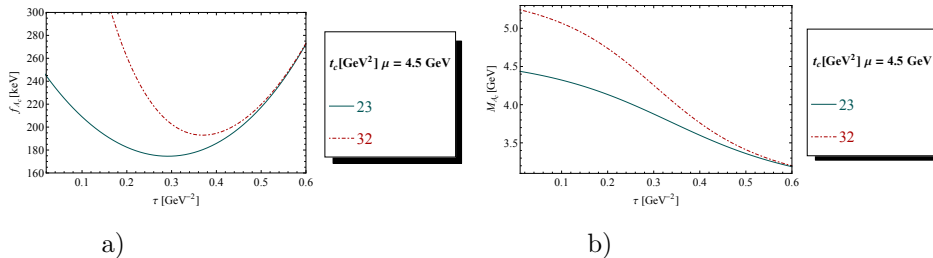


Fig. 67. **a)** f_{A_c} at N2LO as function of τ for different values of t_c , for $\mu = 4.5$ GeV and for the QCD parameters in Tables 2 and 3; **b)** The same as a) but for the mass M_{A_c} .

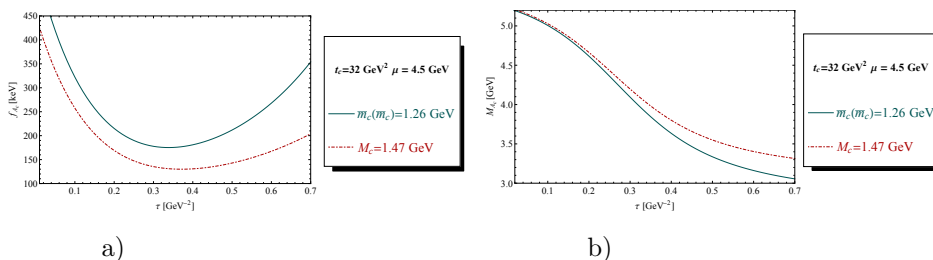


Fig. 68. **a)** f_{A_c} at LO as function of τ for $t_c = 32$ GeV 2 , for $\mu = 4.5$ GeV, for values of the running $\bar{m}_c(\bar{m}_c) = 1.26$ GeV and pole mass $M_c = 1.47$ GeV. We use the QCD parameters in Tables 2 and 3; **b)** The same as a) but for the mass M_{A_c} .

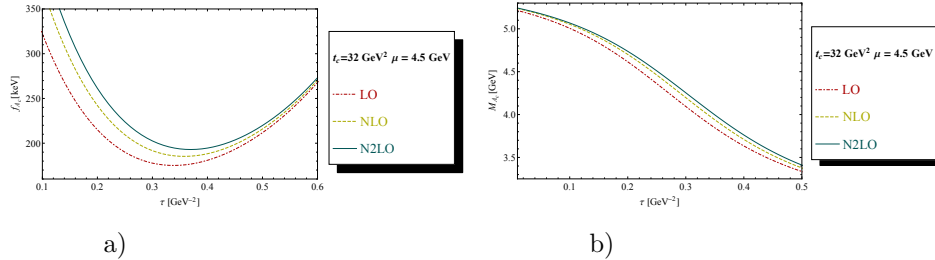


Fig. 69. **a)** f_{A_c} as function of τ for a given value of $t_c = 32 \text{ GeV}^2$, for $\mu = 4.5 \text{ GeV}$, for different truncation of the PT series and for the QCD parameters in Tables 2 and 3; **b)** The same as a) but for the mass M_{A_c} .

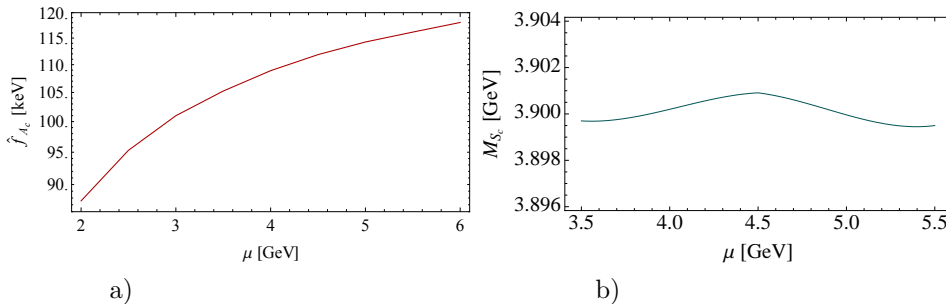


Fig. 70. **a)** Renormalization group invariant coupling \hat{f}_{A_c} at NLO as function of μ , for the corresponding τ -stability region, for $t_c \simeq 32 \text{ GeV}^2$ and for the QCD parameters in Tables 2 and 3; **b)** The same as a) but for the mass M_{A_c} .

10.5. Coupling and mass of the $A_b(1^+)$ four-quark state

We extend the analysis to the b -quark sector which we show in Figs. 71 to 76. The results are summarized in Tables 10 and 14.

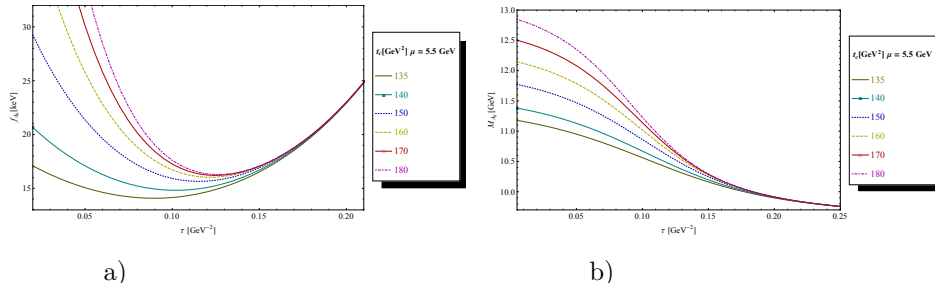


Fig. 71. **a)** f_{A_b} at LO as function of τ for different values of t_c , for $\mu = 5.5$ GeV and for the QCD parameters in Tables 2 and 3; **b)** The same as a) but for the mass M_{A_b} .

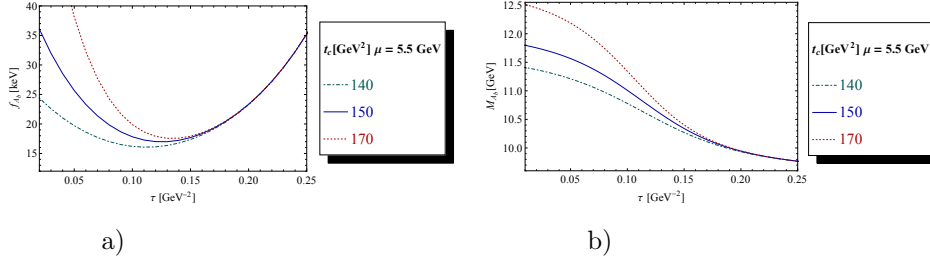


Fig. 72. a) f_{A_b} at NLO as function of τ for different values of t_c , for $\mu = 5.5$ GeV and for the QCD parameters in Tables 2 and 3; b) The same as a) but for the mass M_{A_b} .

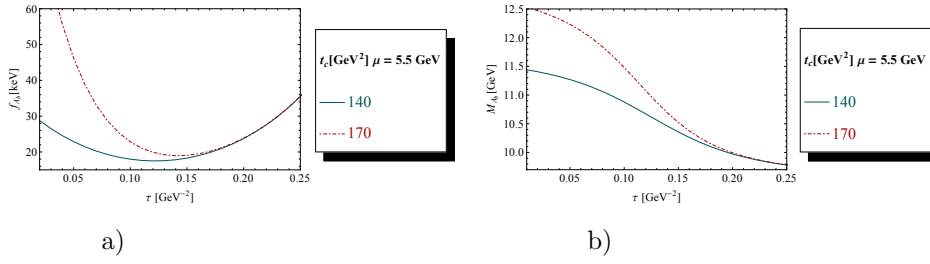


Fig. 73. a) f_{A_b} at N2LO as function of τ for different values of t_c , for $\mu = 5.5$ GeV and for the QCD parameters in Tables 2 and 3; b) The same as a) but for the mass M_{A_b} .

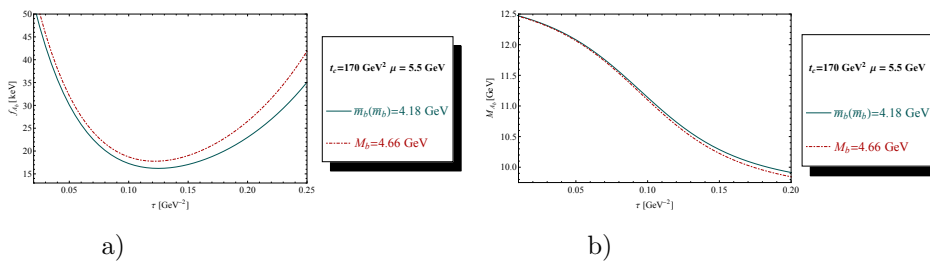


Fig. 74. a) f_{A_b} at LO as function of τ for $t_c = 170$ GeV 2 , for $\mu = 5.5$ GeV, for values of the running $\bar{m}_b(\bar{m}_b) = 4.18$ GeV and pole mass $M_b = 4.66$ GeV. We use the QCD parameters in Tables 2 and 3; b) The same as a) but for the mass M_{A_b} .

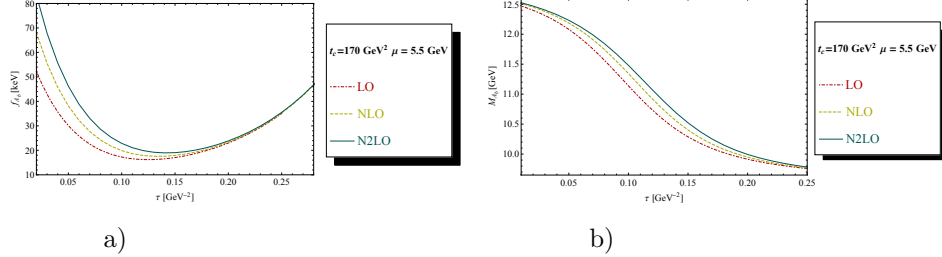


Fig. 75. **a)** f_{A_b} as function of τ for a given value of $t_c = 170 \text{ GeV}^2$, for $\mu = 5.5 \text{ GeV}$, for different truncation of the PT series and for the QCD parameters in Tables 2 and 3; **b)** The same as a) but for the mass M_{A_b} .

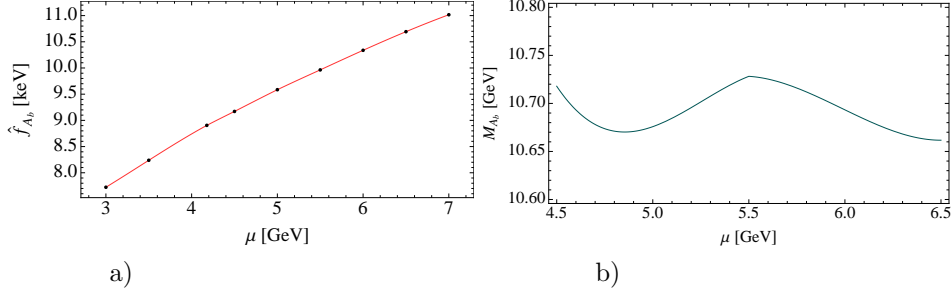


Fig. 76. **a)** Renormalization group invariant coupling \hat{f}_{A_b} at NLO as function of μ , for the corresponding τ -stability region, for $t_c \simeq 170 \text{ GeV}^2$ and for the QCD parameters in Tables 2 and 3; **b)** The same as a) but for the mass M_{A_b} .

10.6. Coupling and mass of the $P_c(0^-)$ four-quark state

Like in the previous cases, we study the coupling and mass of the pseudoscalar $P_c(0^-)$ four-quark state which we show in Figs. 77 to 82. The results are summarized in Tables 9 and 13.

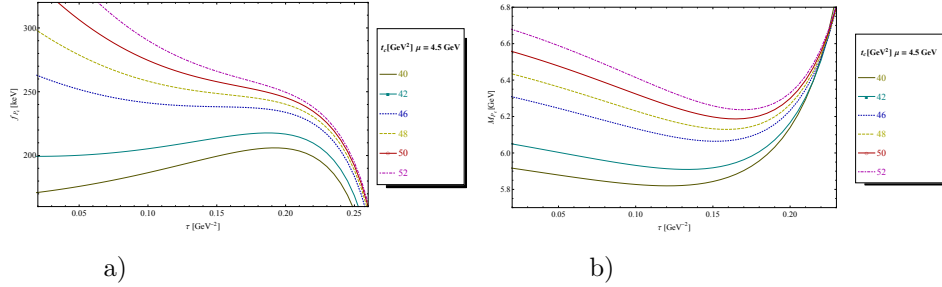


Fig. 77. **a)** f_{P_c} at LO as function of τ for different values of t_c , for $\mu = 4.5 \text{ GeV}$ and for the QCD parameters in Tables 2 and 3; **b)** The same as a) but for the mass M_{P_c} .

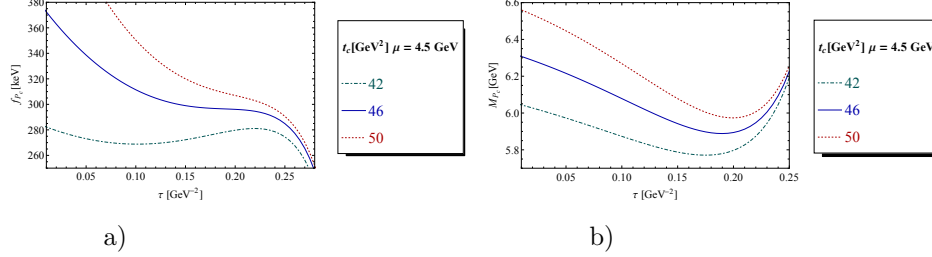


Fig. 78. **a)** f_{P_c} at NLO as function of τ for different values of t_c , for $\mu = 4.5$ GeV and for the QCD parameters in Tables 2 and 3; **b)** The same as a) but for the mass M_{P_c} .

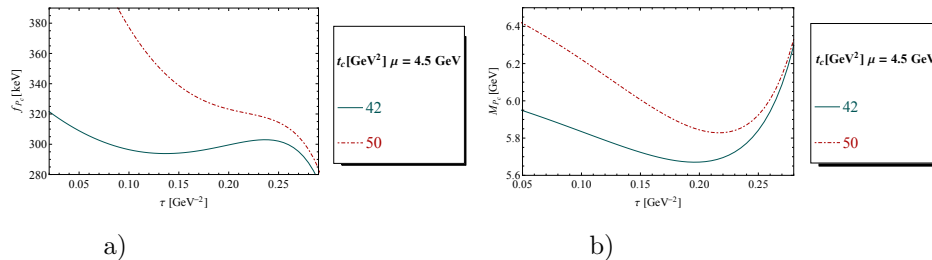


Fig. 79. **a)** f_{P_c} at N2LO as function of τ for different values of t_c , for $\mu = 4.5$ GeV and for the QCD parameters in Tables 2 and 3; **b)** The same as a) but for the mass M_{P_c} .

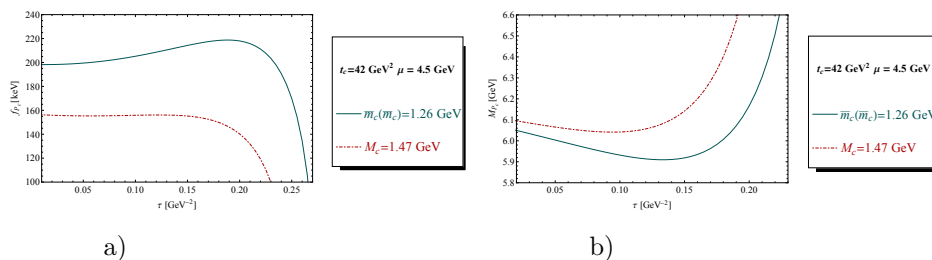


Fig. 80. **a)** f_{P_c} at LO as function of τ for $t_c = 42 \text{ GeV}^2$, for $\mu = 4.5$ GeV, for values of the running $\bar{m}_c(\bar{m}_c) = 1.26$ GeV and pole mass $M_c = 1.47$ GeV. We use the QCD parameters in Tables 2 and 3; **b)** The same as a) but for the mass M_{P_c} .

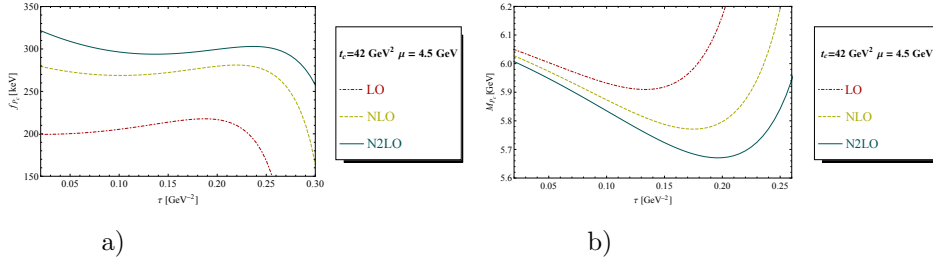


Fig. 81. **a**) f_{P_c} as function of τ for a given value of $t_c = 42 \text{ GeV}^2$, for $\mu = 4.5 \text{ GeV}$, for different truncation of the PT series and for the QCD parameters in Tables 2 and 3; **b**) The same as a) but for the mass M_{P_c} .

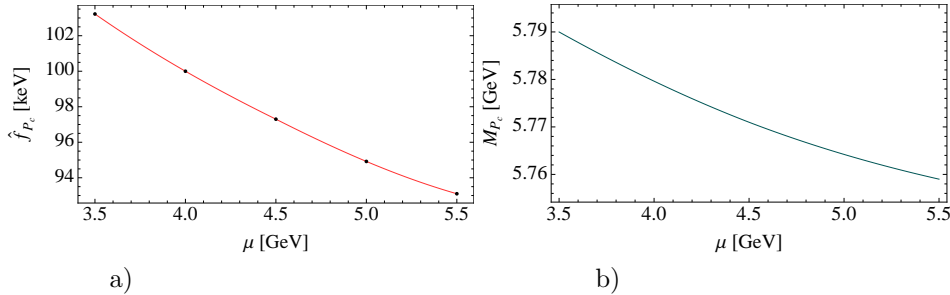


Fig. 82. **a)** Renormalization group invariant coupling \hat{f}_{P_c} at NLO as function of μ , for the corresponding τ -stability region, for $t_c \simeq 42 \text{ GeV}^2$ and for the QCD parameters in Tables 2 and 3; **b)** The same as a) but for the mass M_{P_c} .

10.7. Coupling and mass of the $P_b(0^-)$ four-quark state

We extend the analysis to the b -quark sector which we show in Figs. 83 to 88. The results are summarized in Tables 10 and 14.

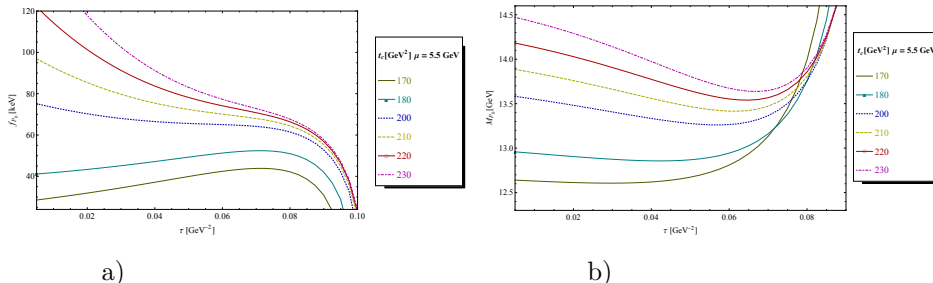


Fig. 83. **a)** f_{P_b} at LO as function of τ for different values of t_c , for $\mu = 5.5$ GeV and for the QCD parameters in Tables 2 and 3; **b)** The same as a) but for the mass M_{P_b} .

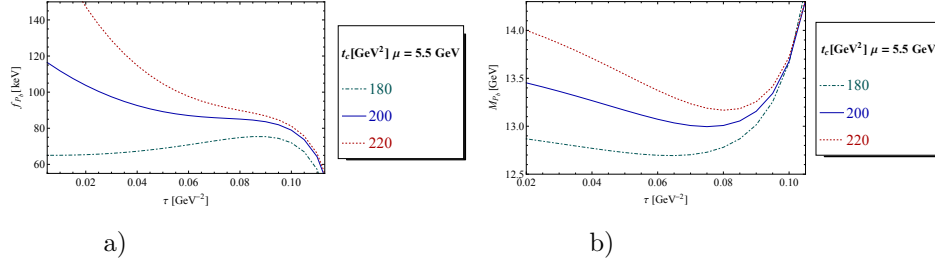


Fig. 84. **a)** f_{P_b} at NLO as function of τ for different values of t_c , for $\mu = 5.5$ GeV and for the QCD parameters in Tables 2 and 3; **b)** The same as a) but for the mass M_{P_b} .

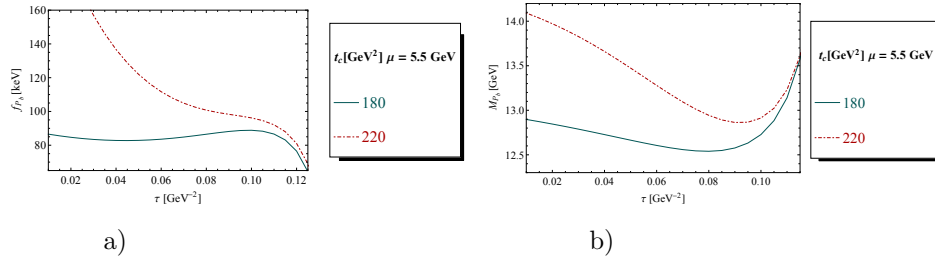


Fig. 85. **a)** f_{P_b} at N2LO as function of τ for different values of t_c , for $\mu = 5.5$ GeV and for the QCD parameters in Tables 2 and 3; **b)** The same as a) but for the mass M_{P_b} .

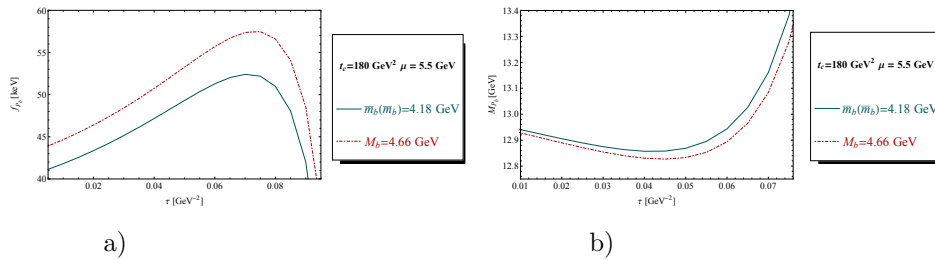


Fig. 86. **a)** f_{P_b} at LO as function of τ for $t_c = 170 \text{ GeV}^2$, for $\mu = 5.5$ GeV, for values of the running $\overline{m}_b(\overline{m}_b) = 4.18 \text{ GeV}$ and pole mass $M_b = 4.66 \text{ GeV}$. We use the QCD parameters in Tables 2 and 3; **b)** The same as a) but for the mass M_{P_b} .

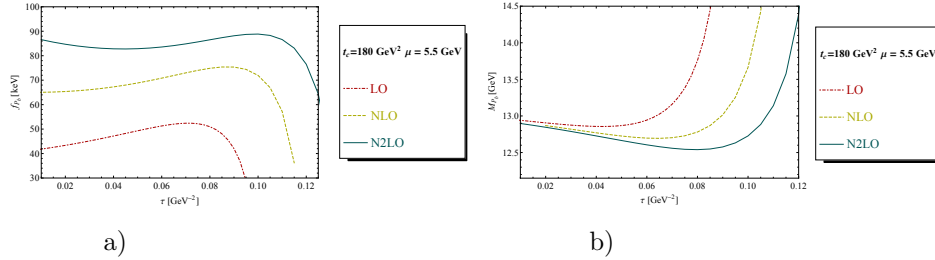


Fig. 87. **a**) f_{P_b} as function of τ for a given value of $t_c = 170 \text{ GeV}^2$, for $\mu = 5.5 \text{ GeV}$, for different truncation of the PT series and for the QCD parameters in Tables 2 and 3; **b**) The same as a) but for the mass M_{P_b} .

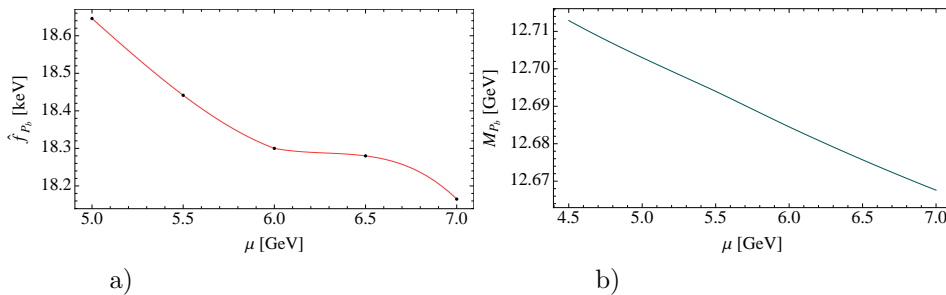


Fig. 88. **a)** Renormalization group invariant coupling \hat{f}_{P_b} at NLO as function of μ , for the corresponding τ -stability region, for $t_c \simeq 170 \text{ GeV}^2$ and for the QCD parameters in Tables 2 and 3; **b)** The same as a) but for the mass M_{P_b} .

10.8. Coupling and mass of the $V_c(1^-)$ four-quark state

Like in the previous cases, we study the coupling and mass of the vector $V_c(1^-)$ four-quark state which we show in Figs. 89 to 94. The results are summarized in Tables 9 and 13.

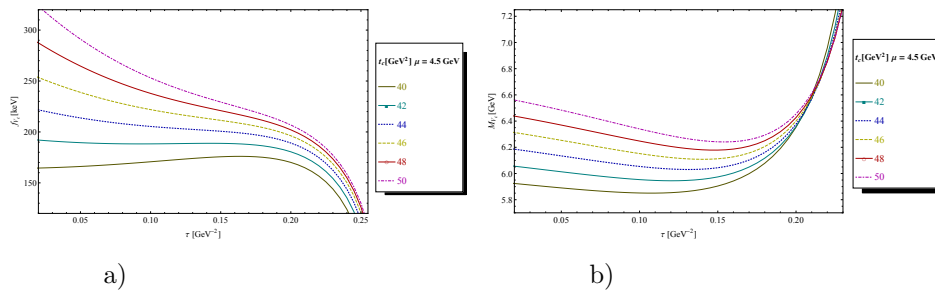


Fig. 89. a) f_{V_c} at LO as function of τ for different values of t_c , for $\mu = 4.5$ GeV and for the QCD parameters in Tables 2 and 3; b) The same as a) but for the mass M_{V_c} .

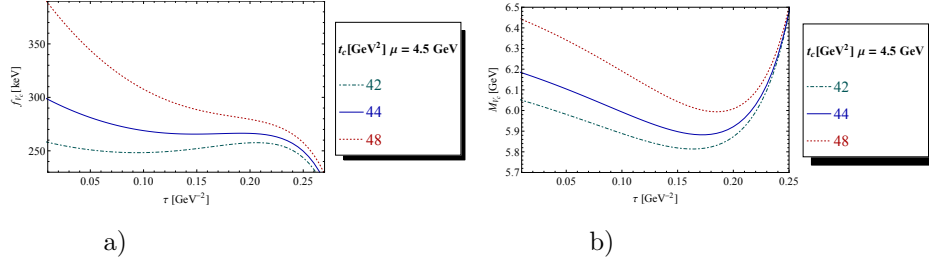


Fig. 90. **a)** f_{V_c} at NLO as function of τ for different values of t_c , for $\mu = 4.5$ GeV and for the QCD parameters in Tables 2 and 3; **b)** The same as a) but for the mass M_{V_c} .

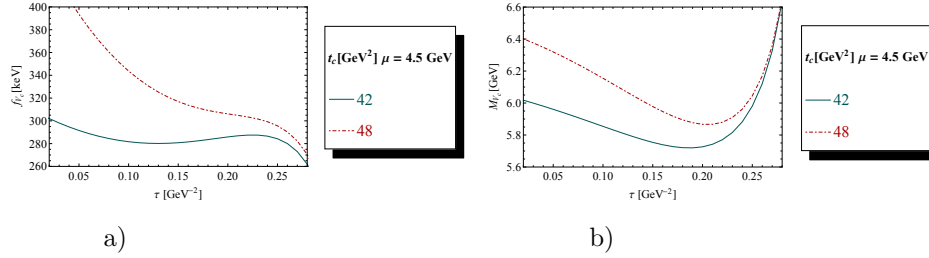


Fig. 91. **a)** f_{V_c} at N2LO as function of τ for different values of t_c , for $\mu = 4.5$ GeV and for the QCD parameters in Tables 2 and 3; **b)** The same as a) but for the mass M_{V_c} .

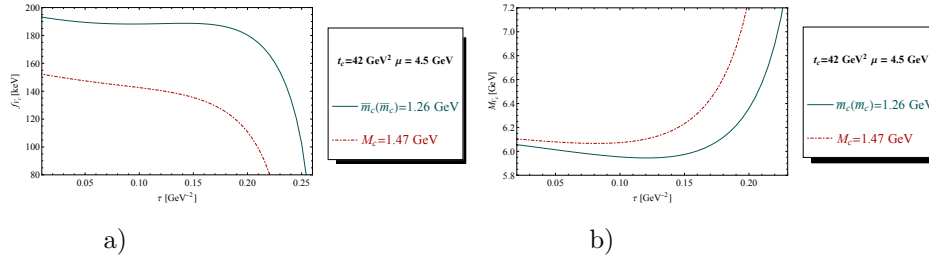


Fig. 92. **a)** f_{V_c} at LO as function of τ for $t_c = 42$ GeV 2 , for $\mu = 4.5$ GeV, for values of the running $\bar{m}_c(\bar{m}_c) = 1.26$ GeV and pole mass $M_c = 1.47$ GeV. We use the QCD parameters in Tables 2 and 3; **b)** The same as a) but for the mass M_{V_c} .

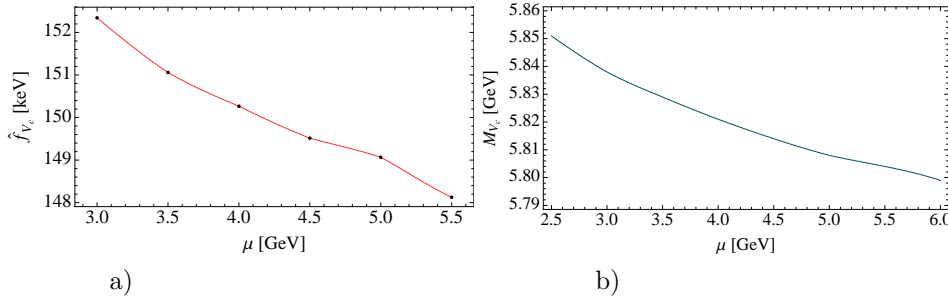


Fig. 94. **a)** Renormalization group invariant coupling \hat{f}_{V_c} at NLO as function of μ , for the corresponding τ -stability region, for $t_c \simeq 42$ GeV 2 and for the QCD parameters in Tables 2 and 3; **b)** The same as a) but for the mass M_{V_c} .

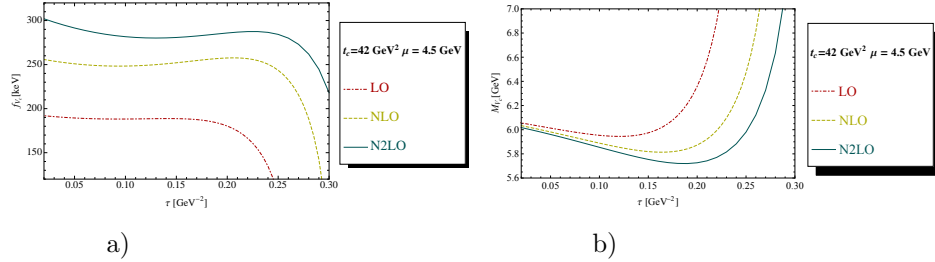


Fig. 93. a) f_{V_c} as function of τ for a given value of $t_c = 42 \text{ GeV}^2$, for $\mu = 4.5 \text{ GeV}$, for different truncation of the PT series and for the QCD parameters in Tables 2 and 3; b) The same as a) but for the mass M_{V_c} .

10.9. Coupling and mass of the $V_b(1^{--})$ four-quark state

We extend the analysis to the b -quark sector which we show in Figs. 83 to 88. The results are summarized in Tables 10 and 14.

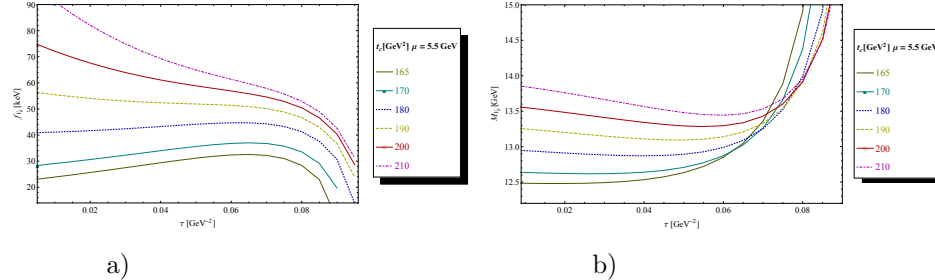


Fig. 95. a) f_{V_b} at LO as function of τ for different values of t_c , for $\mu = 5.5 \text{ GeV}$ and for the QCD parameters in Tables 2 and 3; b) The same as a) but for the mass M_{V_b} .

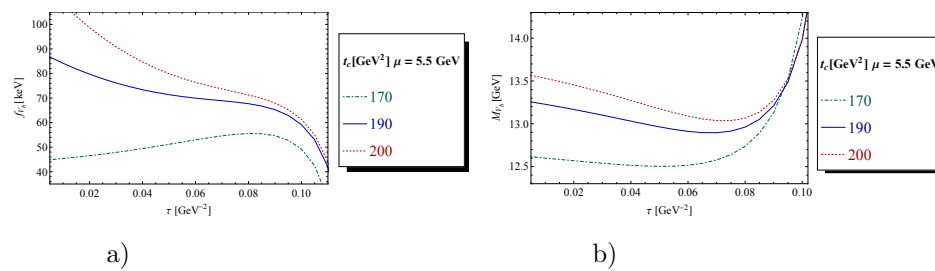


Fig. 96. a) f_{V_b} at NLO as function of τ for different values of t_c , for $\mu = 5.5 \text{ GeV}$ and for the QCD parameters in Tables 2 and 3; b) The same as a) but for the mass M_{V_b} .

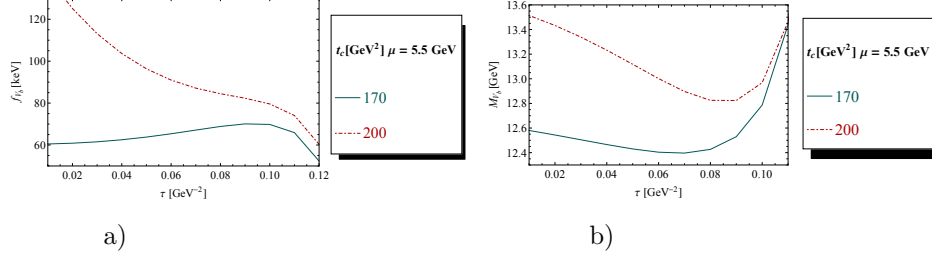


Fig. 97. a) f_{V_b} at N2LO as function of τ for different values of t_c , for $\mu = 5.5$ GeV and for the QCD parameters in Tables 2 and 3; b) The same as a) but for the mass M_{V_b} .

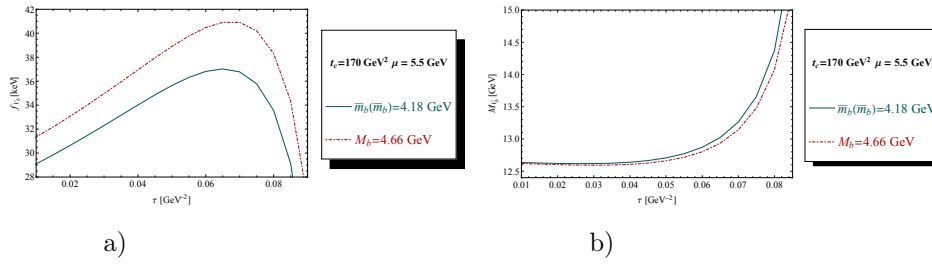


Fig. 98. a) f_{V_b} at LO as function of τ for $t_c = 170$ GeV 2 , for $\mu = 5.5$ GeV, for values of the running $\bar{m}_b(\bar{m}_b) = 4.18$ GeV and pole mass $M_b = 4.66$ GeV. We use the QCD parameters in Tables 2 and 3; b) The same as a) but for the mass M_{V_b} .

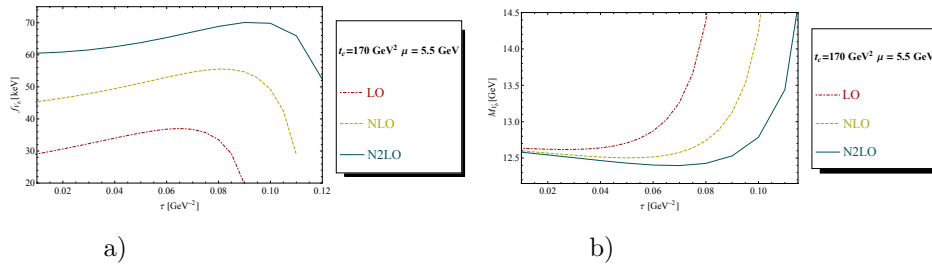


Fig. 99. a) f_{V_b} as function of τ for a given value of $t_c = 170$ GeV 2 , for $\mu = 5.5$ GeV, for different truncation of the PT series and for the QCD parameters in Tables 2 and 3; b) The same as a) but for the mass M_{V_b} .

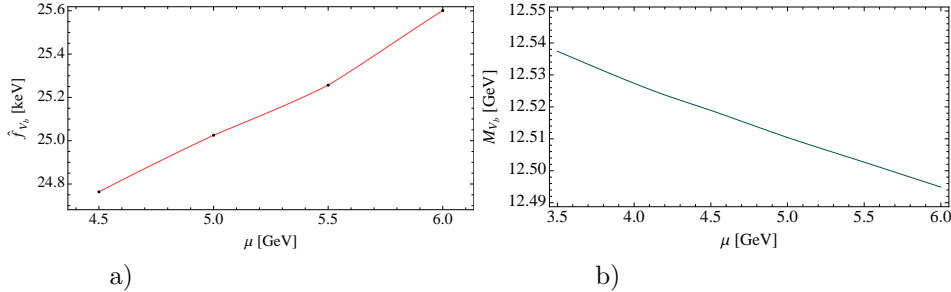


Fig. 100. **a)** Renormalization group invariant coupling \hat{f}_{V_b} at NLO as function of μ , for the corresponding τ -stability region, for $t_c \simeq 170$ GeV 2 and for the QCD parameters in Tables 2 and 3; **b)** The same as a) but for the mass M_{V_b} .

Table 5. Different sources of errors for the estimate of the 0^{++} and 1^{++} $\bar{D}D$ -like molecule masses (in units of MeV) and couplings $f_{MM}(\mu)$ (in units of keV).

Inputs [GeV] ^d	ΔM_{DD}	Δf_{DD}	$\Delta M_{D^* D^*}$	$\Delta f_{D^* D^*}$	$\Delta M_{D^* D}$	$\Delta f_{D^* D}$	$\Delta M_{D_0^* D_1}$	$\Delta f_{D_0^* D_1}$	$\Delta M_{D_0^* D_0^*}$	$\Delta f_{D_0^* D_0^*}$
<i>LSR parameters</i>										
(t_c, τ)	6	7.9	17.4	9.4	3.4	7.6	12.2	2.6	0.67	3.5
$\mu = (4.5 \pm 0.5)$	23	0.32	22.5	3.1	26	2.5	20.5	0.2	2.0	2.0
<i>QCD inputs</i>										
m_c	10.48	4.43	7.44	7.12	10.28	4.05	4.78	2.18	7.78	2.30
α_s	11.66	3.56	11.46	5.83	11.74	3.36	16.32	1.36	14.10	1.24
$N3LO$	0.0	0.35	0.0	0.99	0.0	0.07	0.0	8.67	0.00	11.16
$\langle \bar{q}q \rangle$	6.83	1.94	5.05	1.73	7.89	1.63	12.5	3.8	6.63	4.69
$\langle \alpha_s G^2 \rangle$	1.65	0.63	1.23	0.76	0.21	0.04	0.63	0.1	0.05	1.74
M_0^2	5.64	0.16	4.08	2.36	5.84	1.18	16.09	1.69	13.68	0.23
$\langle \bar{q}q \rangle^2$	3.0	10.4	2.0	25	9.5	10.5	23.5	11.4	6.3	16.5
$\langle g^3 G^3 \rangle$	0.07	0.1	0.11	0.22	0.03	0.07	0.04	0.13	0.51	0.16
$d \geq 8$	19.0	2.1	176	37	52	9.0	158.5	5.6	47	7.5
<i>Total errors</i>	35.5	14.55	178.95	46.77	61.82	16.94	164.16	16.35	53.70	22.39

Table 6. Different sources of errors for the estimate of the 0^{++} and 1^{++} $\bar{B}B$ -like molecule masses (in units of MeV) and couplings $f_{MM}(\mu)$ (in units of keV).

Inputs [GeV] ^d	$\Delta M_{\bar{B}B}$	$\Delta f_{\bar{B}B}$	$\Delta M_{B^*B^*}$	$\Delta f_{B^*B^*}$	ΔM_{B^*B}	Δf_{B^*B}	$\Delta M_{B_0^*B_1}$	$\Delta f_{B_0^*B_1}$	$\Delta M_{B_0^*B_0^*}$	$\Delta f_{B_0^*B_0^*}$
<i>LSR parameters</i>										
(t_c, τ)	54	1.6	102	5.3	44	5.3	122	0.2	0.50	0.16
$\mu = (6.0 \pm 0.5)$	5	2.01	7	0.01	71	0.3	43	0.04	3.0	0.5
<i>QCD inputs</i>										
\tilde{m}_b	2.08	0.08	2.10	0.15	2.85	0.08	1.66	0.08	2.07	0.05
α_s	10.51	0.28	11.01	0.49	12.68	0.31	15.16	0.25	16.30	0.19
$N3LO$	0.0	0.12	0.0	0.22	0.02	0.14	0.01	1.13	0.00	1.11
$\langle \bar{q}q \rangle$	4.24	0.20	2.85	0.21	8.43	0.12	4.05	0.41	3.55	0.23
$\langle \alpha_s G^2 \rangle$	0.50	0.02	0.37	0.02	0.03	0.0	0.03	0.0	1.43	0.02
M_0^2	1.0	1.1	37.0	0.14	58	0.13	20.0	0.20	11.07	0.15
$\langle \bar{q}q \rangle^2$	16.0	1.64	8.0	0.92	22.9	1.15	9.5	1.88	1.95	1.58
$\langle g^3 G^3 \rangle$	0.02	0.0	0.03	0.0	0.0	0.0	0.04	0.0	0.01	0.0
$d \geq 8$	1.0	1.17	37.0	0.07	107	0.07	0.05	0.01	111	3
<i>Total errors</i>	57.72	3.46	115.71	5.41	150.18	5.44	132.18	2.26	112.88	3.62

Table 7. Different sources of errors for the estimate of the $0^{-\pm}$ and 1^{--} $\bar{D}D$ -like molecule masses (in units of MeV) and couplings $f_{MM}(\mu)$ (in units of keV). The errors for the 1^{-+} $\bar{D}_0^*D^*$ and $\bar{D}D_1$ states are similar to the 1^{--} case except for the $\langle\bar{q}q\rangle$ and $\langle\alpha_s G^2\rangle$ condensates where they are equal to zero in the latter.

Inputs [GeV] ^d	$\Delta M_{D_0^*D}$	$\Delta f_{D_0^*D}$	$\Delta M_{D^*D_1}$	$\Delta f_{D^*D_1}$	$\Delta M_{D_0^*D^*}$	$\Delta f_{D_0^*D^*}$	ΔM_{DD_1}	Δf_{DD_1}
<i>LSR parameters</i>								
(t_c, τ)	115	15.86	88.6	25.3	83.41	11.44	150	18.70
$\mu = (4.5 \pm 0.5)$	7.00	3.96	7.00	9.54	3.83	3.34	8.25	3.50
<i>QCD inputs</i>								
\bar{m}_c	14.62	5.19	15.15	10.98	14.79	5.08	13.71	4.62
α_s	3.92	2.20	4.02	4.78	4.77	2.19	4.58	2.09
$N3LO$	2.88	4.47	2.36	20.92	2.40	10.87	2.14	6.04
$\langle\bar{q}q\rangle$	0.00	0.00	0.00	0.00	0.00	0.00	0.00	0.00
$\langle\alpha_s G^2\rangle$	9.33	1.56	2.75	1.00	1.42	0.18	0.00	0.00
M_0^2	0.00	0.00	0.00	0.00	0.00	0.00	9.54	1.14
$\langle\bar{q}q\rangle^2$	68.93	4.85	72.09	9.99	53.78	3.22	56.43	3.16
$\langle g^3 G^3 \rangle$	0.85	0.11	0.95	0.24	0.81	0.10	0.75	0.10
$d \geq 8$	36.0	4.00	80.70	6.70	6.92	0.31	8.0	0.8
<i>Total errors</i>	140.17	19.00	140.94	37.70	100.81	17.36	161.62	11.63

Table 8. Different sources of errors for the estimate of the $0^{-\pm}$ and 1^{--} $\bar{B}B$ -like molecule masses (in units of MeV) and couplings $f_{MM}(\mu)$ (in units of keV). The errors for the 1^{-+} $\bar{B}_0^*B^*$ and $\bar{B}B_1$ are very similar to the ones of the 1^{--} states except for $\langle\bar{q}q\rangle$ and $\langle\alpha_s G^2\rangle$ which are zero here.

Inputs [GeV] ^d	$\Delta M_{B_0^*B}$	$\Delta f_{B_0^*B}$	$\Delta M_{B^*B_1}$	$\Delta f_{B^*B_1}$	$\Delta M_{B_0^*B^*}$	$\Delta f_{B_0^*B^*}$	ΔM_{BB_1}	Δf_{BB_1}
<i>LSR parameters</i>								
(t_c, τ)	254.25	8.66	213.75	14.97	260.85	9.17	249	10.57
$\mu = (5.5 \pm 0.5)$	8.50	1.11	8.00	2.17	8.25	1.11	8.5	1.0
<i>QCD inputs</i>								
\bar{m}_b	1.59	0.19	1.49	0.36	1.45	0.18	1.60	0.19
α_s	3.35	0.52	3.22	1.00	3.24	0.49	3.40	0.56
$N3LO$	2.60	4.79	1.97	6.98	1.96	4.74	2.23	4.23
$\langle\bar{q}q\rangle$	0.00	0.00	0.00	0.00	0.00	0.00	0.00	0.00
$\langle\alpha_s G^2\rangle$	1.47	0.055	0.63	0.051	0.055	0.00	0.00	0.00
M_0^2	0.00	0.00	0.00	0.00	0.00	0.00	1.95	0.050
$\langle\bar{q}q\rangle^2$	49.32	0.65	44.05	1.15	39.12	0.50	49.32	0.63
$\langle g^3 G^3 \rangle$	0.035	0.00	0.04	0.002	0.031	0.00	0.04	0.00
$d \geq 8$	22.00	0.79	53.40	8.60	32.0	1.77	39.0	2.0
<i>Total errors</i>	260.11	10.04	224.86	18.81	265.86	10.56	257.0	11.64

Table 9. Different sources of errors for the estimate of the four-quark $[cq\bar{c}\bar{q}]$ (pseudo)scalar $S_c(P_c)$ and (axial) vector $V_c(A_c)$ states, masses (in units of MeV) and couplings $f(\mu)$ (in units of keV); $q \equiv u, d$.

Inputs [GeV] ^d	ΔM_{S_c}	Δf_{S_c}	ΔM_{A_c}	Δf_{A_c}	ΔM_{P_c}	Δf_{P_c}	ΔM_{V_c}	Δf_{V_c}
<i>LSR parameters</i>								
(t_c, τ)	0.2	9.3	0.23	9.31	101.3	5.66	90.01	14.00
$\mu = (4.5 \pm 0.5)$	0.94	8.12	26.86	8.33	7.7	4.35	6.31	4.24
<i>QCD inputs</i>								
\bar{m}_c	10.22	4.97	10.04	4.61	15.46	6.25	14.59	5.69
α_s	11.75	4.05	11.73	3.85	4.01	2.60	3.34	2.28
$N3LO$	0.00	0.41	0.38	0.72	3.55	4.56	2.89	8.61
$\langle\bar{q}q\rangle$	7.58	1.96	8.10	1.77	0.0	0.0	0.13	0.19
$\langle\alpha_s G^2\rangle$	0.52	0.35	0.50	0.048	3.73	0.66	0.84	0.21
M_0^2	6.27	1.39	6.12	1.91	0.0	0.0	6.66	0.84
$\langle\bar{q}q\rangle^2$	1.4	14.62	93.94	14.87	73.37	6.09	71.97	5.50
$\langle g^3 G^3 \rangle$	0.03	0.09	0.03	0.09	0.92	0.14	0.82	0.12
$d \geq 8$	5.60	0.07	83.0	22.0	10.0	1.0	37.0	3.0
<i>Total errors</i>	54.25	20.34	129.53	30.08	126.83	12.50	122.35	19.13

Table 10. Different sources of errors for the estimate of the four-quark $[b\bar{q}\bar{b}\bar{q}]$ (pseudo)scalar $S_b(P_b)$ and (axial) vector $V_b(A_b)$ states, masses (in units of MeV) and couplings $f(\mu)$ (in units of keV); $q \equiv u, d$.

Inputs [GeV] ^d	ΔM_{S_b}	Δf_{S_b}	ΔM_{A_b}	Δf_{A_b}	ΔM_{P_b}	Δf_{P_b}	ΔM_{V_b}	Δf_{V_b}
<i>LSR parameters</i>								
(t_c, τ)	0.10	0.14	8.9	0.87	235	9	213.6	7.60
$\mu = (5.5 \pm 0.5)$	2.9	1.0	43.65	0.99	9.0	1.65	7.75	1.28
<i>QCD inputs</i>								
\bar{m}_b	2.85	0.09	2.59	0.091	2.01	0.29	1.47	0.21
α_s	13.20	0.35	12.30	0.35	4.06	0.79	3.12	0.56
$N3LO$	0.00	0.13	0.30	0.00	4.54	3.88	1.10	3.94
$\langle \bar{q}q \rangle$	7.39	0.15	7.33	0.16	0.0	0.0	0.18	0.022
$\langle \alpha_s G^2 \rangle$	0.10	0.005	0.12	0.0035	0.54	0.02	0.29	0.014
M_0^2	7.02	0.16	7.46	0.17	0.0	0.0	1.23	0.036
$\langle \bar{q}q \rangle^2$	1.2	1.47	112.82	1.42	69.01	1.24	43.77	0.66
$\langle g^3 G^3 \rangle$	0.002	0.0	0.0035	0.001	0.05	0.002	0.032	0.001
$d \geq 8$	108	3	120.4	2.3	68.0	3.35	105.0	1.5
<i>Total errors</i>	109.37	3.52	171.68	3.03	254.43	10.60	242.16	8.83

Table 11. $\bar{D}D$ -like molecules masses, invariant and running couplings from LSR within stability criteria at LO to N2LO of PT. The errors are the quadratic sum of the ones in Tables 5 and 7.

Nature	\hat{f}_X [keV]						Mass [MeV]			Threshold	Exp.
	LO	NLO	N2LO	LO	NLO	N2LO	LO	NLO	N2LO		
$J^{PC} = 0^{++}$											
$\bar{D}D$	56	60	62(6)	155	164	170(15)	3901	3901	3898(36)	3739	—
\bar{D}^*D^*	—	—	—	269	288	302(47)	3901	3903	3903(179)	4020	
$D_0^*D_0^*$	27	42	50(8)	74	116	136(22)	4405	4402	4398(54)	4636	
$J^{PC} = 1^{+\pm}$											
\bar{D}^*D	87	93	97(10)	146	154	161(17)	3901	3901	3903(62)	3880	X_c, Z_c
$D_0^*D_1$	48	71	83(10)	81	118	137(16)	4394	4395	4401(164)	4739	
$J^{PC} = 0^{-\pm}$											
\bar{D}_0^*D	68	88	94(7)	190	240	257(19)	5956	5800	5690(140)	4188	—
\bar{D}^*D_1	—	—	—	382	490	564(38)	6039	5898	5797(141)	4432	
$J^{PC} = 1^{--}$											
$\bar{D}_0^*D^*$	112	143	157(10)	186	238	261(17)	6020	5861	5748(101)	4328	Y_c
$\bar{D}D_1$	98	126	139(13)	164	209	231(21)	5769	5639	5544(162)	4291	
$J^{PC} = 1^{-+}$											
\bar{D}^*D^*	105	135	150(13)	174	224	249(22)	6047	5920	5828(132)	4328	Y_c
$\bar{D}D_1$	97	128	145(15)	162	213	241(25)	5973	5840	5748 (179)	4328	

Table 12. $\bar{B}B$ -like molecules masses, invariant and running couplings from LSR within stability criteria from LO to N2LO of PT. The errors are the quadratic sum of the ones in Tables 6 and 8.

Nature	\hat{f}_X [keV]			$f_X(5.5)$ [keV]			Mass [MeV]			Threshold	Exp.
	LO	NLO	N2LO	LO	NLO	N2LO	LO	NLO	N2LO		
$J^{PC} = 0^{++}$											
$\bar{B}B$	4.0	4.4	5(1)	14.4	15.6	17(4)	10605	10598	10595(58)	10559	—
\bar{B}^*B^*	—	—	—	27	30	32(5)	10626	10646	10647(184)	10650	—
$B_0^*B_0^*$	2.1	3.2	4(1)	7.7	11.3	14(4)	10653	10649	10648(113)	—	—
$J^{PC} = 1^{+\pm}$											
\bar{B}^*B	7	8	9(3)	14	16	17(5)	10680	10673	10646(150)	10605	X_b, Z_b
$\bar{B}_0^*B_1$	4	6	7(1)	8	11	14(2)	10670	10679	10692(132)	—	—
$J^{PC} = 0^{-\pm}$											
\bar{B}_0^*B	11	16	20(3)	39	55	67(10)	12930	12737	12562(260)	—	—
\bar{B}^*B_1	—	—	—	71	105	136(19)	12967	12794	12627(225)	11046	—
$J^{PC} = 1^{--}$											
$\bar{B}_0^*B^*$	21	29	35(6)	39	54	66(11)	12936	12756	12592(266)	—	Y_b
$\bar{B}B_1$	21	29	35(7)	39	54	65(12)	12913	12734	12573(257)	11000	—
$J^{PC} = 1^{-+}$											
$\bar{B}_0^*B^*$	20	29	34(4)	38	54	64(8)	12942	12774	12617(220)	—	Y_b
BB_1	20	29	35(5)	37	53	65(9)	12974	12790	12630(236)	11000	—

Table 13. Four-quark masses, invariant and running couplings from LSR within stability criteria from LO to N2LO of PT. The errors are the quadratic sum of the ones in Tables 5 and 7.

Nature	\hat{f}_X [keV]			$f_X(4.5)$ [keV]			Mass [MeV]			Exp.
	LO	NLO	N2LO	LO	NLO	N2LO	LO	NLO	N2LO	
c-quark										
$S_c(0^+)$	62	67	70(7)	173	184	191(20)	3902	3901	3898(54)	—
$A_c(1^+)$	100	106	112(18)	166	176	184(30)	3903	3890	3888(130)	X_c, Z_c
$P_c(0^-)$	84	106	113(5)	233	292	310(13)	6048	5872	5750(127)	—
$V_c(1^-)$	123	162	178(11)	205	268	296(19)	6062	5904	5793(122)	Y_c

Table 14. Four-quark masses, invariant and running couplings from LSR within stability criteria from LO to N2LO of PT. The errors are the quadratic sum of the ones in Tables 5 and 7.

Nature	\hat{f}_X [keV]			$f_X(5.5)$ [keV]			Mass [MeV]			Exp.
	LO	NLO	N2LO	LO	NLO	N2LO	LO	NLO	N2LO	
\bar{b}-quark										
$S_b(0^+)$	4.6	5.0	5.3(1.1)	16	17	19(4)	10652	10653	10654(109)	—
$A_b(1^+)$	8.7	9.5	10(2)	16	18	19(3)	10730	10701	10680(172)	Z_b
$P_b(0^-)$	18	23	27(3)	62	83	94(11)	13186	12920	12695(254)	—
$V_b(1^-)$	24	33	40(5)	45	62	75(9)	12951	12770	12610(242)	Y_b

11. Confrontation with the data and some LO results

11.1. Axial-vector (1^{++}) states

As mentioned in the introduction, there are several observed states in this channel. In addition to the well-established $X_c(3872)$, we have the $X_c(4147, 4273)$ and the

$Z_c(3900, 4025, 4050, 4430)$.

- For the non-strange states found from their decays into $J/\psi\pi^+\pi^-$, one can conclude from the results given in Table 11 that the $X_c(3872)$ and $Z_c(3900)$ can be well described with an almost pure \bar{D}^*D molecule or/and four quark [$cq\bar{c}\bar{q}$] states, ($q \equiv u, d$) while the one of the $Z_c(4200, 4430)$ might be a $\bar{D}_0^*D_1$ molecule state. Our result for the $X_c(3872)$ confirm our previous LO results in.^{69–71}
- One can notice that the values of these masses below the corresponding $\bar{D}D$, $\bar{B}B$ -like thresholds are much lower than the ones predicted $\simeq 5.12$ (resp 11.32) GeV for the 1^{++} $\bar{c}gc$ (resp. $\bar{b}gb$) hybrid mesons.^{96, 202–205}
- Assuming that the value of $\sqrt{t_c} \approx 6 - 7$ GeV, where the optimal values of the masses have been extracted, are approximately the mass of the 1st radial excitation, one can deduce that the higher masses experimental states cannot be such radial excitations.
- In the bottom sector, experimental checks of our predictions are required.

11.2. *Scalar (0^{++}) states*

Our analysis in Tables 11 and 14 predicts that:

- The 0^{++} $\bar{D}D$, \bar{D}^*D^* molecule and four-quark non-strange states are almost degenerated with the 1^{++} ones and have masses around 3900 MeV. This prediction is comparable with the $Z_c(3900)$ quoted by PDG⁷ as a 0^{++} state.
- The predicted mass of the $\bar{D}_0^*D_0^*$ molecule is higher [4402(30) MeV] but is still below the $\bar{D}_0^*D_0^*$ threshold.

11.3. *Vector ($1^{-\pm}$) states*

Our predictions in Tables 11 to 14 for molecules and four-quark vector states in the range of (5646-5961) MeV are too high compared with the observed $Y_c(4140)$ to $Y_c(4660)$ states. Our N2LO results confirm previous LO ones in^{72, 73, 115} but do not support the result in⁴⁵ which are too low. Our results indicate that the observed states might result from a mixing of the molecule / four-quark with ordinary quarkonia-states (if the description of these states in terms of molecules and/or four-quark states are the correct one). The NP contribution to this kind of mixing has been estimated to leading order in.¹¹⁹ The same conclusion holds for the $Y_b(9898, 10260, 10870)$ where the predicted unmixed molecule / four-quark states are in the range (12326-12829) MeV. As these pure molecule states are well above the physical threshold, they should be broad and may be difficult to separate from backgrounds. They might not even be bound states, a result which goes in lines with the one of.²⁰⁸

11.4. *Pseudoscalar ($0^{-\pm}$) states*

- One expects from Tables 11 to 14 that the $0^{-\pm}$ molecules will populate the region 5656-6020 (resp 12379-12827) MeV for the charm (resp bottom) channels

like in the case of the $1^{-\pm}$ vector states. One can notice that these states are much heavier than the predicted 0^- hybrid $\bar{c}gc$ (resp. $\bar{b}gb$) ones $\simeq 3.82$ (resp. $\simeq 10.64$) GeV from QSSR.^{96,203–205,209} Like in the case of vector states, these pseudoscalar states are well above the physical threshold. Therefore, like in the case of vector states, these molecule states should be broad and may be difficult to separate from backgrounds or / and eventually weakly bounded.

- One can also notice that the $D_0^*D(0^{--})$ and (0^{-+}) states are almost degenerate despite the opposite signs of the $\langle\bar{q}q\rangle$ and $\langle\bar{q}Gq\rangle$ contributions to the spectral functions in the two channels (see Appendix A.6).

11.5. Isospin breakings and almost degenerate states

In our approach, isospin breakings are controlled by the running light quark mass $\bar{m}_d - \bar{m}_u$ and condensate $\langle\bar{u}u - \bar{d}d\rangle$ differences which are tiny quantities. Their effects are hardly noticeable within the accuracy of our approach. Therefore, for the neutral combination of currents which we have taken in Table 1, one expects that the molecules built from the corresponding charged currents will be degenerate in masses because their QCD expressions are the same in the chiral limit.

11.6. Radial excitations

If one consider the value of the continuum threshold t_c , at which the optimal value of the ground state is obtained (see their values in the corresponding figures), as an approximate value of the mass of the 1st radial excitation, one expects that the radial excitations are in the region of about 0.4 to 1.6 GeV above the ground state mass. A more accurate prediction can be obtained by combining LSR with Finite Energy Sum Rule (FESR)^{69,70,72,73} where the mass-splitting is expected to be around 250-300 MeV at LO. Among these different observed states, the $Z_c(4430)$ and $X_c(4506, 4704)$ could eventually be considered as radial excitation candidates.

12. Quark Mass Behaviour of the Decay Constants

The couplings or decay constants given in Tables 11 to 14 are normalized in Eq. 13 in the same way as $f_\pi = 130.4(2)$ MeV through its coupling to the pseudoscalar current : $\langle 0 | (m_u + m_d) \bar{u}(i\gamma_5) d | \pi \rangle = f_\pi m_\pi^2 \phi_\pi(x)$, where $\phi_\pi(x)$ is the pion field.

- One can find from Table 11 that $f_{DD} \simeq 170(15)$ keV which is about 10^{-3} of f_π and of $f_B \simeq f_D \simeq 206(7)$ MeV.^{159,160,164,165,168–170} The same observation holds for the other molecule and four-quark states indicating the weak coupling of these states to the associated interpolating currents.

• Comparing the size of the couplings in the c and b quark channels in Tables 11 to 14, one can observe that the ratio decreases by a factor about 10 from the c to the b channels for the 0^{++} and 1^{++} states which is about the value of the ratio $(m_b/m_c)^{3/2}$, while it decreases but about a factor 4 for the 0^{--} and 1^{--} states which is about the value (m_b/m_c) . These behaviours can be compared with the

well-known one of f_B from HQET and can motivate further theoretical studies of the molecule and four-quark state couplings.

13. Summary and Conclusions

We have systematically revisited in this paper the LO estimate of the molecule and four-quark state masses and couplings using QCD Laplace sum rule (LSR) at N2LO of PT and including the non-perturbative (NP) contributions of condensates having dimension $\leq 6\text{-}8$.

- The different PT and NP QCD expressions at LO of the spectral functions corresponding to the interpolating currents given in Tables 1 and 4 used in the analysis are given in integrated compact forms in the Appendix. They are new and more suitable for a phenomenological analysis than the non-integrated forms given in the existing literature.
- Due to the technical difficulties for evaluating directly the PT $(\alpha_s)^n$ corrections, we have assumed the factorization of the four-quark spectral function into the convolution of two spectral functions built from bilinear currents. We have tested the accuracy of this assumption in Section 4 leading to the conclusions that it can provide an accurate determination of the hadron masses and decay constants. We expect that, within this assumption, one can reproduce with a good accuracy the full radiative corrections. Indeed, it has been shown in¹⁵³ that non-factorizable α_s corrections give small contribution of the order of 10% of the full α_s one, while it is also known^{95,96} that radiative corrections partially cancel in the ratio of LSR used to extract the mass of the resonance (Eq. 11) within the minimal duality ansatz approximation (MDA) for parametrizing the spectral function.
- Our results show that radiative corrections are relatively smaller for the masses than for the couplings which can explain the agreement of our results for the masses with the LO ones given in the literature. However, radiative corrections to some couplings are large which may invalidate some results on the hadronic widths from vertex sum rules where LO value of the decay constants have been used.
- Our analysis has been done within stability criteria with respect to the LSR variable τ , the QCD continuum threshold t_c and the subtraction constant μ which have provided successful predictions in different hadronic channels (see e.g. 95, 96 159, 160, 164, 165, 168–170). The optimal values of the masses and couplings have been extracted at the same value of these parameters where the stability appear as an extrema and/or inflection point. The analysis is shown in details in different Sections for transparency such that the readers can appreciate and check explicitly the procedure used for extracting the results.
- We have also studied the effects of the choice of the value of the quark masses which definitions (running or pole) are ambiguous at LO. The effects are often large for the coupling as one can inspect in the different figures given in previous Sections. The additional error induced by this ad hoc choice is always bypassed by different authors.

- We have estimated the error due to higher order PT given in Tables 7 to 10 by an estimate of the N3LO contribution based on a geometric growth of the numerical coefficients of the a_s^n terms following the works in.^{130,147–150} We can see from the estimate given for each truncation of the PT series from LO to N2LO given in Tables 11 to 14 the good convergence of the PT series.

- The error due to the high dimension condensates come from the $\langle\bar{q}q\rangle\langle\bar{q}Gq\rangle$ condensates (part of the full $d = 8$ condensate contributions) where we have assumed the same violation of factorization as that of the $\langle\bar{q}q\rangle^2$ dimension-six condensates. One can deduce from Tables 7 to 10 a good convergence of the OPE. Due to the inaccurate control of the size of high-dimension condensates, we refrain to include these contributions in our estimate but only consider them as a source of the errors.

- The results for the XYZ-like spectra are summarized in Tables 11 to 14, where one can observe that the N2LO predictions for the masses differ only slightly from the LO ones when the value of the running mass is used for the latter. However, the size of the meson couplings is strongly affected by the radiative corrections in some channels which consequently may modify the existing estimates of the meson hadronic widths based on vertex functions.

- One can notice that the masses of the $J^P = 1^+, 0^+$ states are most of them below the corresponding $\bar{D}D$, $\bar{B}B$ -like thresholds and are compatible with some of the observed XZ masses suggesting that these states can be interpreted as almost pure molecules or/and four-quark states.

- One also note that the predictions for the $J^P = 1^-, 0^-$ states are about 1.5 GeV higher than the observed Y_c mesons masses and (1.7-2.6) GeV higher than the observed Y_b ones. Our results do not favour their interpretation as pure molecule or/and four-quark states. These theoretical predictions are far above the corresponding hadronic threshold which may suggest that they are broad and then difficult to separate from backgrounds. They can also indicate that they can be weakly bounded in line with the results of.²⁰⁸

- A confrontation of our results with the observed XYZ states are done in details in Section 11.

- Finally, we observe that, normalized to $f_\pi = 130$ MeV, the $\bar{D}D$, $\bar{B}B$ -like molecule and four-quark states couple weakly to the associated interpolating currents than ordinary D , B mesons ($f_{DD} \approx 10^{-3}f_D$). Our numerical results also indicate that the corresponding decay constants behave as $1/\bar{m}_b^{3/2}$ (resp. $1/\bar{m}_b$) for the $1^+, 0^+$ (resp. $1^-, 0^-$) states compared to the usual $1/\bar{m}_b^{1/2}$ behaviour of f_B . These results can stimulate further theoretical studies of the molecule and four-quark state decay constants.

Appendix A. Molecule Spectral Functions in QCD

They are defined from Eq. 2 as: $\frac{1}{\pi}\text{Im}\Pi_{mol}^{(1)}(t)$ for spin 1 particles and $\frac{1}{\pi}\text{Im}\psi_{mol}^{(s,p)}(t)$ from Eq. 3 from spin 0 ones. In the following, we shall use the notations and definitions:

$$\begin{aligned} Q &\equiv c, b, \quad x = M_Q^2/t, \quad v = \sqrt{1-4x}, \\ \mathcal{L}_v &= \text{Log}_{(1-v)}^{(1+v)}, \quad \mathcal{L}_+ = \text{Li}_2\left(\frac{1+v}{2}\right) - \text{Li}_2\left(\frac{1-v}{2}\right). \end{aligned}$$

Appendix A.1. (0⁺⁺) $\bar{D}D$, $\bar{B}B$ Molecules

$$\begin{aligned} pert &: \frac{M_Q^8}{5 \cdot 2^{14} \pi^6} \left[v \left(480 + \frac{1460}{x} - \frac{274}{x^2} - \frac{38}{x^3} + \frac{1}{x^4} \right) \right. \\ &\quad \left. + 120\mathcal{L}_v \left(8x - 1 - 6 \text{Log}(x) - \frac{8}{x} + \frac{2}{x^2} \right) - 1440\mathcal{L}_+ \right] \\ \langle \bar{q}q \rangle &: \frac{M_Q^5 \langle \bar{q}q \rangle}{2^7 \pi^4} \left[v \left(6 - \frac{5}{x} - \frac{1}{x^2} \right) + 6\mathcal{L}_v \left(2x - 2 + \frac{1}{x} \right) \right] \\ \langle G^2 \rangle &: -\frac{M_Q^4 \langle g_s^2 G^2 \rangle}{3 \cdot 2^{11} \pi^6} \left[v \left(6 - \frac{5}{x} - \frac{1}{x^2} \right) + 6\mathcal{L}_v \left(2x - 2 + \frac{1}{x} \right) \right] \\ \langle \bar{q}Gq \rangle &: -\frac{3M_Q^3 \langle \bar{q}Gq \rangle}{2^7 \pi^4} \left[v \left(1 - \frac{3}{x} \right) + \mathcal{L}_v \left(2x + 1 + \frac{1}{x} \right) \right] \\ \langle \bar{q}q \rangle^2 &: \frac{M_Q^2 \rho \langle \bar{q}q \rangle^2 v}{2^4 \pi^2} \\ \langle G^3 \rangle &: \frac{M_Q^2 \langle g_s^3 G^3 \rangle}{3 \cdot 2^{14} \pi^6} \left[v \left(6 - \frac{25}{x} + \frac{1}{x^2} \right) + 6\mathcal{L}_v \left(2x + 2 + \frac{1}{x} \right) \right] \\ \langle \bar{q}q \rangle \langle \bar{q}Gq \rangle &: -\frac{\langle \bar{q}q \rangle \langle \bar{q}Gq \rangle}{2^5 \pi^2} v \left[1 - \frac{M_Q^2 \tau}{x} (1 - M_Q^2 \tau) \right] \end{aligned} \tag{A.1}$$

Appendix A.2. (0⁺⁺) \bar{D}^*D^* , \bar{B}^*B^* Molecules

$$\begin{aligned} pert &: \frac{M_Q^8}{5 \cdot 2^{12} \pi^6} \left[v \left(480 + \frac{1460}{x} - \frac{274}{x^2} - \frac{38}{x^3} + \frac{1}{x^4} \right) \right. \\ &\quad \left. + 120\mathcal{L}_v \left(8x - 1 - 6 \text{Log}(x) - \frac{8}{x} + \frac{2}{x^2} \right) - 1440\mathcal{L}_+ \right] \\ \langle \bar{q}q \rangle &: \frac{M_Q^5 \langle \bar{q}q \rangle}{2^6 \pi^4} \left[v \left(6 - \frac{5}{x} - \frac{1}{x^2} \right) + 6\mathcal{L}_v \left(2x - 2 + \frac{1}{x} \right) \right] \\ \langle G^2 \rangle &: \frac{M_Q^4 \langle g_s^2 G^2 \rangle}{3 \cdot 2^{10} \pi^6} \left[v \left(6 - \frac{5}{x} - \frac{1}{x^2} \right) + 6\mathcal{L}_v \left(2x - 2 + \frac{1}{x} \right) \right] \\ \langle \bar{q}Gq \rangle &: \frac{3M_Q^3 \langle \bar{q}Gq \rangle}{2^7 \pi^4} \left[\frac{v}{x} - 2\mathcal{L}_v \right] \\ \langle \bar{q}q \rangle^2 &: \frac{M_Q^2 \rho \langle \bar{q}q \rangle^2 v}{4 \pi^2} \\ \langle G^3 \rangle &: \frac{M_Q^2 \langle g_s^3 G^3 \rangle}{3 \cdot 2^{12} \pi^6} \left[v \left(6 - \frac{25}{x} + \frac{1}{x^2} \right) + 6\mathcal{L}_v \left(2x + 2 + \frac{1}{x} \right) \right] \\ \langle \bar{q}q \rangle \langle \bar{q}Gq \rangle &: -\frac{\langle \bar{q}q \rangle \langle \bar{q}Gq \rangle}{8 \pi^2} \frac{M_Q^4 \tau^2}{x} \end{aligned} \tag{A.2}$$

Appendix A.3. $(0^{++}) \bar{D}_0^* D_0^*$, $\bar{B}_0^* B_0^*$ Molecules

$$\begin{aligned}
pert &: \frac{M_Q^8}{5 \cdot 2^{14} \pi^6} \left[v \left(480 + \frac{1460}{x} - \frac{274}{x^2} - \frac{38}{x^3} + \frac{1}{x^4} \right) \right. \\
&\quad \left. + 120 \mathcal{L}_v \left(8x - 1 - 6 \operatorname{Log}(x) - \frac{8}{x} + \frac{2}{x^2} \right) - 1440 \mathcal{L}_+ \right] \\
\langle \bar{q}q \rangle &: -\frac{M_Q^5 \langle \bar{q}q \rangle}{2^7 \pi^4} \left[v \left(6 - \frac{5}{x} - \frac{1}{x^2} \right) + 6 \mathcal{L}_v \left(2x - 2 + \frac{1}{x} \right) \right] \\
\langle G^2 \rangle &: -\frac{M_Q^4 \langle g_s^2 G^2 \rangle}{3 \cdot 2^{11} \pi^6} \left[v \left(6 - \frac{5}{x} - \frac{1}{x^2} \right) + 6 \mathcal{L}_v \left(2x - 2 + \frac{1}{x} \right) \right] \\
\langle \bar{q}Gq \rangle &: \frac{3M_Q^3 \langle \bar{q}Gq \rangle}{2^7 \pi^4} \left[v \left(1 - \frac{3}{x} \right) + \mathcal{L}_v \left(2x + 1 + \frac{1}{x} \right) \right] \\
\langle \bar{q}q \rangle^2 &: \frac{M_Q^2 \rho \langle \bar{q}q \rangle^2 v}{2^4 \pi^2} \\
\langle G^3 \rangle &: \frac{M_Q^2 \langle g_s^3 G^3 \rangle}{3 \cdot 2^{14} \pi^6} \left[v \left(6 - \frac{25}{x} + \frac{1}{x^2} \right) + 6 \mathcal{L}_v \left(2x + 2 + \frac{1}{x} \right) \right] \\
\langle \bar{q}q \rangle \langle \bar{q}Gq \rangle &: -\frac{\langle \bar{q}q \rangle \langle \bar{q}Gq \rangle}{2^5 \pi^2} v \left[1 - \frac{M_Q^2 \tau}{x} (1 - M_Q^2 \tau) \right], \tag{A.3}
\end{aligned}$$

Appendix A.4. $(1^{+\pm}) \bar{D}^* D$, $\bar{B}^* B$ Molecules

The QCD spectral functions of the 1^{++} and 1^{+-} states are the same.

$$\begin{aligned}
pert &: \frac{M_Q^8}{5 \cdot 3 \cdot 2^{15} \pi^6} \left[v \left(840x + 140 + \frac{5248}{x} - \frac{1164}{x^2} - \frac{182}{x^3} + \frac{5}{x^4} \right) \right. \\
&\quad \left. + 120 \mathcal{L}_v \left(14x^2 + 15 - 18 \operatorname{Log}(x) - \frac{32}{x} + \frac{9}{x^2} \right) - 4320 \mathcal{L}_+ \right] \\
\langle \bar{q}q \rangle &: \frac{M_Q^5 \langle \bar{q}q \rangle}{3 \cdot 2^{10} \pi^4} \left[v \left(60x + 82 - \frac{94}{x} - \frac{21}{x^2} \right) + 24 \mathcal{L}_v \left(5x^2 + 6x - 9 + \frac{5}{x} \right) \right] \\
\langle G^2 \rangle &: -\frac{M_Q^4 \langle g_s^2 G^2 \rangle}{3^2 \cdot 2^{14} \pi^6} \left[v \left(60x - 62 + \frac{26}{x} + \frac{3}{x^2} \right) + 24 \mathcal{L}_v \left(5x^2 - 6x + 3 - \frac{1}{x} \right) \right] \\
\langle \bar{q}Gq \rangle &: -\frac{M_Q^3 \langle \bar{q}Gq \rangle}{3 \cdot 2^{10} \pi^4} \left[v \left(66x + 11 - \frac{86}{x} \right) + 6 \mathcal{L}_v \left(22x^2 + 9 + \frac{4}{x} \right) \right] \\
\langle \bar{q}q \rangle^2 &: \frac{M_Q^2 \rho \langle \bar{q}q \rangle^2 v}{16 \pi^2} \\
\langle G^3 \rangle &: \frac{M_Q^2 \langle g_s^3 G^3 \rangle}{3^2 \cdot 2^{16} \pi^6} \left[v \left(132x + 22 - \frac{190}{x} + \frac{9}{x^2} \right) + 24 \mathcal{L}_v \left(11x^2 + 3 + \frac{2}{x} \right) \right] \\
\langle \bar{q}q \rangle \langle \bar{q}Gq \rangle &: -\frac{\langle \bar{q}q \rangle \langle \bar{q}Gq \rangle}{2^6 \pi^2} v \left[1 - \frac{M_Q^2 \tau}{x} (1 - 2M_Q^2 \tau) \right] \tag{A.4}
\end{aligned}$$

Appendix A.5. $(1^{+\pm}) \bar{D}_0^* D_1, \bar{B}_0^* B_1$ Molecules

The QCD spectral functions of the 1^{++} and 1^{+-} states are the same.

$$\begin{aligned}
pert &: \frac{M_Q^8}{5 \cdot 3 \cdot 2^{15} \pi^6} \left[v \left(840x + 140 + \frac{5248}{x} - \frac{1164}{x^2} - \frac{182}{x^3} + \frac{5}{x^4} \right) \right. \\
&\quad \left. + 120\mathcal{L}_v \left(14x^2 + 15 - 18 \text{Log}(x) - \frac{32}{x} + \frac{9}{x^2} \right) - 4320\mathcal{L}_+ \right] \\
\langle \bar{q}q \rangle &: -\frac{M_Q^5 \langle \bar{q}q \rangle}{3 \cdot 2^{10} \pi^4} \left[v \left(60x + 82 - \frac{94}{x} - \frac{21}{x^2} \right) + 24\mathcal{L}_v \left(5x^2 + 6x - 9 + \frac{5}{x} \right) \right] \\
\langle G^2 \rangle &: -\frac{M_Q^4 \langle g_s^2 G^2 \rangle}{3^2 \cdot 2^{14} \pi^6} \left[v \left(60x - 62 + \frac{26}{x} + \frac{3}{x^2} \right) + 24\mathcal{L}_v \left(5x^2 - 6x + 3 - \frac{1}{x} \right) \right] \\
\langle \bar{q}Gq \rangle &: \frac{M_Q^3 \langle \bar{q}Gq \rangle}{3 \cdot 2^{10} \pi^4} \left[v \left(66x + 11 - \frac{86}{x} \right) + 6\mathcal{L}_v \left(22x^2 + 9 + \frac{4}{x} \right) \right] \\
\langle \bar{q}q \rangle^2 &: \frac{M_Q^2 \rho \langle \bar{q}q \rangle^2 v}{16\pi^2} \\
\langle G^3 \rangle &: \frac{M_Q^2 \langle g_s^3 G^3 \rangle}{3^2 \cdot 2^{16} \pi^6} \left[v \left(132x + 22 - \frac{190}{x} + \frac{9}{x^2} \right) + 24\mathcal{L}_v \left(11x^2 + 3 + \frac{2}{x} \right) \right] \\
\langle \bar{q}q \rangle \langle \bar{q}Gq \rangle &: -\frac{\langle \bar{q}q \rangle \langle \bar{q}Gq \rangle}{2^6 \pi^2} v \left[1 - \frac{M_Q^2 \tau}{x} \left(1 - 2M_Q^2 \tau \right) \right]
\end{aligned} \tag{A.5}$$

Appendix A.6. $(0^{-\pm}) \bar{D}_0^* D, \bar{B}_0^* B$ Molecules

The QCD spectral functions of the 0^{--} and 0^{-+} states are the same.

$$\begin{aligned}
pert &: \frac{M_Q^8}{5 \cdot 2^{14} \pi^6} \left[v \left(480 + \frac{1460}{x} - \frac{274}{x^2} - \frac{38}{x^3} + \frac{1}{x^4} \right) \right. \\
&\quad \left. + 120\mathcal{L}_v \left(8x - 1 - 6 \text{Log}(x) - \frac{8}{x} + \frac{2}{x^2} \right) - 1440\mathcal{L}_+ \right] \\
\langle \bar{q}q \rangle &: 0 \\
\langle G^2 \rangle &: -\frac{M_Q^4 \langle g_s^2 G^2 \rangle}{3 \cdot 2^{11} \pi^6} \left[v \left(6 - \frac{5}{x} - \frac{1}{x^2} \right) + 6\mathcal{L}_v \left(2x - 2 + \frac{1}{x} \right) \right] \\
\langle \bar{q}Gq \rangle &: 0 \\
\langle \bar{q}q \rangle^2 &: -\frac{M_Q^2 \rho \langle \bar{q}q \rangle^2 v}{16\pi^2} \\
\langle G^3 \rangle &: \frac{M_Q^2 \langle g_s^3 G^3 \rangle}{3 \cdot 2^{14} \pi^6} \left[v \left(6 - \frac{25}{x} + \frac{1}{x^2} \right) + 6\mathcal{L}_v \left(2x + 2 + \frac{1}{x} \right) \right] \\
\langle \bar{q}q \rangle \langle \bar{q}Gq \rangle &: \frac{\langle \bar{q}q \rangle \langle \bar{q}Gq \rangle}{2^5 \pi^2} v \left[1 - \frac{M_Q^2 \tau}{x} (1 - M_Q^2 \tau) \right].
\end{aligned} \tag{A.6}$$

Appendix A.7. $(0^{-\pm}) \bar{D}^* D_1, \bar{B}^* B_1$ Molecules

The QCD spectral functions of the 0^{--} and 0^{-+} states are the same.

$$\begin{aligned}
pert &: \frac{M_Q^8}{5 \cdot 2^{12} \pi^6} \left[v \left(480 + \frac{1460}{x} - \frac{274}{x^2} - \frac{38}{x^3} + \frac{1}{x^4} \right) \right. \\
&\quad \left. + 120 \mathcal{L}_v \left(8x - 1 - 6 \text{Log}(x) - \frac{8}{x} + \frac{2}{x^2} \right) - 1440 \mathcal{L}_+ \right], \\
\langle \bar{q}q \rangle &: 0 \\
\langle G^2 \rangle &: \frac{M_Q^4}{3 \cdot 2^{10} \pi^6} \langle g_s^2 G^2 \rangle \left[v \left(6 - \frac{5}{x} - \frac{1}{x^2} \right) + 6 \mathcal{L}_v \left(2x - 2 + \frac{1}{x} \right) \right], \\
\langle \bar{q}Gq \rangle &: 0 \\
\langle \bar{q}q \rangle^2 &: -\frac{M_Q^2}{4\pi^2} \rho \langle \bar{q}q \rangle^2 v, \\
\langle G^3 \rangle &: \frac{M_Q^2}{3 \cdot 2^{12} \pi^6} \langle g_s^3 G^3 \rangle \left[v \left(6 - \frac{25}{x} + \frac{1}{x^2} \right) + 6 \mathcal{L}_v \left(2x + 2 + \frac{1}{x} \right) \right], \\
\langle \bar{q}q \rangle \langle \bar{q}Gq \rangle &: \frac{1}{4\pi^2} \langle \bar{q}q \rangle \langle \bar{q}Gq \rangle \frac{x}{v} (x + M_Q^2 \tau). \\
\end{aligned} \tag{A.7}$$

Appendix A.8. $(1^{--}) \bar{D}_0^* D^*, \bar{B}_0^* B^*$ Molecules

The factorized expression corresponds to the value $\epsilon = 0$ and the full one to $\epsilon = 1$.

$$\begin{aligned}
pert &: \frac{M_Q^8}{5 \cdot 3 \cdot 2^{15} \pi^6} \left[v \left(840x + 140 + \frac{5248}{x} - \frac{1164}{x^2} - \frac{182}{x^3} + \frac{5}{x^4} \right) \right. \\
&\quad \left. + 120 \mathcal{L}_v \left(14x^2 + 15 - 18 \text{Log}(x) - \frac{32}{x} + \frac{9}{x^2} \right) - 4320 \mathcal{L}_+ \right] \\
&\quad - \frac{\epsilon M_Q^8}{5 \cdot 3 \cdot 2^{14} \pi^6} \left[v \left(420x - 1730 - \frac{4966}{x} - \frac{477}{x^2} - \frac{6}{x^3} \right) \right. \\
&\quad \left. + 60 \mathcal{L}_v \left(14x^2 - 60x - 12 + 12(3 + 1/x) \text{Log}(x) + \frac{56}{x} + \frac{3}{x^2} \right) + 1440(3 + 1/x) \mathcal{L}_+ \right] \\
\langle \bar{q}q \rangle &: -\frac{(1-\epsilon) M_Q^5 \langle \bar{q}q \rangle}{3 \cdot 2^{10} \pi^4} \left[v \left(60x - 62 + \frac{26}{x} + \frac{3}{x^2} \right) + 24 \mathcal{L}_v \left(5x^2 - 6x + 3 - \frac{1}{x} \right) \right] \\
\langle G^2 \rangle &: -\frac{(1-\epsilon) M_Q^4 \langle g_s^2 G^2 \rangle}{3^2 \cdot 2^{14} \pi^6} \left[v \left(60x - 62 + \frac{26}{x} + \frac{3}{x^2} \right) + 24 \mathcal{L}_v \left(5x^2 - 6x + 3 - \frac{1}{x} \right) \right] \\
\langle \bar{q}Gq \rangle &: \frac{M_Q^3 \langle \bar{q}Gq \rangle}{3 \cdot 2^{10} \pi^4} \left[v \left(66x + 11 - \frac{50}{x} \right) + 6 \mathcal{L}_v \left(22x^2 - 3 + \frac{4}{x} \right) \right] \\
&\quad - \frac{3\epsilon M_Q^3 \langle \bar{q}Gq \rangle}{2^{10} \pi^4} \left[3v(2x - 1) + 2 \mathcal{L}_v(6x^2 - 4x + 1) \right] \\
\langle \bar{q}q \rangle^2 &: -\frac{M_Q^2 \rho \langle \bar{q}q \rangle^2}{3 \cdot 2^6 \pi^2} v \left(12 + \epsilon(4 - 1/x) \right)
\end{aligned}$$

$$\begin{aligned} \langle G^3 \rangle &: \frac{M_Q^2 \langle g_s^3 G^3 \rangle}{3^2 \cdot 2^{16} \pi^6} \left[v \left(132x + 22 - \frac{190}{x} + \frac{9}{x^2} \right) + 24\mathcal{L}_v \left(11x^2 + 3 + \frac{2}{x} \right) \right] \\ &\quad - \frac{\epsilon M_Q^2 \langle g_s^3 G^3 \rangle}{3^2 \cdot 2^{16} \pi^6} \left[v \left(204x - 182 + \frac{2}{x} + \frac{3}{x^2} \right) + 24\mathcal{L}_v \left(17x^2 - 18x + 9 - \frac{1}{x} \right) \right] \\ \langle \bar{q}q \rangle \langle \bar{q}Gq \rangle &: \frac{\langle \bar{q}q \rangle \langle \bar{q}Gq \rangle}{2^6 \pi^2} v \left[1 - \frac{M_Q^2 \tau}{x} \left(1 - 2M_Q^2 \tau \right) - \epsilon(x + M_Q^2 \tau) \right] \end{aligned} \quad (\text{A.8})$$

Appendix A.9. $(1^{-+}) \bar{D}_0^* D^*$, $\bar{B}_0^* B^*$ Molecules

$$\begin{aligned} pert &: \frac{M_Q^8}{5 \cdot 3 \cdot 2^{15} \pi^6} \left[v \left(1680x - 3320 - \frac{4684}{x} - \frac{2118}{x^2} - \frac{194}{x^3} + \frac{5}{x^4} \right) \right. \\ &\quad \left. + 120\mathcal{L}_v \left(28x^2 - 60x + 3 + 6 \left(3 + \frac{2}{x} \right) \text{Log}(x) + \frac{24}{x} + \frac{12}{x^2} \right) + 1440 \left(3 + \frac{2}{x} \right) \mathcal{L}_+ \right] \\ \langle \bar{q}q \rangle &: -\frac{M_Q^5 \langle \bar{q}q \rangle}{3 \cdot 2^9 \pi^4} \left[v \left(60x - 62 + \frac{26}{x} + \frac{3}{x^2} \right) + 24\mathcal{L}_v \left(5x^2 - 6x + 3 - \frac{1}{x} \right) \right] \\ \langle G^2 \rangle &: -\frac{M_Q^4 \langle g_s^2 G^2 \rangle}{3^2 \cdot 2^{13} \pi^6} \left[v \left(60x - 62 + \frac{26}{x} + \frac{3}{x^2} \right) + 24\mathcal{L}_v \left(5x^2 - 6x + 3 - \frac{1}{x} \right) \right] \\ \langle \bar{q}Gq \rangle &: \frac{M_Q^3 \langle \bar{q}Gq \rangle}{3 \cdot 2^9 \pi^4} \left[v \left(60x - 8 - \frac{25}{x} \right) + 12\mathcal{L}_v \left(10x^2 - 3x + \frac{1}{x} \right) \right] \\ \langle \bar{q}q \rangle^2 &: -\frac{M_Q^2 \rho \langle \bar{q}q \rangle^2}{3 \cdot 2^6 \pi^2} v \left(8 + \frac{1}{x} \right) \\ \langle G^3 \rangle &: \frac{M_Q^2 \langle g_s^3 G^3 \rangle}{3^2 \cdot 2^{14} \pi^6} \left[v \left(84x - 40 - \frac{47}{x} + \frac{3}{x^2} \right) + 6\mathcal{L}_v \left(28x^2 - 18x + 12 + \frac{1}{x} \right) \right] \\ \langle \bar{q}q \rangle \langle \bar{q}Gq \rangle &: \frac{\langle \bar{q}q \rangle \langle \bar{q}Gq \rangle}{2^6 \pi^2} v \left[1 + x - \frac{M_Q^2 \tau}{x} \left(1 - x - 2M_Q^2 \tau \right) \right]. \end{aligned} \quad (\text{A.9})$$

Note that one also can obtain this expression of the $(1^{-+}) \bar{D}_0^* D^*$ molecule by the choice $\epsilon = -1$ in Eq. Appendix A.8 for $(1^{--}) \bar{D}_0^* D^*$ molecule.

Appendix A.10. $(1^{--}) \bar{D}D_1$, $\bar{B}B_1$ Molecules

$$\begin{aligned} pert &: \frac{M_Q^8}{3 \cdot 2^{15} \pi^6} \left[v \left(720 + \frac{3036}{x} - \frac{42}{x^2} - \frac{34}{x^3} + \frac{1}{x^4} \right) \right. \\ &\quad \left. + 24\mathcal{L}_v \left(60x + 27 - 6 \left(9 + \frac{2}{x} \right) \text{Log}(x) - \frac{88}{x} + \frac{6}{x^2} \right) - 288 \left(9 + \frac{2}{x} \right) \mathcal{L}_+ \right] \\ \langle \bar{q}q \rangle &: 0 \\ \langle G^2 \rangle &: 0 \\ \langle \bar{q}Gq \rangle &: -\frac{M_Q^3 \langle \bar{q}Gq \rangle}{3 \cdot 2^9 \pi^4} \left[v \left(6x + 19 - \frac{25}{x} \right) + 6\mathcal{L}_v \left(2x^2 + 6x - 3 + \frac{2}{x} \right) \right] \\ \langle \bar{q}q \rangle^2 &: -\frac{M_Q^2 \rho \langle \bar{q}q \rangle^2}{3 \cdot 2^6 \pi^2} v \left(16 - \frac{1}{x} \right) \\ \langle G^3 \rangle &: -\frac{M_Q^2 \langle g_s^3 G^3 \rangle}{3 \cdot 2^{15} \pi^6} \left[v \left(12x - 34 + \frac{32}{x} - \frac{1}{x^2} \right) + 12\mathcal{L}_v \left(2x^2 - 6x + 2 - \frac{1}{x} \right) \right] \\ \langle \bar{q}q \rangle \langle \bar{q}Gq \rangle &: \frac{\langle \bar{q}q \rangle \langle \bar{q}Gq \rangle}{2^6 \pi^2} v \left[1 - x - M_Q^2 \tau \left(1 + \frac{1}{x} - \frac{2M_Q^2 \tau}{x} \right) \right]. \end{aligned} \quad (\text{A.10})$$

Appendix A.11. (1^-) $\bar{D}D_1, \bar{B}B_1$ Molecules

$$\begin{aligned}
pert &: \frac{M_Q^8}{5 \cdot 3 \cdot 2^{15} \pi^6} \left[v \left(1680x - 3320 - \frac{4684}{x} - \frac{2118}{x^2} - \frac{194}{x^3} + \frac{5}{x^4} \right) \right. \\
&\quad \left. + 120\mathcal{L}_v \left(28x^2 - 60x + 3 + 6 \left(3 + \frac{2}{x} \right) \text{Log}(x) + \frac{24}{x} + \frac{12}{x^2} \right) + 1440 \left(3 + \frac{2}{x} \right) \mathcal{L}_+ \right] \\
\langle \bar{q}q \rangle &: \frac{M_Q^5 \langle \bar{q}q \rangle}{3 \cdot 2^9 \pi^4} \left[v \left(60x - 62 + \frac{26}{x} + \frac{3}{x^2} \right) + 24\mathcal{L}_v \left(5x^2 - 6x + 3 - \frac{1}{x} \right) \right] \\
\langle G^2 \rangle &: -\frac{M_Q^4 \langle g_s^2 G^2 \rangle}{3^2 \cdot 2^{13} \pi^6} \left[v \left(60x - 62 + \frac{26}{x} + \frac{3}{x^2} \right) + 24\mathcal{L}_v \left(5x^2 - 6x + 3 - \frac{1}{x} \right) \right] \\
\langle \bar{q}Gq \rangle &: -\frac{M_Q^3 \langle \bar{q}Gq \rangle}{3 \cdot 2^9 \pi^4} \left[v \left(60x - 8 - \frac{25}{x} \right) + 12\mathcal{L}_v \left(10x^2 - 3x + \frac{1}{x} \right) \right] \\
\langle \bar{q}q \rangle^2 &: -\frac{M_Q^2 \rho \langle \bar{q}q \rangle^2}{3 \cdot 2^6 \pi^2} v \left(8 + \frac{1}{x} \right) \\
\langle G^3 \rangle &: \frac{M_Q^2 \langle g_s^3 G^3 \rangle}{3^2 \cdot 2^{14} \pi^6} \left[v \left(84x - 40 - \frac{47}{x} + \frac{3}{x^2} \right) + 6\mathcal{L}_v \left(28x^2 - 18x + 12 + \frac{1}{x} \right) \right] \\
\langle \bar{q}q \rangle \langle \bar{q}Gq \rangle &: \frac{\langle \bar{q}q \rangle \langle \bar{q}Gq \rangle}{2^6 \pi^2} v \left[1 + x - \frac{M_Q^2 \tau}{x} \left(1 - x - 2M_Q^2 \tau \right) \right]. \tag{A.12}
\end{aligned}$$

Appendix B. Four-Quark Spectral Functions

They are defined from Eq. 2 as: $\frac{1}{\pi} \text{Im}\Pi_{mol}^{(1)}(t)$ for spin 1 particles and $\frac{1}{\pi} \text{Im}\psi_{mol}^{(s,p)}(t)$ from Eq. 3 from spin 0 ones.

Appendix B.1. (0^+) Scalar State

$$\begin{aligned}
pert &: \frac{(1+k^2)M_c^8}{5 \cdot 3 \cdot 2^{12} \pi^6} \left[v \left(480 + \frac{1460}{x} - \frac{274}{x^2} - \frac{38}{x^3} + \frac{1}{x^4} \right) \right. \\
&\quad \left. + 120\mathcal{L}_v \left(8x - 1 - 6 \log x - \frac{8}{x} + \frac{2}{x^2} \right) - 1440 \mathcal{L}_+ \right] \\
\langle \bar{q}q \rangle &: \frac{(1-k^2)M_c^5 \langle \bar{q}q \rangle}{3 \cdot 2^5 \pi^4} \left[v \left(6 - \frac{5}{x} - \frac{1}{x^2} \right) + 6\mathcal{L}_v \left(2x - 2 + \frac{1}{x} \right) \right] \\
\langle G^2 \rangle &: -\frac{(1+k^2)M_c^4 \langle g_s^2 G^2 \rangle}{3^2 \cdot 2^{11} \pi^6} \left[v \left(6 - \frac{5}{x} - \frac{1}{x^2} \right) + 6\mathcal{L}_v \left(2x - 2 + \frac{1}{x} \right) \right] \\
\langle \bar{q}Gq \rangle &: -\frac{(1-k^2)M_c^3 \langle \bar{q}Gq \rangle}{2^7 \pi^4} \left[v \left(2 - \frac{7}{x} \right) + 2\mathcal{L}_v \left(2x + 2 + \frac{1}{x} \right) \right] \\
\langle \bar{q}q \rangle^2 &: \frac{(1+k^2)M_c^2 \rho \langle \bar{q}q \rangle^2 v}{12 \pi^2} \\
\langle G^3 \rangle &: \frac{(1+k^2)M_c^2 \langle g_s^3 G^3 \rangle}{3^2 \cdot 2^{12} \pi^6} \left[v \left(6 - \frac{25}{x} + \frac{1}{x^2} \right) + 6\mathcal{L}_v \left(2x + 2 + \frac{1}{x} \right) \right] \\
\langle \bar{q}q \rangle \langle \bar{q}Gq \rangle &: -\frac{(1+k^2) \langle \bar{q}q \rangle \langle \bar{q}Gq \rangle}{3 \cdot 2^4 \pi^2} v \left[1 - \frac{M_c^2 \tau}{x} \left(1 - 2M_c^2 \tau \right) \right], \tag{B.1}
\end{aligned}$$

where we use the same definitions as in the case of the molecule states; k is the mixing of interpolating currents where $k = 0$ ^{72,73} is its optimal value.

Appendix B.2. (1^+) Axial-vector state

$$\begin{aligned}
pert &: \frac{(1+k^2)M_Q^8}{5 \cdot 3^2 \cdot 2^{13} \pi^6} \left[v \left(840x + 140 + \frac{5248}{x} - \frac{1164}{x^2} - \frac{182}{x^3} + \frac{5}{x^4} \right) \right. \\
&\quad \left. + 120\mathcal{L}_v \left(14x^2 + 15 - 18 \log x - \frac{32}{x} + \frac{9}{x^2} \right) - 4320 \mathcal{L}_+ \right] \\
\langle \bar{q}q \rangle &: \frac{(1-k^2)M_Q^5 \langle \bar{q}q \rangle}{3^2 \cdot 2^8 \pi^4} \left[v \left(60x + 82 - \frac{94}{x} - \frac{21}{x^2} \right) + 24\mathcal{L}_v \left(5x^2 + 6x - 9 + \frac{5}{x} \right) \right] \\
\langle G^2 \rangle &: \frac{(1+k^2)M_Q^4 \langle g_s^2 G^2 \rangle}{3^2 \cdot 2^{11} \pi^6} \left[v \left(6 - \frac{5}{x} - \frac{1}{x^2} \right) + 6\mathcal{L}_v \left(2x - 2 + \frac{1}{x} \right) \right] \\
\langle \bar{q}Gq \rangle &: -\frac{(1-k^2)M_Q^3 \langle \bar{q}Gq \rangle}{3^2 \cdot 2^8 \pi^4} \left[v \left(42x + 7 - \frac{58}{x} \right) + 6\mathcal{L}_v \left(14x^2 + 9 + \frac{2}{x} \right) \right] \\
\langle \bar{q}q \rangle^2 &: \frac{(1+k^2)M_Q^2 \rho \langle \bar{q}q \rangle^2 v}{12 \pi^2} \\
\langle G^3 \rangle &: \frac{(1+k^2)M_Q^2 \langle g_s^3 G^3 \rangle}{3^3 2^{14} \pi^6} \left[v \left(132x + 22 - \frac{190}{x} + \frac{9}{x^2} \right) + 24\mathcal{L}_v \left(11x^2 + 3 + \frac{2}{x} \right) \right] \\
\langle \bar{q}q \rangle \langle \bar{q}Gq \rangle &: -\frac{(1+k^2) \langle \bar{q}q \rangle \langle \bar{q}Gq \rangle}{3 \cdot 2^5 \pi^2} v \left[1 - \frac{M_c^2 \tau}{x} \left(1 - 4M_c^2 \tau \right) \right], \tag{B.2}
\end{aligned}$$

Appendix B.3. (0^-) Pseudoscalar state

$$\begin{aligned}
pert &: \frac{(1+k^2)M_c^8}{5 \cdot 3 \cdot 2^{12} \pi^6} \left[v \left(480 + \frac{1460}{x} - \frac{274}{x^2} - \frac{38}{x^3} + \frac{1}{x^4} \right) + 120\mathcal{L}_v \left(8x - 1 - 6 \log x - \frac{8}{x} + \frac{2}{x^2} \right) - 1440 \mathcal{L}_+ \right] \\
\langle \bar{q}q \rangle &: 0 \\
\langle G^2 \rangle &: -\frac{(1+k^2)M_c^4 \langle g_s^2 G^2 \rangle}{3^2 \cdot 2^{11} \pi^6} \left[v \left(6 - \frac{5}{x} - \frac{1}{x^2} \right) + 6\mathcal{L}_v \left(2x - 2 + \frac{1}{x} \right) \right] \\
\langle \bar{q}Gq \rangle &: 0 \\
\langle \bar{q}q \rangle^2 &: -\frac{(1+k^2)M_c^2 \rho \langle \bar{q}q \rangle^2 v}{12 \pi^2} \\
\langle G^3 \rangle &: \frac{(1+k^2)M_c^2 \langle g_s^3 G^3 \rangle}{3^2 \cdot 2^{12} \pi^6} \left[v \left(6 - \frac{25}{x} + \frac{1}{x^2} \right) + 6\mathcal{L}_v \left(2x + 2 + \frac{1}{x} \right) \right] \\
\langle \bar{q}q \rangle \langle \bar{q}Gq \rangle &: \frac{(1+k^2) \langle \bar{q}q \rangle \langle \bar{q}Gq \rangle}{3 \cdot 2^4 \pi^2} v \left[1 - \frac{M_c^2 \tau}{x} \left(1 - 2M_c^2 \tau \right) \right] \tag{B.3}
\end{aligned}$$

Appendix B.4. (1^-) Vector State

$$\begin{aligned}
pert &: \frac{(1+k^2)M_Q^8}{5 \cdot 3^2 \cdot 2^{13} \pi^6} \left[v \left(840x + 140 + \frac{5248}{x} - \frac{1164}{x^2} - \frac{182}{x^3} + \frac{5}{x^4} \right) \right. \\
&\quad \left. + 120\mathcal{L}_v \left(14x^2 + 15 - 18 \log x - \frac{32}{x} + \frac{9}{x^2} \right) - 4320 \mathcal{L}_+ \right] \\
\langle \bar{q}q \rangle &: \frac{(1-k^2)M_Q^5 \langle \bar{q}q \rangle}{3^2 \cdot 2^8 \pi^4} \left[v \left(60x - 62 + \frac{26}{x} + \frac{3}{x^2} \right) + 24\mathcal{L}_v \left(5x^2 - 6x + 3 - \frac{1}{x} \right) \right]
\end{aligned}$$

$$\begin{aligned}
\langle G^2 \rangle &: \frac{(1+k^2)M_Q^4 \langle g_s^2 G^2 \rangle}{3^2 \cdot 2^{11} \pi^6} \left[v \left(6 - \frac{5}{x} - \frac{1}{x^2} \right) + 6\mathcal{L}_v \left(2x - 2 + \frac{1}{x} \right) \right] \\
\langle \bar{q}Gq \rangle &: -\frac{(1-k^2)M_Q^3 \langle \bar{q}Gq \rangle}{3^2 \cdot 2^8 \pi^4} \left[v \left(42x + 7 - \frac{22}{x} \right) + 6\mathcal{L}_v \left(14x^2 - 3 + \frac{2}{x} \right) \right] \\
\langle \bar{q}q \rangle^2 &: -\frac{(1+k^2)M_Q^2 \rho \langle \bar{q}q \rangle^2 v}{12 \pi^2} \\
\langle G^3 \rangle &: \frac{(1+k^2)M_Q^2 \langle g_s^3 G^3 \rangle}{3^3 2^{14} \pi^6} \left[v \left(132x + 22 - \frac{190}{x} + \frac{9}{x^2} \right) + 24\mathcal{L}_v \left(11x^2 + 3 + \frac{2}{x} \right) \right] \\
\langle \bar{q}q \rangle \langle \bar{q}Gq \rangle &: \frac{(1+k^2)\langle \bar{q}q \rangle \langle \bar{q}Gq \rangle}{3 \cdot 2^5 \pi^2} v \left[1 - \frac{M_c^2 \tau}{x} \left(1 - 4M_c^2 \tau \right) \right]. \tag{B.4}
\end{aligned}$$

References

1. S.-K. Choi *et al.* [Belle Collaboration], *Phys. Rev. Lett.* **91** (2003) 262001.
2. B. Aubert *et al.* [BABAR Collaboration], *Phys. Rev.* **D71** (2005) 071103.
3. B. Aubert *et al.* [BABAR Collaboration], *Phys. Rev. Lett.* **95** (2005) 142001.
4. D. Acosta *et al.* [CDF II Collaboration], *Phys. Rev. Lett.* **93** (2004) 072001.
5. V. M. Abazov *et al.* [D0 Collaboration], *Phys. Rev. Lett.* **93** (2004) 162002.
6. R. Aaij *et al.* [LHCb collaboration], *Nucl. Phys.* **B886** (2014) 665.
7. K.A. Olive *et al.* [Particle Data Group], *Chin. Phys.* **C38** (2014) 090001.
8. R. Albuquerque et al, work in preparation.
9. T. Skwarnicki [LHCb collaboration] talk given at Meson2016.
10. T. Aaltonen *et al.* [CDF Collaboration], *Phys. Rev. Lett.* **102** (2009) 242002.
11. T. Aaltonen *et al.* [CDF Collaboration], arXiv:1101.6058 [hep-ex] (2011).
12. C. P. Shen *et al.* [Belle Collaboration], *Phys. Rev. Lett.* **104** (2010) 112004.
13. K. Abe *et al.* [Belle Collaboration], *Phys. Rev. Lett.* **94** (2005) 182002.
14. B. Aubert *et al.* [BABAR Collaboration], *Phys. Rev. Lett.* **95** (2005) 142001.
15. T. E. Coan *et al.* [CLEO Collaboration], *Phys. Rev.* **D74** (2006) 091104.
16. M. Albikim *et al.* [BESIII Collaboration], *Phys. Rev. Lett.* **110** (2013) 252001.
17. W. Shan [BESIII Collaboration], review talk given at QCD16 (19th HEP Int. Conf. in QCD), 4-8 july, Montpellier-FR.
18. Z. Q. Liu *et al.* [Belle Collaboration], *Phys. Rev. Lett.* **110** (2013) 252002.
19. U. Tamponi [Belle Collaboration], SLAC-econf/C130904 (2013).
20. M. Albikim *et al.* [BESIII Collaboration], *Phys. Rev. Lett.* **112** (2014) 132001.
21. M. Albikim *et al.* [BESIII Collaboration], *Phys. Rev. Lett.* **113** (2014) 212002.
22. M. Albikim *et al.* [BESIII Collaboration], *Phys. Rev. Lett.* **115** (2015) 182002.
23. X. L. Wang *et al.* [Belle Collaboration], *Phys. Rev.* **D91** (2015) 112007.
24. S. K. Choi *et al.* [Belle Collaboration], *Phys. Rev. Lett.* **100** (2008) 142001.
25. R. Aaij *et al.* [LHCb collaboration], *Phys. Rev. Lett.* **112** (2014) 222002.
26. I. Adachi *et al.* [Belle Collaboration], *Phys. Rev. Lett.* **108** (2012) 032001.
27. K.-F Chen *et al.* [Belle Collaboration], *Phys. Rev. Lett.* **100** (2008) 112001.
28. A. Bondar *et al.* [Belle Collaboration], *Phys. Rev. Lett.* **108** (2012) 122001.
29. C.P Chen *et al.* [Belle Collaboration], arXiv:1605.00990v1 (2016).
30. E.S. Swanson, *Phys. Rept.* **429**, 243 (2006).
31. J.M. Richard, *Nucl. Phys. (Proc. Suppl.)* **B164** (2007) 131.
32. S.-L. Zhu, *Int. J. Mod. Phys. E* **17** (2008) 283.
33. S. Godfrey and S. Olsen, *Ann. Rev. Nucl. Part. Sci.* **58** (2008) 51.
34. F. S. Navarra, M. Nielsen, S. H. Lee, *Phys. Rep.* **497** (2010) 41.

35. W. Chen and S.-L Zhu, *Phys. Rev.* **D83** (2011) 034010.
36. N. Brambilla, et al., *Eur. Phys. J.* **C71** (2011) 1534.
37. R. Albuquerque, PhD thesis, arXiv:1306.4671 [hep-ph] (2013).
38. X. Liu, *Chin. Sci. Bull.* **59** (2014) 3815.
39. G.T. Bodwin et al., arXiv:1307.7425 (2013).
40. M. Nielsen, *Nucl. Part. Phys. Proc.* **258-259** (2015) 139.
41. E. Braaten, *EPJ Web Conf.* **113** (2016) 01015.
42. A. Esposito et al., *Int. J. Mod. Phys.* **A30** (2015) 1530002.
43. H.-X. Chen et al., *Phys. Rep.* **631** (2016) 1.
44. R.A. Briceno et al., *Chin. Phys.* **C40** (2016) n.4, 042001.
45. Z.-G. Wang, arXiv: 1601.0554 [hep-ph] (2016).
46. A. Ali, arXiv:1605.05954 (2016) and references therein.
47. Z.-G. Wang, arXiv: 1606.05872 [hep-ph] (2016).
48. Z.-G. Wang, arXiv: 1607.00701 [hep-ph] (2016).
49. D.V. Bugg, *Europhys. Lett.* **96** (2011) 1102.
50. A.P. Szczepaniak, *Phys. Lett.* **B747** (2015) 410.
51. E.S. Swanson, *AIP Conf. Proc.* **1735** (2016) 020013.
52. M. B. Voloshin and L. B. Okun, *JETP Lett.* **23** (1976) 333.
53. A. D. Rujula, H. Georgi, and S. L. Glashow, *Phys. Rev. Lett.* **38** (1977) 317.
54. N.A. Tornqvist, *Phys. Lett.* **B590** (2004) 209-215.
55. Z.-F. Sun, J. He, X. Liu, Z.-G. Luo and S.-L. Zhu, *Phys. Rev.* **D84** (2011) 054002.
56. Y.J. Zhang, H.C. Chiang, P.N. Shen and B.S. Zou, *Phys. Rev.* **D74** (2006) 014013.
57. R.L Jaffe, *Phys. Rev.* **D15** (1977) 267.
58. L. Maiani et al., *Phys. Rev.* **D71** (2005) 014028.
59. H. Hogaasen, E. Kou, J.-M Richard, P. Sorba, *Phys. Lett.* **B732** (2014) 97.
60. S. Weinberg, *Phys. Rev. Lett.* **110** (2013) 261601.
61. M. Knecht and S. Peris, *Phys. Rev.* **D88** (2013) 036016.
62. G. Rossi and G. Veneziano, *JHEP* **1606** (2016) 041.
63. S. Narison and G. Veneziano, *Int. J. Mod. Phys.* **A4** (1989) 2751.
64. S. Narison, *Nucl. Phys.* **B509** (1998) 312.
65. G. Mennessier, S. Narison and W. Ochs, *Phys. Lett.* **B665** (2008) 205.
66. R. Kaminski, G. Mennessier and S. Narison, *Phys. Lett.* **B680** (2009) 148.
67. G. Mennessier, S. Narison and X.-G. Wang, *Phys. Lett.* **B688** (2010) 59.
68. G. Mennessier, S. Narison and X.-G. Wang, *Phys. Lett.* **B696** (2011) 40.
69. R.D. Matheus, S. Narison, M. Nielsen and J.M. Richard, *Phys. Rev.* **D75** (2007) 014005.
70. J. M. Dias, S. Narison, F.S. Navarra, M. Nielsen and J. M. Richard, *Phys. Lett.* **B703** (2011) 274.
71. S. Narison, F.S. Navarra and M. Nielsen, *Phys. Rev.* **D83** (2011) 016004.
72. R.M. Albuquerque, F. Fanomezana, S. Narison and A. Rabemananjara, *Phys. Lett.* **B715** (2012) 129-141.
73. R.M. Albuquerque, F. Fanomezana, S. Narison and A. Rabemananjara, *Nucl. Phys. Proc. Suppl.* **234** (2013) 158-161.
74. R.M. Albuquerque, M. Nielsen and R. Rodrigues da Silva, *Phys. Rev.* **D84** (2012) 116004.
75. S.H. Lee, A. Mihara, F.S. Navarra and M. Nielsen, *Phys. Lett.* **B661** (2008) 28.
76. S.I. Finazzo, X. Liu and M. Nielsen, *Phys. Lett.* **B701** (2011) 101.
77. J-R Zhang, *Phys. Rev.* **D 87** (2013) 116004.
78. J-R Zhang and M.-Q. Huang, *J. Phys.* **G37** (2010) 025005.
79. C.-Y. Cui, X.-H. Liao, Y.-L. Liu and M.-Q. Huang, *J. Phys.* **G41** (2014) 075003.

80. C.-Y. Cui, Y.-L. Liu and M.-Q. Huang, *Phys. Rev.* **D85** (2012) 074014.
81. Z.-G. Wang, *Int. J. Mod. Phys.* **A30** (2015) 1550168.
82. Z.-G. Wang, *Eur. Phys. J.* **C63** (2009) 115.
83. Z.-G. Wang, *Eur. Phys. J.* **C74** (2014) 2963.
84. W. Chen, T. G. Steele, H.-X. Chen and S.-L. Zhu, *Phys. Rev.* **D92** (2015) 054002.
85. M.-Q. Huang and J.-R. Zhang, *Phys. Rev.* **D 80** (2009) 056004.
86. R. Albuquerque, X. Liu and M. Nielsen, *Phys. Lett.* **B718** (2012) 492.
87. S. Narison, E. de Rafael, *Phys. Lett.* **B103** (1981) 57.
88. J.S. Bell and R.A. Bertlmann, *Nucl. Phys.* **B227** (1983) 435.
89. R.A. Bertlmann, *Acta Phys. Austriaca* **53** (1981) 305.
90. R.A. Bertlmann and H. Neufeld, *Z. Phys.* **C27** (1985) 437.
91. R.A. Bertlmann, G. Launer and E. de Rafael, *Nucl. Phys.* **B250** (1985) 61.
92. R.A. Bertlmann, C.A. Dominguez, M. Loewe, M. Perrottet and E. de Rafael, *Z. Phys.* **C39** (1988) 231.
93. M.A. Shifman, A.I. Vainshtein and V.I. Zakharov, *Nucl. Phys.* **B147** (1979) 385.
94. M.A. Shifman, A.I. Vainshtein and V.I. Zakharov, *Nucl. Phys.* **B147** (1979) 448.
95. S. Narison, *QCD as a theory of hadrons*, Cambridge Monogr. Part. Phys. Nucl. Phys. Cosmol. **17** (2002) 1 [hep-ph/0205006].
96. S. Narison, *QCD spectral sum rules*, World Sci. Lect. Notes Phys. **26** (1989) 1.
97. S. Narison, *Phys. Rept.* **84** (1982) 263.
98. S. Narison, *Acta Phys. Pol.* **B26** (1995) 687.
99. S. Narison, hep-ph/9510270 (1995).
100. L.J. Reinders, H. Rubinsteing and S. Yazaki, *Phys. Rept.* **127** (1985) 1.
101. E. de Rafael, hep-ph/9802448.
102. S. Narison, *Phys. Lett.* **B210** (1988) 238.
103. S. Narison, *Phys. Lett.* **B337** (1994) 166.
104. S. Narison, *Phys. Lett.* **B322** (1994) 327.
105. S. Narison, *Phys. Lett.* **B387** (1996) 162.
106. S. Narison, *Phys. Lett.* **B358** (1995) 113.
107. S. Narison, *Phys. Lett.* **B466** (1999) 345.
108. S. Narison, *Phys. Lett.* **B605** (2005) 319.
109. S. Narison, *Phys. Rev.* **D74** (2006) 034013.
110. S. Narison, *Phys. Lett.* **B668** (2008) 308.
111. R.M. Albuquerque and S. Narison, *Phys. Lett.* **B694** (2010) 217.
112. R.M. Albuquerque, S. Narison and M. Nielsen, *Phys. Lett.* **B684** (2010) 236.
113. S. Narison, F. Navarra and M. Nielsen, *Phys. Rev.* **D83** (2011) 016004.
114. R. D. Matheus, F. S. Navarra, M. Nielsen and C. M. Zanetti, *Phys. Rev.* **D80** (2009) 056002.
115. R.M. Albuquerque and M. Nielsen, *Nucl. Phys.* **A815** (2009) 53; Erratum-ibid. **A857** (2011) 48.
116. J.M. Dias, F. S. Navarra, M. Nielsen and C.M. Zanetti, *Phys. Rev.* **D88** (2013) 1,016004.
117. F. S. Navarra, M. Nielsen, J.M. Dias and C.M. Zanetti, *Nucl. Part. Phys. Proc.* **258-259** (2015) 145.
118. R.M. Albuquerque and R. D. Matheus, *Nucl. Part. Phys. Proc.* **258-259** (2015) 148.
119. R.M. Albuquerque, J.M. Dias, M. Nielsen and C.M. Zanetti, *Phys. Rev.* **D89** (2014) 076007.
120. F. Fanomezana, S. Narison and A. Rabemananjara, *Nucl. Part. Phys. Proc.* **258-259** (2015) 152.
121. F. Fanomezana, S. Narison and A. Rabemananjara, *Nucl. Part. Phys. Proc.* **258-259**

- (2015) 156.
122. R. Albuquerque, S. Narison, A. Rabemananjara and D. Rabetiarivony, *Int. J. Mod. Phys. A***31** (2016) no. 17, 1650093.
 123. C.M. Zanetti, M. Nielsen and K.P. Khemchandani, *Phys. Rev. D***93** (2016) no. 9, 096011.
 124. W. Chen et al., *Phys. Rev. Lett.* **117** (2016) no. 2, 022002.
 125. S. S. Agaev and K. Azizi and H. Sundu, *Phys. Rev. D***93** (2016) no. 7, 074024.
 126. S. S. Agaev and K. Azizi and H. Sundu, arXiv:1603.02708 [hep-ph].
 127. Z.-G. Wang, arXiv:1602.08711v1 [hep-ph].
 128. V.M. Abazov et al., [D0 collaboration], *Phys. Rev. Lett.* **117** (2016) 022003.
 129. J. van Tilburg, [LHCb collaboration], LHCb-CONF-2016-004, 51ème Rencontre de Moriond, La Thuile, Italy (2016).
 130. S. Narison and V.I. Zakharov, *Phys. Lett. B***679** (2009) 355.
 131. S. Narison, *Phys. Lett. B***673** (2009) 30.
 132. G. Launer, S. Narison and R. Tarrach, *Z. Phys. C***26** (1984) 433.
 133. Y. Chung et al., *Z. Phys. C***25** (1984) 151.
 134. H.G. Dosch, *Non-Perturbative Methods (Montpellier 1985)* ed. S. Narison, World Scientific (Singapore).
 135. H.G. Dosch, M. Jamin and S. Narison, *Phys. Lett. B***220** (1989) 251.
 136. S. Narison and R. Tarrach, *Phys. Lett. B***125** (1983) 217.
 137. R. Tarrach, *Nucl. Phys. B***183** (1981) 384.
 138. R. Coquereaux, *Annals of Physics* **125** (1980) 401.
 139. P. Binetruy and T. Sücker, *Nucl. Phys. B***178** (1981) 293.
 140. S. Narison, *Phys. Lett. B***197** (1987) 405.
 141. S. Narison, *Phys. Lett. B***216** (1989) 191.
 142. N. Gray, D.J. Broadhurst, W. Grafe, and K. Schilcher, *Z. Phys. C***48** (1990) 673.
 143. L.V. Avdeev and M. Yu. Kalmykov, *Nucl. Phys. B***502** (1997) 419.
 144. J. Fleischer, F. Jegerlehner, O.V. Tarasov, and O.L. Veretin, *Nucl. Phys. B***539** (1999) 671.
 145. K.G. Chetyrkin and M. Steinhauser, *Nucl. Phys. B***573** (2000) 617.
 146. K. Melnikov and T. van Ritbergen, *Phys. Lett. B***482** (2000) 99.
 147. K. Chetyrkin, S. Narison and V.I. Zakharov, *Nucl. Phys. B***550** (1999) 353.
 148. S. Narison and V.I. Zakharov, *Phys. Lett. B***522** (2001) 266.
 149. V.I. Zakharov, *Nucl. Phys. Proc. Suppl.* **164** (2007) 240.
 150. S. Narison, *Nucl. Phys. Proc. Suppl.* **164** (2007) 225.
 151. A. Pich and E. de Rafael, *Phys. Lett. B***158** (1985) 477.
 152. A. Pich, *Phys. Lett. B***206** (1988) 322.
 153. S. Narison and A. Pivovarov, *Phys. Lett. B***327** (1994) 341.
 154. K. Hagiwara, S. Narison and D. Nomura, *Phys. Lett. B***540** (2002) 233.
 155. D.J. Broadhurst, *Phys. Lett. B***101** (1981) 423.
 156. K.G. Chetyrkin and M. Steinhauser, *Phys. Lett. B***502** (2001) 104.
 157. K.G. Chetyrkin and M. Steinhauser, *Eur. Phys. J. C***21** (2001) 319 and references therein.
 158. W. Lucha, D. Melikhov and S. Simula, *Phys. Lett. B***735** (2014) 12.
 159. S. Narison, *Phys. Lett. B***718** (2013) 1321.
 160. S. Narison, *Nucl. Phys. Proc. Suppl.* **234** (2013) 187.
 161. E. de Rafael, *Nucl. Phys. Proc. Suppl.* **96** (2001) 316.
 162. S. Peris, B. Phily and E. de Rafael, *Phys. Rev. Lett.* **86** (2001) 14.
 163. S. Narison, *Phys. Lett. B***520** (2001) 115.
 164. S. Narison, *Nucl. Phys. Proc. Suppl.* **258-259** (2015) 189 and references therein.

165. S. Narison, *Nucl. Phys. Proc. Supp.* **270-272** (2016) 143 and references therein.
166. J. Rosner and S. Stone, arXiv:1509.02220 [hep-ph] (2015).
167. S. Aoki et al., FLAG working group, *Eur. Phys. J.* **C74** (2014) 2890 .
168. S. Narison, *Phys. Lett.* **B721** (2013) 269.
169. S. Narison, *Phys. Lett.* **B738** (2014) 346.
170. S. Narison, *Int. J. Mod. Phys.* **A30** (2015) no.20, 1550116
171. P.M. Stevenson, *Nucl.Phys.* **B868** (2013) 38.
172. S. J. Brodsky, G. P. Lepage and P. B. Mackenzie, *Phys. Rev.* **D28** (1983) 228.
173. X.-G. Wu et al., *Rep. Prog. Phys.* **78** (2015) 126201.
174. A.L. Kataev and S.V. Mikhailov, *Phys.Rev.* **D91** (2015) no.1, 014007.
175. J. -L. Kneur and A. Neveu, *Phys.Rev.* **D88** (2013) 074025.
176. E. Braaten, S. Narison and A. Pich, *Nucl. Phys.* **B373** (1992) 581.
177. S. Narison and A. Pich, *Phys. Lett.* **B211** (1988) 183.
178. S. Narison, arXiv:hep-ph/0202200 (2002).
179. S. Narison, *Phys. Lett.* **B693** (2010) 559; Erratum ibid 705 (2011) 544.
180. S. Narison, *Phys. Lett.* **B706** (2011) 412.
181. S. Narison, *Phys. Lett.* **B707** (2012) 259.
182. B.L. Ioffe and K.N. Zyablyuk, *Eur. Phys. J.* **C27** (2003) 229.
183. B.L. Ioffe, *Prog. Part. Nucl. Phys.* **56** (2006) 232.
184. H.G. Dosch and S. Narison, *Phys. Lett.* **B417** (1998) 173.
185. S. Narison, *Phys. Lett.* **B216** (1989) 191.
186. B.L. Ioffe, *Nucl. Phys.* **B188** (1981) 317.
187. B.L. Ioffe, *Nucl. Phys.* **B191** (1981) 591.
188. A.A.Ovchinnikov and A.A.Pivovarov, *Yad. Fiz.* **48** (1988) 1135.
189. S. Narison, *Phys. Lett.* **B300** (1993) 293.
190. S. Narison, *Phys. Lett.* **B361** (1995) 121.
191. F.J. Yndurain, *Phys. Rept.* **320** (1999) 287.
192. S. Narison, *Phys. Lett.* **B361** (1995) 121.
193. S. Narison, *Phys. Lett.* **B624** (2005) 223.
194. S. Narison, *Phys. Lett.* **B387** (1996) 162.
195. A. Pich and A. Rodriguez-Sánchez, arXiv:1605.06830 [hep-ph] (2016).
196. See e.g: S. Bethke, talk given at QCD16, 4-8 july 2016, Montpellier (FR).
197. E.G. Floratos, S. Narison and E. de Rafael, *Nucl. Phys.* **B155** (1979) 155.
198. G. S. Bali, C. Bauer and A. Pineda, *Phys. Rev. Lett.* **113** (2014) 092001.
199. T. Lee, *Phys. Rev.* **D82**(2010)114021.
200. M. Davier et al., *Eur. Phys. J.* **C56** (2008) 305.
201. D. Boito et al, *Phys. Rev.* **D95** (2015) n⁰**3**, 034003.
202. R.T. Kleiv, D. Harnett, T.G. Steele and H.Y. Jin, *Nucl. Phys. Proc. Suppl.* **234** (2013) 150.
203. J. Govaerts, L. J. Reinders, H. R. Rubinstein, and J. Weyers, *Nucl. Phys.* **B258** (1985) 215.
204. J. Govaerts, L. J. Reinders, and J. Weyers, *Nucl. Phys.* **B262** (1985) 575.
205. J. Govaerts, L. J. Reinders, P. Francken, X. Gonze, and J. Weyers, *Nucl. Phys.* **B284** (1987) 674.
206. R. F Lebed and A. D Polosa, *Phys. Rev.* **D93** (2016) 094024.
207. H.-X Chen et al, arXiv: 1606.03179v1 (2016).
208. Y. Liu and I. Zahed, arXiv:1608.06535 [hep-ph] (2016).
209. D. Harnett, R. Berg, R.T. Kleiv and T.G. Steele, *Nucl. Phys. Proc. Suppl.* **234** (2013) 154.